XN-NF-80-19(NP)

VOLUME 1

EXXON NUCLEAR METHODOLOGY FOR BOILING WATER REACTORS

VOLUME 1
NEUTRONICS METHODS FOR DESIGN AND ANALYSIS

AUGUST 1980

RICHLAND, WA 99352

EXXON NUCLEAR COMPANY, Inc.

XN-NF-80-19(NP)

Vol. 1
08/07/80

EXXON NUCLEAR METHODOLOGY FOR BOILING WATER REACTORS VOLUME 1 NEUTRONIC METHODS FOR DESIGN AND ANALYSIS

Approved: T L Krysinski 8/1/80

T. L. Krysinski, Manager
BWR Neutronics

Approved: David H. Timmons 8/1/80

D. H. Timmons, Manager
Neutronics Development

Approved: R B Stout 4 Aug 80

R. B. Stout, Manager
Neutronics & Fuel Management

Approved: George A Sofer 5 Aug 80

G. A. Sofer, Manager
Nuclear Fuels Engineering

TABLE OF CONTENTS

TABLE OF CONTENTS CONTINUED

TABLE OF CONTENTS CONTINUED

TABLE OF CONTENTS CONTINUED

LIST OF TABLES

LIST OF FIGURES

LIST OF FIGURES CONTINUED

LIST OF FIGURES CONTINUED

LIST OF FIGURES CONTINUED

1.0 INTRODUCTION

The purpose of this report is to document the Exxon Nuclear Company (ENC) methods for the neutronic analysis of boiling water reactors (BWR's). The report is being issued at this time for NRC and utility customer review. Included in this report are local neutronic analysis models applicable to individual fuel assemblies and neutronics core analysis methodology applicable to the entire core. Uncertainty analysis methodology and verification of the calculational results are also covered. The neutronics core analysis methodology includes control rod drop, control rod withdrawal, fuel misloading, reactor core and channel hydrodynamic stability, and neutronic input to the total nuclear plant transient analysis. The neutronic methods are verified by comparing the calculational results with measured reactor data and with higher order calculations. The power distribution uncertainty methodology considers the neutronic models and the measured reactor data. The neutronic methods presented in this report will be used by ENC and utility customers for the design of reload fuel, for reactor in-core physics calculations and for safety and licensing calculations which include accident and transient analyses.

2.0 SUMMARY

Included in this section is a brief description of the computer codes used in the neutronic calculations for boiling water reactors. A summary of the core analysis methodology, verification of the neutronic and fuel management methods, and the method of determining the power distribution uncertainty is provided in the following.

The ENC neutronic methods include the five modules: (1) XFYRE for calculation of fuel neutronic parameters and assembly burnup, (2) XTGBWR for reactor core simulation, (3) COTRAN for transient calculations, (4) XDT for diffusion theory calculations and (5) XMC for Monte Carlo benchmark calculations.

2.1 FUEL ASSEMBLY DEPLETION MODEL (XFYRE)

The nuclear parameters for the BWR assemblies are calculated with the XFYRE computer code. The XFYRE code combines the HRG and THERMOS cross section generating codes, diffusion theory, and an isotopics depletion model to generate fuel neutronic parameters as a function of voids and exposure for both controlled and uncontrolled assemblies.

The calculations performed by the XFYRE code include generation of cross sections for each fuel assembly region, neutron flux and power shapes across the fuel assembly, isotopic depletion, flux and volume weighted bundle parameters, and incore detector parameters.

The code uses two dimensional four energy group diffusion theory methods for the microscopic depletion of BWR assemblies. The code alternates between a spatial calculation of the average flux in each pin cell and

a burnup calculation for each pin over an exposure interval, maintaining a constant pin power over the interval. The four energy group cross sections are collapsed from fine group thermal and epithermal spectrum calculations for each pin type within an assembly. The spectrum calculations are repeated at intervals to adjust the multigroup cross sections for the spectral change with burnup.

2.2 CORE SIMULATOR MODEL (XTGBWR)

The ENC core simulator program for the analysis of BWR cores is the XTGBWR code. The XTGBWR code requires two-group cross sections as input and utilizes simulated two-group diffusion theory models to solve for flux and power. The XTGBWR program uses coarse mesh diffusion theory to solve for the fast group flux in each node. The thermal flux is calculated from the fast flux assuming the only source of thermal neutrons is slowing from the fast group and that no thermal leakage occurs within each node. Corrections to the above assumption are made to account for thermal flux gradients at controlled nodes and on the core edge. Inner iterations are performed on the fast group flux, but the thermal flux is updated only after each outer iteration. After a specified number of outer iterations, the cross sections are updated to reflect power dependence on xenon, Doppler and thermal hydraulic feedback.

For fuel management calculations, the XTGBWR code has the following primary capabilities:

1. Core calculations in 1/4, 1/2 and full core geometry.
2. Control rod dependent parameters.
3. Thermal hydraulic void feedback including subcooled boiling.
4. Equilibrium and time dependent xenon and samarium.
5. Power dependent Doppler broadening.
6. Void history correction to cross sections.
7. Calculation of core K-effective and nodal power distribution.
8. Calculation of critical power ratio (CPR), linear heat generation rate (LHGR), and average planar linear heat generation rate (APLHGR), at each node.
9. Prediction of the traveling incore probe (TIP) measurements.
10. Haling calculations in two or three dimensions.
11. Fuel shuffling option.
12. Zero power critical option.

2.3 REACTOR KINETICS MODEL (COTRAN)

The ENC program for kinetics analysis of BWR cores is the COTRAN code. COTRAN is a two dimensional (r-z) computer program which solves the space and time dependent neutron diffusion equation with fuel temperature and reactivity feedback. These reactivity feedbacks are determined from a solution of equations of mass, energy and momentum for the coolant coupled with a fuel conduction model.

The COTRAN code requires input from the XFYRE and XTGBWR codes including cross sections, rod worths, initial flux and power shapes, peaking factors and other initial condition parameters. The COTRAN code has the capability to accept forcing functions as a function of time for several system parameters. These forcing functions allow COTRAN to model the reactor while including as input the total system feedback.

2.4 DIFFUSION THEORY MODEL (XDT)

The ENC computer program which is used for special single and multi-bundle diffusion theory calculations is the XDT code. These special diffusion theory calculations include four and sixteen bundle calculations, fuel misloading calculations and incore detector calculations. The XDT code calculates the eigenvalue, relative powers, multigroup neutron fluxes, and region cross sections.

2.5 MONTE CARLO MODEL (XMC)

The Exxon Monte Carlo Code (XMC) is a general purpose Monte Carlo code designed primarily to calculate benchmark problems for thermal reactors. These benchmarks are then used as one of the methods to calibrate the other ENC methods. With XMC, the geometrical configuration can be described exactly. This geometrical capability and a coupled space-energy solution of the transport problem makes the Monte Carlo method as contained in XMC superior to other calculational methods for evaluting key bundle nuclear parameters and for calculating the effects of water gaps, control blades and burnable poisor rods.

The neutron flux, isotopic reaction rates, group-averaged cross sections, and neutron leakage are calculated in three-dimensional space over the energy range from 0 to 10 MeV. The reaction types considered are fission, capture, inelastic and n-2n scattering, elastic scattering with isotropic or anisotropic angular distributions, and thermal elastic scattering using the ideal gas scattering model. The energy distribution of the neutrons is continuous. However, the cross sections are averaged over up to 2000 microscopic energy groups. Resolved resonance cross sections are caluclated by XMC for each neutron energy using the Doppler-broadened Breit-Wigner single-level formula.

2.6 CORE ANALYSIS METHODOLOGY

Special neutronic calculations are performed to evaluate the control rod drop accident, fuel misloading incident, reactor core and channel hydrodynamic stability, control rod withdrawal incident, and to determine the neutronic input parameters for the plant transients and loss of coolant accidents.

Control Rod Drop

The control rod drop accident assumes that a control rod becomes uncoupled from the drive and remains stuck fully inserted in the reactor core as the control rod drive is withdrawn. The uncoupled control rod is then assumed to drop out of core. The control rod drop calculations are performed with COTRAN in two-dimensional (r-z) geometry with fuel temperature

and moderator density reactivity feedbacks. The reactor neutronic parameters which significantly affect the rod drop analysis include the Doppler reactivity coefficient, the maximum control rod worth, the power peaking (peaking with control rod removed from core) and the delayed neutron fraction.

Fuel Misloading

Two separate incidents are analyzed as part of the fuel misloading analysis. The first incident, which is termed the fuel misorientation error, assumes that a fuel assembly is misoriented, by rotation through 90^{o} or 180^{o} from the correct orientation, when loaded into the reactor core. The second incident, the fuel mislocation error, assumes a fuel assembly is placed in the wrong core location during refueling. For both the fuel misorientation error and the fuel mislocation error, the assumption is made that the error is not discovered during the core verification and the reactor is operated during the cycle with a fuel assembly misloaded. The fuel misorientation calculations are performed using the XFYRE, XDT, and XTGBWR codes. The fuel mislocation calculation is performed with the XTGBWR code. The limiting parameter of interest for the fuel misloading error is the MCPR in the misloaded fuel assembly. The fuel misloading analysis determines the difference between the MCPR for the correctly loaded core and the MCPR for the core with a fuel assembly misloaded.

Stability

Stability analysis is concerned with two basic phenomenon, reactor core (reactivity) stablity and channel hydrodynamic stability. Reactor core instability is when the reactivity feedback of the entire core drives the

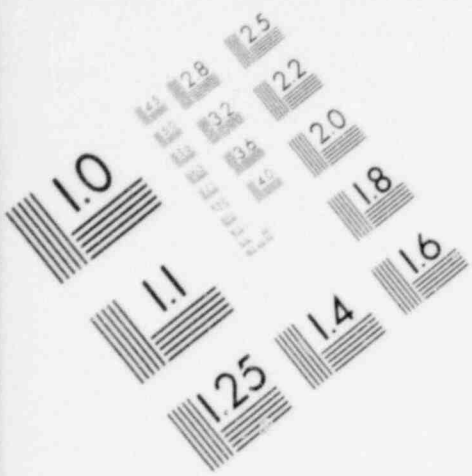

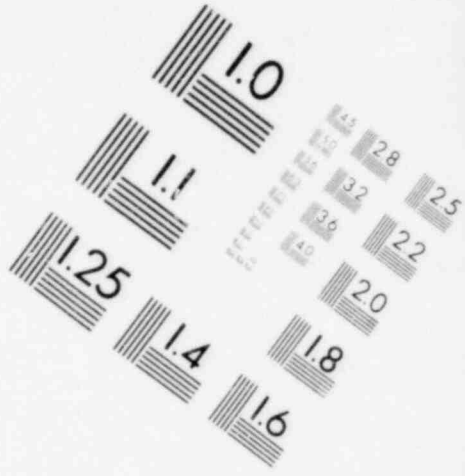

IMAGE EVALUATION
TEST TARGET (MT-3)

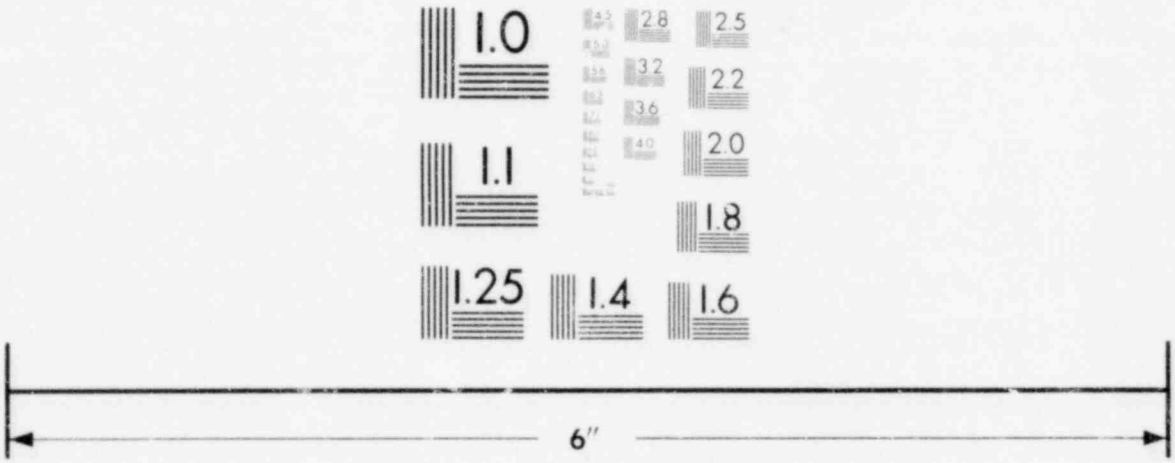

MICROCOPY RESOLUTION TEST CHART

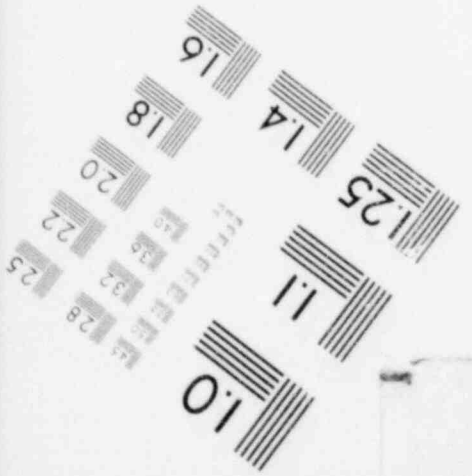

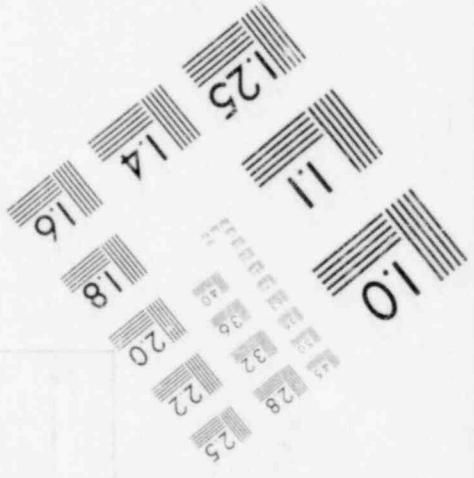

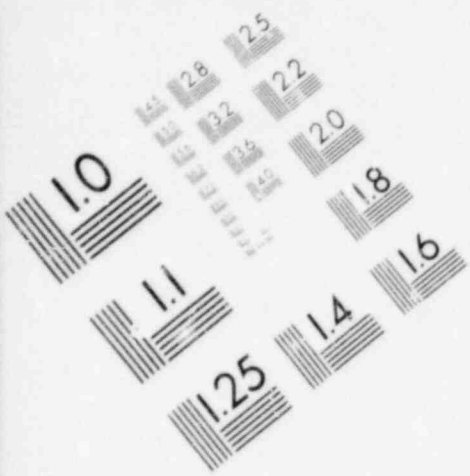

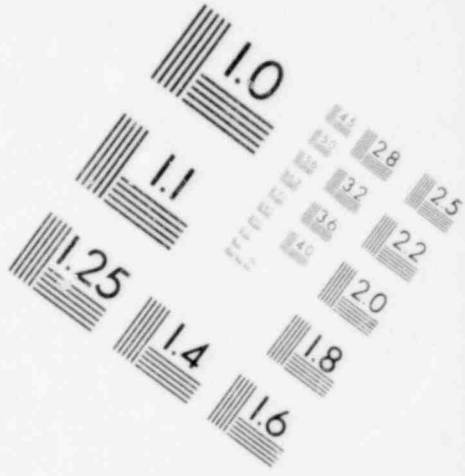

IMAGE EVALUATION
TEST TARGET (MT-3)

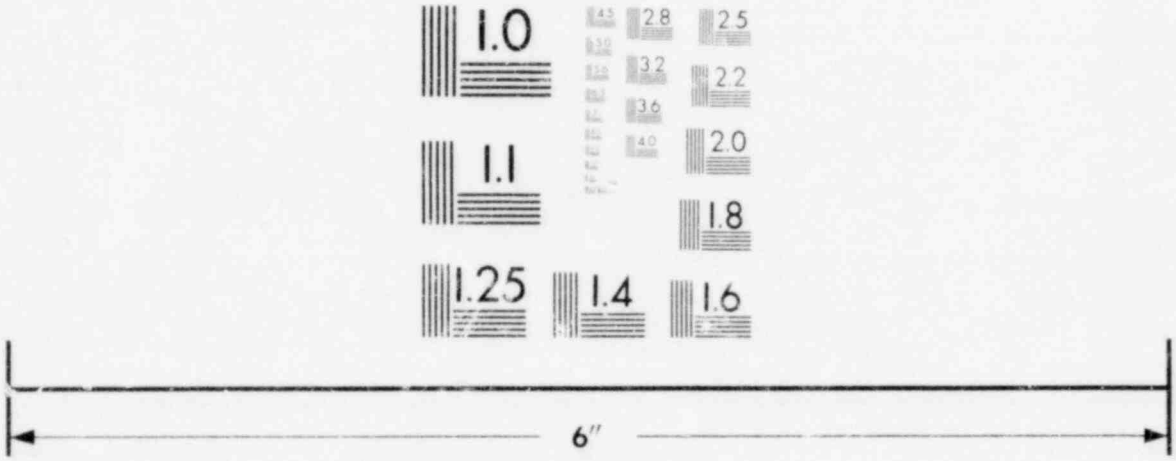

MICROCOPY RESOLUTION TEST CHART

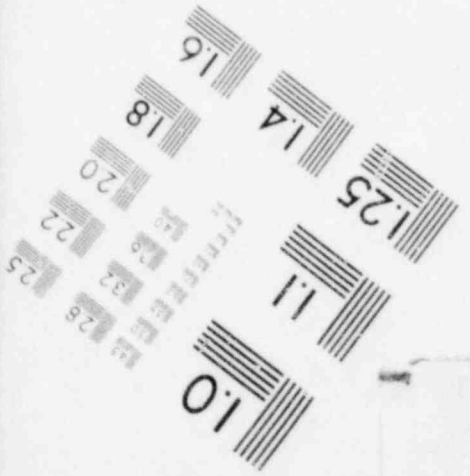

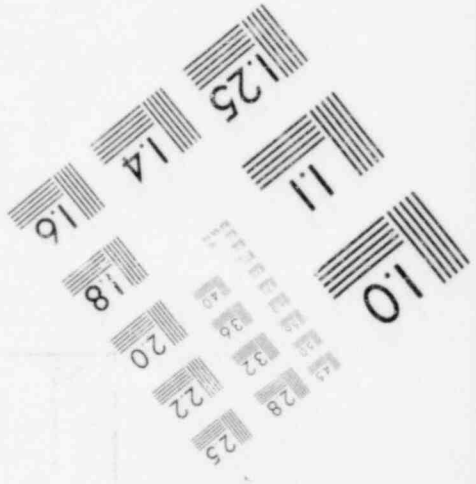

reactor into power oscillations. Channel hydrodynamic instability is flow oscillations which may impede heat transfer to the moderator resulting in localized power oscillations. Stability is analytically demonstrated if no divergent oscillations develop as a result of perturbations of any critical variable such as core pressure, control rod position, and recirculation flow. The stability analysis is performed with the COTRAN computer code.

Neutronic Input to Plant Transient Analysis

The ENC plant transient and loss of coolant accident calculations require the following neutronic parameters as input:

1. Void reactivity coefficient,
2. Doppler reactivity coefficient,
3. Scram reactivity,
4. Delayed neutron fraction, and
5. Prompt neutron lifetime.

The above parameters are calculated with the XFYRE, XTG, and COTRAN codes.

Control Rod Withdrawal

The control rod withdrawal error is the widthdrawal of a control rod by the reactor operator from a fully inserted position until the control rod motion is stopped by the rod block. While the control rod is being withdrawn, the reactor power and the local power in the area of the rod which is being withdrawn will increase. The reactor thermal limit of concern as the power increases is the transient minimum critical power ratio (MCPR) limit which protects against critical heat flux. The control rod withdrawn calculation is performed with the XTGBWR code.

2.7 NEUTRONICS METHODS VERIFICATION

The ENC neutronics methods are principally verified by comparing calculated results to measured reactor data. The XFYRE calculated local power distribution and isotopics are compared to gamma scan measurements and destructive isotopic data. In addition the XFYRE code has been benchmarked against the higher order Monte Carlo code. The XTGBWR reactor simulator code is verified by calculating reactor K_{eff} data, measured TIP traces, and bundle gamma scan data. The kinetics calculations performed by the COTRAN code are compared to the measured Peach Bottom-2 data.

2.8 MEASURED POWER DISTRIBUTION UNCERTAINTY

The determination of the uncertainty associated with a measured power distribution is necessary from a reactor safety viewpoint. The safety analyses are performed to assure safe reactor operation with a certain quantified degree of confidence. The uncertainty associated with the reactor power distribution is defined in terms of the relative standard deviations of the independent variables involved in determining power distribution.

The reactor power distributions are combinations of measured reactor data and computer calculated data. The measured reactor data include the fixed local power range monitor (LPRM) in-core detector data and the traveling in-core probe (TIP) detector data. The computer calculated data include the relative core nodal power distribution, the in-core detector

response distribution, and the local peaking factors for the fuel rods within each bundle. The predicted relative nodal power and detector response distributions are calculated with the XTGBWR reactor simulator code.

The relative standard deviations of the detector measurements, the calculated detector response distribution, the calculated nodal power distribution, and the local pin power distribution are determined by comparison to measured data. The measured data consist of distributions of TIP and fixed in-core detector responses plus gamma scans of bundles and pins.

3.0 NEUTRONICS MODELS FOR BWR REACTOR CORE CALCULATIONS

The ENC code package for performing reactor core neutronics calculations includes a fuel assembly depletion model (XFYRE), a core simulator model (XTGBWR), a reactor kinetics model (COTRAN), a multigroup diffusion theory model (XDT), and a Monte Carlo model (XMC). The XFYRE code calculates the basic fuel assembly neutronic parameters including the local rod power distribution, the local rod exposure distribution, the two and four group cross section sets and the fuel assembly reactivity. The parameters are calculated as a function of temperature, voids, exposure, power, and control.

The XTGBWR reactor simulator code models the reactor core in two dimensional (X-Y) or three dimensional (X-Y-Z) geometry. The reactor calculations can be performed in one-quarter, one-half, or full core geometry. The code calculates the reactor core reactivity, core flow distribution, nodal power distribution, reactor thermal limit values, and incore detector response.

The reactor kinetics calculations are performed with the COTRAN code. The COTRAN code models the time dependent core neutronics and thermal hydraulics in two dimensional (r-z) geometry with void and Doppler feedback. The code calculates the axial and radial temperature distribution for the fuel rods.

The special single fuel assembly and multi-fuel assembly diffusion theory calculations are performed with the XDT code. The XDT code is a two dimensional-multigroup model for reactor analysis. The code calculates the eigenvalue, relative powers, neutron fluxes, and flux and volume weighted neutronic parameters.

The XMC code is a general purpose Monte Carlo code used primarily to benchmark the bundle depletion code XFYRE. XMC utilizes an exact geometrical description and a coupled space-energy solution of the transport problem which makes XMC higher order than the other methods for evaluating key nuclear parameters.

These computer codes are described in Sections 3.1, 3.2, 3.3, 3.4, and 3.5, respectively.

3.1 FUEL ASSEMBLY DEPLETION MODEL (XFYRE)

The nuclear parameters for the BWR fuel assemblies are calculated with the XFYRE computer code. The XFYRE code combines the basic cross section generating codes, diffusion theory, and depletion models to generate fuel neutronic parameters as a function of voids and exposure for both controlled and uncontrolled assemblies.

The XFYRE code is automated to perform all calculations for the BWR fuel designs with a minimum of required input. A typical 8x8 BWR fuel design with two inert water rods and a control rod is shown in Figure 3.1-1. The XFYRE code can be used to analyze fuel rod arrays up to 11x11, with non-symmetrical or symmetrical water gaps and with water or zirconium filled inert rods.

The input to the XFYRE code consists of basic fuel rod and fuel assembly dimensions, fuel rod enrichments and material densities.

The calculations performed by the XFYRE code include generation of cross sections for each fuel assembly region, calculation of neutron flux and power shapes across the fuel assembly, depletion calculations, calculation of flux and volume weighted bundle parameters, and calculation of incore detector parameters. The methods used by the code to calculate each of the above are described in the following sections.

3.1.1 Basic Cross Section Library

The cross sections in the XFYRE code with the exception of the hydrogen scattering kernel are derived from the Battelle Northwest Master Library.[3-1] The ENDF/B[3-2] scattering kernel (Haywood Kernel)[3-3] for hydrogen in water was incorporated into the cross section library for the THERMOS[3-4] program. The hydrogen kernel is generated using the FLANGE II code.[3-5] The scattering kernels for the other nuclides are calculated by a Brown-St. ohn model, using free atom scattering cross sections.

The isotopes normally used in the XFYRE calculations are listed in Table 3.1-1.

3.1.2 Thermal Cross Sections

The thermal cross sections for the fuel rods are calculated with the Exxon revised THERMOS program. The THERMOS code calculates the scalar thermal neutron spectrum as a function of position in a lattice by solving numerically, the integral transport equation. The calculations are performed for 30 energy groups over the energy range $0 \leq E \leq 0.683$ ev.

For a standard fuel rod with no burnable poison, the fuel rod and surrounding water are transformed into a cylindrical pin cell for calculation of the thermal cross section. The cylindrical cell has a fuel region, a clad region, and an outer water region as shown in Figure 3.1-2. The gap between the fuel pellet and the clad is homogenized with the fuel. The outer diameter of the water region in the cylindrical geometry is selected to give the true volume of the unit cell.

For the standard feul rod, the cell is divided into 15 cylindrical rings, with eight equal thickness rings of fuel, two rings of clad and five rings of water moderator. The THERMOS calculation uses the white boundary condition at the edge of the cell with an albedo of 1.0.

For fuel rods containing gadolinia, the cylindrical geometry is expanded to include an extra region of homogenized cells. The extra region is necessary to obtain the correct thermalization spectrum in the fuel rods containing gadolinia. The cylindrical geometry for the gadolinia pin cells is shown in Figure 3.1-3. [ ]

The cylindrical pin cell and extra region are divided into [ ] rings for the THERMOS calculation. Since the thermal flux is strongly depressed in the gadolinia-fuel region, the gadolinium cross sections have a strong spatial dependence resulting in a non-uniform depletion of the gadolinium. [ ]

The reflecting boundary condition is used in the THERMOS calculations for the fuel cells with extra regions.

For both the standard fuel rod and the gadolinia fuel rod, the cross sections are flux and volume weighted over the 30 fine energy groups and the fuel pin cell to obtain a one thermal energy group macroscopic cross section.

3.1.3 Epithermal Cross Sections

The epithermal cross sections for each region in the fuel assembly are calculated in XFYRE with the JRG program. The JRG program combines the HRG[3-6] program and the DASQHE[3-7] Dancoff calculation. The epithermal slowing down spectrum calculation is performed with 68 equal lethargy width five energy groups using the P_1 approximation. The calculation is performed over the energy range 10 MeV to 0.414 ev. The 68 fine group fluxes and currents are calculated by one sweep through the group structure, starting from the U-235 or Pu-239 source distribution. The multigroup model uses a full down-scattering matrix, with inelastic, n-2n, and P_0 and P_1 components of elastic scattering explicitly included.

For each fuel rod type in the BWR fuel assembly, the isotopic concentrations are homogenized over the unit cell consisting of the fuel, clad and water associated with each fuel rod. The macroscopic fine group parameters are constructed from the homogenized isotopic concentrations and the microscopic parameters on the HRG data tape.

A special calculation is made in the resonance range for U-235, U-238, Pu-239, Pu-240, and Pu-241 nuclides, using an adaptation of the

Alder, Hinman, and Nordheim[3-8] method to an intermediate resonance approximatation for both the absorber nuclide and an admixed moderator. The Dancoff correction factors that account for the effect of the adjacent fuel rods on the resonance absorption are calculated with the DASQHE program for a square lattice. The resonance contribution for each isotope is allocated to the fine groups in a consistent manner providing self-shielding in both space and energy.

3.1.4 Control Rod Cross Sections

Control rod cross sections are calculated for each fuel type as a function of exposure and void. The control rod cross sections are calculated after the THERMOS and JRG calculations are carried out for each fuel rod type in the fuel assembly. The calculation model includes the fuel assembly and the detailed control rod blade configuration including dimensions and number of poison pins per wing.

The blade is constituted of stainless steel for the support, stiffener (if present) and sheath, B_4C powder in stainless steel clad absorber pins, and the space between the absorber pins and the sheath can be either voided or unvoided water.

In the thermal energy range, a special one-dimensional slab geometry integral transport theory calculation is performed. The control rod blade and fuel assembly are converted into a one-dimensional slab preserving the relative areas of each component. The actual control rod geometry and the geometry for the THERMOS calculation of the control rod blade is shown in Figure 3.1-4.

[ ]

The thermal macroscopic cross sections of the control rod blade are obtained from the THERMOS calculations by editing over the blade region of the fuel assembly. The stainless steel microscopic cross sections for the control rod support are obtained from the blade sheath region.

The concentrations of the fuel isctopes, the clad, and the water in the pin cells are flux and volume weighted to obtain the homogenized concentrations for the fuel regions. The thermal flux for the flux weighting is obtained from the THERMOS pin cell calculations. [ ]

In the epithermal energy range, the control rod cross sections are obtained from a special HRG calculation. The calculation is performed by homogenizing all regions of the fuel assemlby including the control rod to obtain bundle average number densities. The HRG calculation is then performed for the fuel bundle to obtain the slowing down spectrum and the multigroup microscopic cross sections for each nuclide in the fuel assembly.

The epithermal macroscopic cross sections of the control blade are calculated from the boron, carbon, stainless steel, and water isotopic concentrations in the blade and the respective microscopic cross sections.

3.1.5 Neutron Flux and Power Calculation

Controlled and uncontrolled local pin powers, neutron flux, and bundle reactivity are calculated within XFYRE utilizing a four group diffusion theory calculation in two dimensional geometry. This portion of

the program is a modified version of the XDT code described in Section 3.4. These calculations are performed after the detailed energy and spatial calculations have been carried out for each fuel pin type in the assembly.

For the diffusion theory calculations the fuel assembly is transformed into an X-Y geometry as shown in Figure 3.1-5. [ ] The arrangement of pin cells is symmetric about the assembly diagonal which bisects the control blade slot. Additional regions representing the film water-channel mixture, gap water, incore detectors, inert rods, control blade, and control support complete the geometrical description of the fuel assembly. [

]

The broad group cross section parameters for the diffusion theory calculations are averaged over the following four broad energy groups:

Broad Energy Groups	Energy Range
1	11.7 kev - 10 Mev
2	2.38 ev - 11.7 kev
3	0.683 ev - 2.38 ev
4	0 ev - .683 ev

The four energy group diffusion equations can be written as:

$$D_g \nabla^2 \phi_g - \Sigma_g^r \phi_g + S_g = 0, \; g = 1, \ldots 4 \qquad (3.1\text{-}1)$$

where

$$S_g = \frac{\chi_g}{K_{eff}} \sum_{g'=1}^{4} (\nu\Sigma_f)_{g'} \phi_{g'} + \sum_{g'=1}^{g-1} \Sigma(g' \to g) \phi_{g'}, \qquad (3.1\text{-}2)$$

and

g = the energy group

χ_g = the fraction of neutrons generated in energy group g

For mesh points which are situated in the center of the mesh interval as shown in the mesh description below

integration over the volume associated with each mesh point yields the difference equations in the following form:

$$\sum_{k=1}^{4} \frac{\bar{D}_k A_k}{\ell_k} (\phi_k - \phi_o) - \Sigma_o^r \phi_o V_o + S_o V_o = 0, \qquad (3.1\text{-}3)$$

where, for simplicity, the group indices have been omitted, and:

Σ_o^r = removal cross section associated with mesh point o,

S_o = source rate associated with mesh point o,

V_o = volume associated with mesh point o,

ϕ_k = flux associated with mesh point k,

ℓ_k = distance between mesh point k and mesh point o,

A_k = area of boundary between mesh point k and mesh point o,

$\bar{D}_k$ = effective diffusion constant between mesh point k and mesh point o.

$$\bar{D}_k = \frac{D_o D_k (\delta R_o + \delta R_k)}{D_o \delta R_K + D_k \delta R_o} \qquad (3.1\text{-}4)$$

An iterative process is used to solve the difference equation (3.1-3). In XFYRE a successive line over-relaxation algorithm is used to accelerate convergence in the iteration that produces the group fluxes. After the spatial four energy group neutron fluxes are calculated, the power in each fuel pin is calculated from the fission rate and normalized to the average pin power.

The XTGBWR core simulator code requires as input the nodal average two energy group macroscopic cross sections for each fuel type in the reactor. These node average macroscopic cross section parameters are obtained by collapsing the four group cross sections in XFYRE to two energy groups.

3.1.6 Depletion Calculation

The burnup calculation is performed over exposure intervals which are specified by input. A typical set of exposure intervals for a BWR assembly containing gadolinia as a burnable poison is given in Table 3.1-2. The depletion is performed separately for each pin cell in the fuel assembly,

assuming diagonal symmetry of the cells in the assembly. The isotopes which are burned are listed in Table 3.1-3. The four isotopes FPA, FPB, FPC, and FPD are lumped pseudo-isotopes for U-235 in the Nephew[3-9] fission product model. In all fuel pins the non-gadolinia isotopes are burned using an average isotopic concentration for the fuel area. [ ]

The isotopic transmutation calculations performed in the XFYRE program follow the process depicted in Figure 3.1-6. The set of differential equations that govern the transmutation of the subchain, i.e. U-238, Pu-239, Pu-240, Pu-241, Pu-242, can be written as follows using standard notation:

$$\frac{dN^8}{dt} = - \langle \sigma_a^8 \rangle \cdot \langle \phi \rangle \cdot N^8 \qquad (3.1\text{-}5)$$

$$\frac{dN^9}{dt} = - \langle \sigma_a^9 \rangle \cdot \langle \phi \rangle \cdot N^9 - \lambda^9 \cdot N^9 + \langle \sigma_c^8 \rangle \cdot \langle \phi \rangle \cdot N^8 \qquad (3.1\text{-}6)$$

$$\frac{dN^0}{dt} = - \langle \sigma_a^0 \rangle \cdot \langle \phi \rangle \cdot N^0 - \lambda^0 \cdot N^0 + \langle \sigma_c^9 \rangle \cdot \langle \phi \rangle \cdot N^9 \qquad (3.1\text{-}7)$$

$$\frac{dN^1}{dt} = - \langle \sigma_a^1 \rangle \cdot \langle \phi \rangle \cdot N^1 - \lambda^1 \cdot N^1 + \langle \sigma_c^0 \rangle \cdot \langle \phi \rangle \cdot N^0 \qquad (3.1\text{-}8)$$

$$\frac{dN^2}{dt} = - \langle \sigma_a^2 \rangle \cdot \langle \phi \rangle \cdot N^2 + \langle \sigma_c^1 \rangle \cdot \langle \phi \rangle \cdot N^1. \qquad (3.1\text{-}9)$$

The depletion calculations are performed with a one group flux which is obtained by collapsing the four group fluxes from the diffusion theory calculation. The XFYRE code takes advantage of the fact that for constant fluxes and cross sections, the solution to the depletion equations can be expressed analytically.

The assumption of constant fluxes and cross sections is a reasonable assumption if the exposure steps are small. [ ]

When the cross sections are regenerated, the average concentration of each isotope for a fuel type is calculated, and then the THERMOS-JRG fine group calculations are performed to obtain new microscopic cross sections for each isotope. The number of fuel types in the fuel assembly is specified as input. Usually all fuel rods with the same uranium enrichment, gadolinia concentration, dimensions, and fuel density are considered as one rod type in the calculation.

[ ] A typical plot of the gadolinium-157 thermal absorption cross section for each region as a function of exposure is shown in Figure 3.1-7. A typical plot of the gadolium-157 concentration as a function of exposure is shown in Figure 3.1-8.

Since the gadolinium concentrations and cross sections are changing more rapidly than the other isotopes, over each burnup subinterval the gadolinium cross sections [ ]

3.1.7 Xenon and Samarium

For depletion calculations the XFYRE code includes time and power dependent xenon and samarium. The time is calculated by the code from the power, exposure, and fuel weight. At zero exposure there is no xenon or samarium in the calculations.

For restart calculations the code can calculate time dependent xenon and samarium based on the isotopic concentrations from the restart

tape and an input shutdown time. The code has the options of calculating (1) no xenon and no samarium, or (2) no xenon and the samrium from the restart tape in addition to the time dependent option.

3.1.8 Restart Calculations

During an XFYRE depletion calculation, a restart tape can be written that saves sufficient information to perform additional calculations without repeating the burnup calculation. Such additional calculations can include solutions at different temperatures, void conditions, or control conditions.

When a restart and burn calculation is performed where a parameter is changed or when the gadolinia is not depleted, a small burn step of 250 MWD/MT with cross section regeneration is desirable prior to resuming calculations with larger burn steps. The small step is necessary for the accurate extrapolation of cross section during a larger burn interval.

3.1.9 Incore Detector Parameters

The XFYRE code uses a dilute macroscopic thermal fission cross section at the location of the incore detector to calculate the T factor. The T factor is defined as follows:

[ ]

If desired, the homogenized four energy group macroscopic cross sections of the incore detector can be input. The code then uses the input cross sections in the diffusion theory calculations and in calculating

Table 3.1-1 Isotopes Normally Used in XFYRE

Isotopes	Isotopes
C12	Am241
O16	Am243
H2O W/UPSCAT	Cm242
ZIRCONIUM	Cm243
304SS	Cm244
BORON	PFP4-235
U238	PFP1-235
Pu240	PFP2-235
Pu242	PFP3-235
U235	Sm151
Pu239	Gd154
Pu241	Gd155
Xe135	Gd156
Sm149	Gd157
U236	Gd158
Np237	Pu238

Table 3.1-2 Typical Exposures (MWD/MTU) for XFYRE Depletion Calculations

[ ]

Table 3.1-3 Burnable Isotopes in XFYRE

U-235	Pu-238	Am-241	Xe-135	Gd-154*
U-236	Pu-239	Am-243	Sm-149	Gd-155
U-238	Pu-240	Cm-242	Sm-151	Gd-156
Np-237	Pu-241	Cm-243	PFP4-235	Gd-157
	Pu-242	Cm-244	PFP1-235	Gd-158
			PFP2-235	
			PFP3-235	

* The gadolinia isotopes are burned only in Gd-poisoned pins.

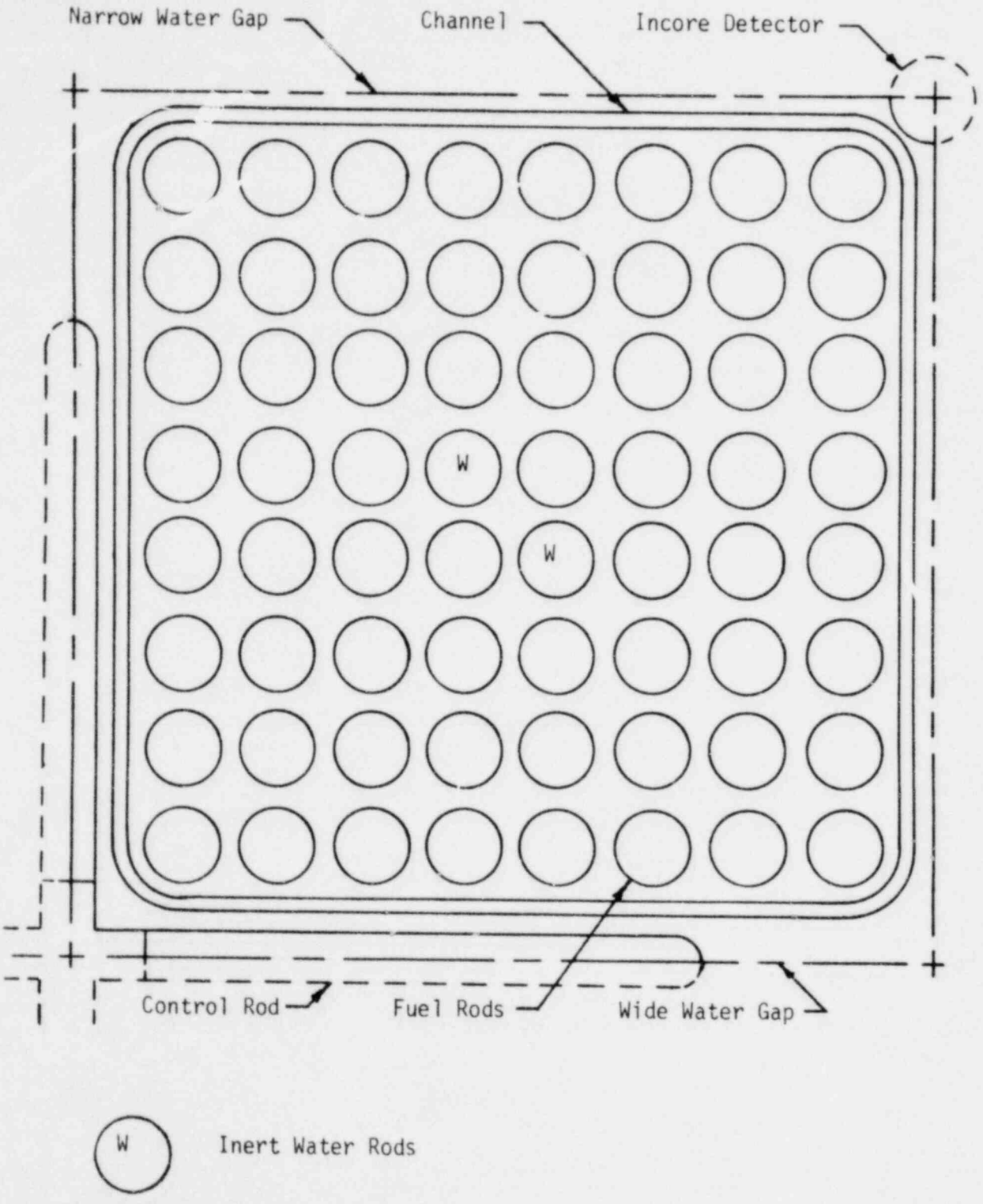

Figure 3.1-1 Typical 8x8 BWR Fuel Assembly with a Wide and Narrow Water Gap

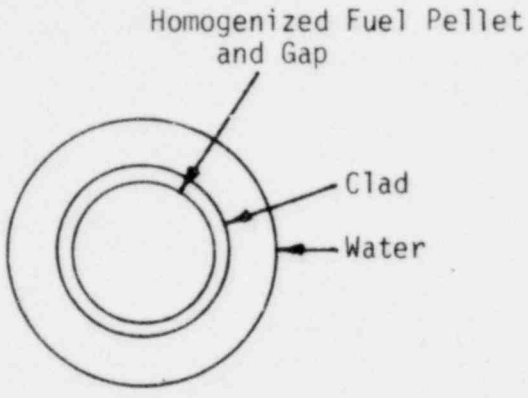

Figure 3.1-2 Cylindrical Geometry for THERMOS Calculation of Non-Gadolinia Fuel Rod

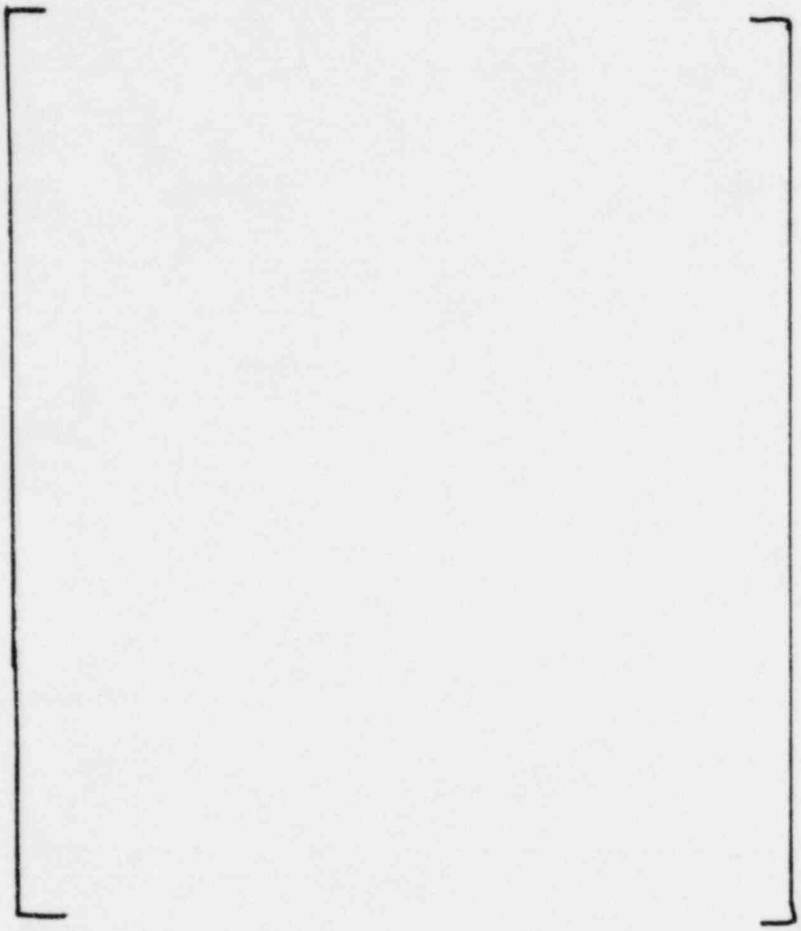

Figure 3.1-3 Cylindrical Geometry for THERMOS Calculation of Fuel Rod Containing Gadolinia

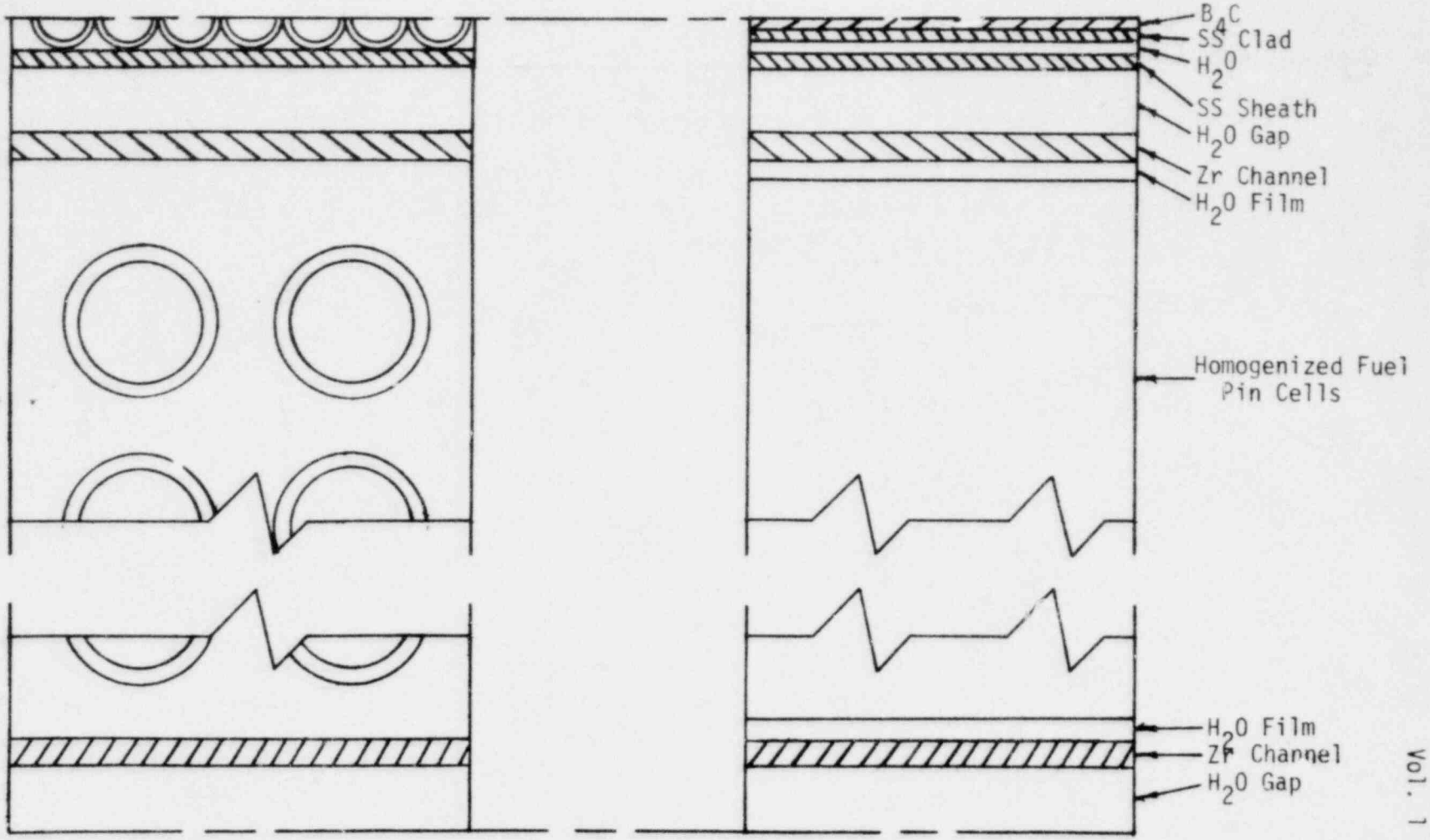

Figure 3.1-4 Actual Geometry and Slab Geometry for THERMOS Control Rod Cross Section Calculation

Figure 3.1-5 XFYRE Mesh Boundaries for an 8x8 BWR Fuel Assembly with a Wide and Narrow Water Gap

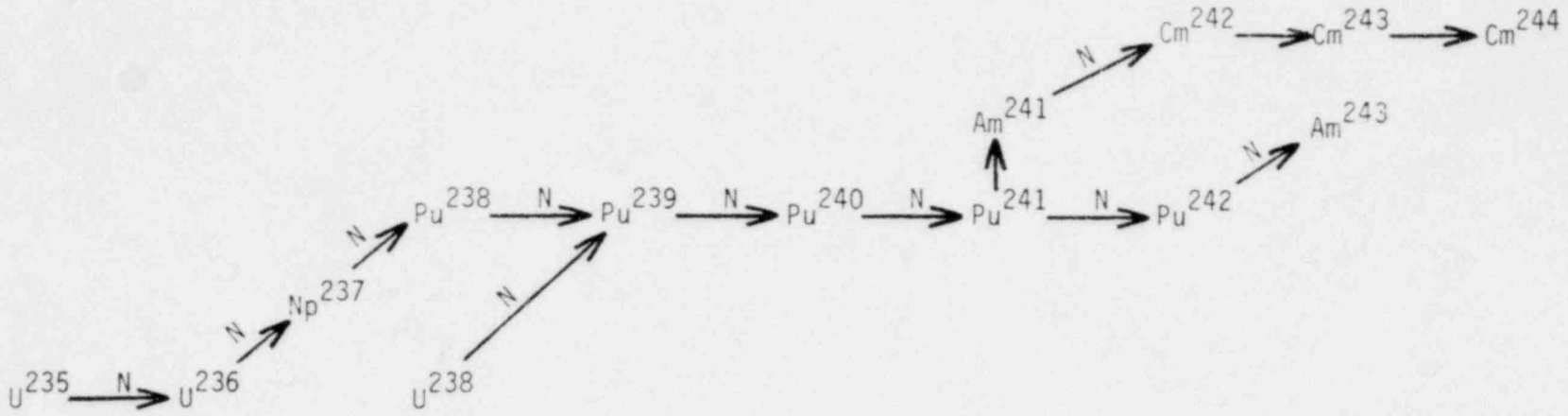

Figure 3.1-6 XFYRE Isotopic Chain

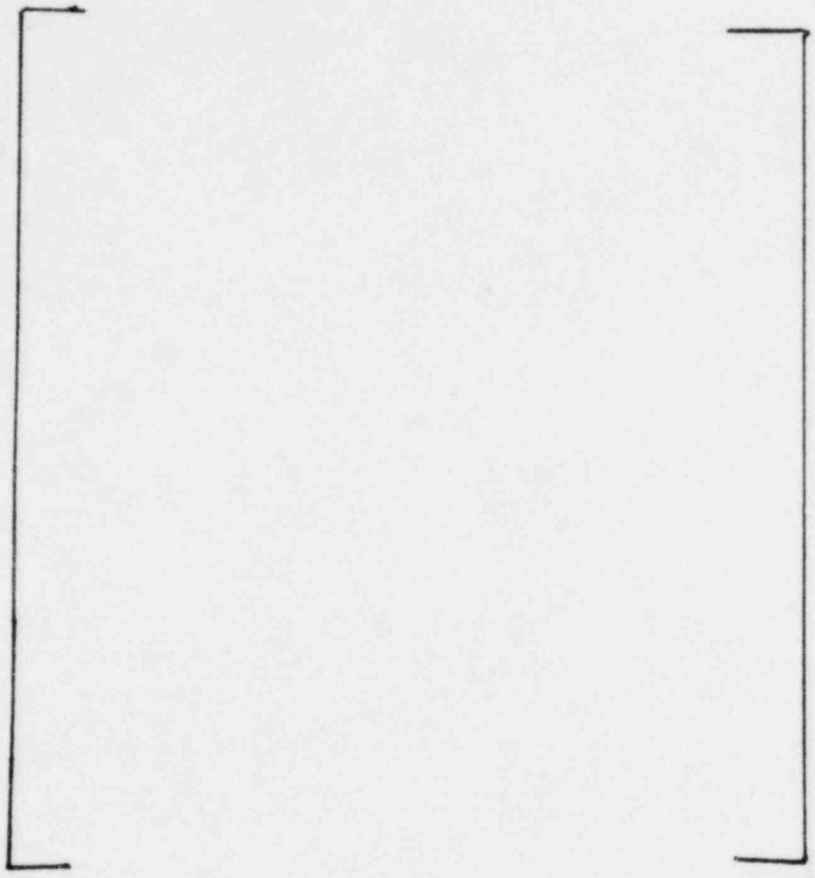

Figure 3.1-7 Relative Thermal Absorption Cross Section of Gadolinium-157 as a Function of Fuel Assembly Exposure

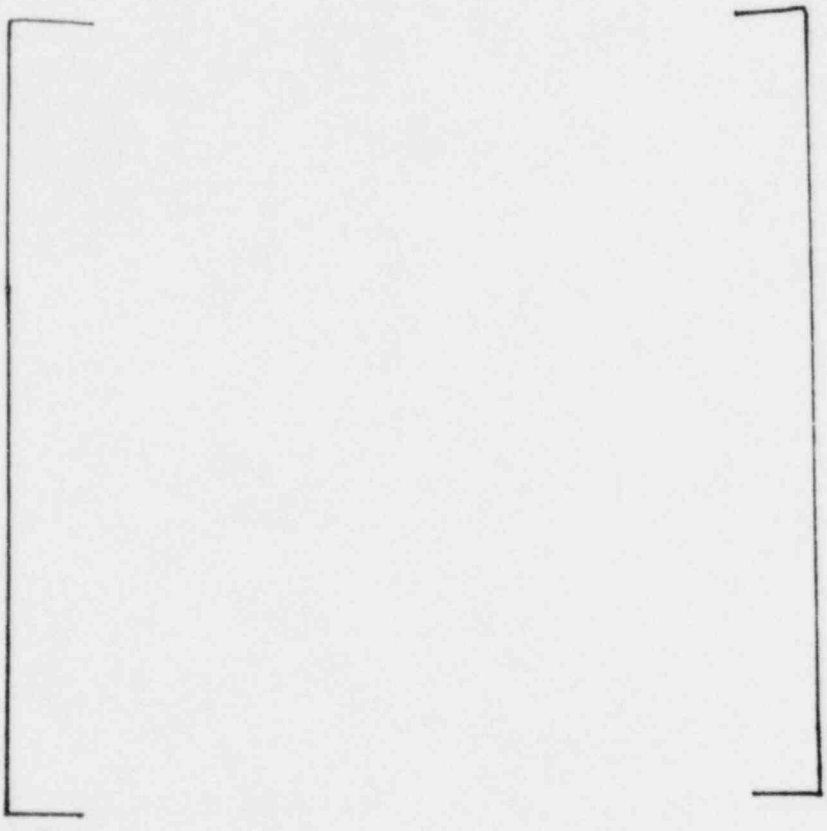

Figure 3.1-8 Relative Gadolinium-157 Number Density by Subregion as a Function of Fuel Assembly Exposure

the T factor. The incore detector region for the diffusion theory calculation is defined by the width of the water gaps on the side of the bundle of the control rods. The incore detector location is shown in Figure 3.1-1. The incore detector region in X-Y geometry for the diffusion calculation is shown in the upper right hand corner of Figure 3.1-5.

3.2 CORE SIMULATOR MODEL (XTGBWR)

The Exxon Nuclear core simulator program for the analysis of BWR reactor cores is the XTGBWR code. The XTGBWR code uses the same modified two group diffusion theory as the Exxon Nuclear reactor simulator code for pressurized water reactors (XTGPWR).[3-10] The XTGBWR program uses coarse mesh diffusion theory to solve for the fast flux assuming the only source of thermal neutrons is slowing down from the fast group and no thermal leakage occurs within each node. Corrections to this assumption are made to account for thermal flux gradients at controlled nodes and on the core edge. Inner iterations are performed on the fast group flux, but the thermal flux is updated only after each outer iteration. After a specified number of outer iterations, the cross sections are updated to reflect power dependence on xenon, Doppler and thermal-hydraulic feedback. This method of solution results in rapid convergence.

For fuel management calculations, the XTGBWR code has the following capabilities:

1. Core calculations in 1/4, 1/2 and full core geometry with several boundary conditions.
2. Control rod dependent parameters.

3. Thermal hydraulic model including void feedback, subcooled boiling, and pressure drop flow calculation.
4. Equilibrium and time dependent xenon and samarium.
5. Power dependent Doppler broadening.
6. Void history correction to cross sections.
7. Calculation of core K-effective and nodal power distribution.
8. Calculation of critical power ratio (CPR), linear heat generation rate (LHGR), and average planar linear heat generation rate (APLHGR) at each node.
9. Core exposure calculated from inputs of burnup (MWD/MT), energy (GWD), or time (hours).
10. Full edit capability in either two or three dimensions for all arrays.
11. Prediction of the traveling incore probe (TIP) measurements.
12. Tape or file outputs for restart capability.
13. Haling calculations in two or three dimensions.
14. Fuel shuffling option.
15. Zero power critical option.

3.2.1 Core Geometry

X-Y-Z geometry is used in the three dimensional model of XTGBWR. When two dimensional geometry is used the axial nodes are averaged into one plane in the Z direction. A typical X-Y geometry full core configuration is shown in Figure 3.2-1. The code requires the node in the

radial direction (X-Y) to be the same size for all fuel assemblies. All nodes in the axial direction must also be the same size but may be a different size than in the radial direction. [ ] In addition to the full core geometry, the code can be used for quarter core and half core geometry with reflective, repetitive, or 90^{o} rotational boundaries. The boundary conditions for quarter core symmetry are shown in Figure 3.2-2.

For the analysis of cores with axially distributed gadolinia or enrichment, each fuel type may be made up of two or more material types. XTGBWR is capable of handling a different fuel type for each axial plane of the reactor for each bundle location.

For core analysis in two dimensions, the core is modeled in X-Y geometry and the neutron leakage in the axial direction is calculated using either an input axial buckling or the internally calculated geometric axial buckling. The reactivity effects of the axial buckling are treated through adjustment of the absorption cross sections.

3.2.2 Diffusion Theory Model

The XTGBWR program uses a modified coarse mesh two energy group diffusion theory model for steady state analysis of the reactor core. The model is designed to accept void and exposure dependent two group cross sections. The cross sections can be specified on a nodal basis allowing axial and radial effects to be modeled. The conditions under which the cross sections were generated are input, and the XTGBWR code utilizes this information to adjust the cross sections to fit the actual reactor conditions

in each node. This includes adjustment for control rods, instantaneous void, void history, power dependent Doppler, and time and power dependent xenon and samarium.

[ ]

Using standard notation, the basic diffusion theory equation is

$$-D_g \nabla^2 \phi_g + \Sigma_g^R \phi_g = \frac{\chi_g}{k_{eff}} \sum_{g'=1}^{G} (\nu\Sigma_f)_{g'} \phi_{g'} + \sum_{g'=1}^{g-1} \Sigma_{s1}(g' \to g) \phi_{g'} \qquad (3.2\text{-}1)$$

Assuming all neutrons are born in the fast group, the two group diffusion equations are

$$-D_1 \nabla^2 \phi_1 + \Sigma_{R_1} \phi_1 = \frac{1}{k_{eff}} (\nu_1 \Sigma_{f_1} \phi_1 + \nu_2 \Sigma_{f_2} \phi_2) \qquad (3.2\text{-}2)$$

$$-D_2 \nabla^2 \phi_2 + \Sigma_{a_2} \phi_2 = \Sigma_{s1} (1 \to 2) \phi_1 \qquad (3.2\text{-}3)$$

These equations are integrated over the volume of a three-dimensional node. To evaluate the leakage term, the volume integral over the Laplacian is changed to a surface integral using Green's theorem

$$\int D \nabla^2 \phi dV = \int D \vec{\nabla} \phi \cdot d\vec{A} \qquad (3.2\text{-}4)$$

Using mesh points at the node centers, the volume integration of equation (3.2-2) yields

$$\sum_{k=1}^{6} \frac{\bar{D}_k A_k}{dk} (\phi_k - \phi_0) - \Sigma_{R_0} \bar{\phi}_0 V_0 = -S_0 V_0 \bar{\phi}_0 \qquad (3.2.5)$$

where 0 refers to the node being calculated and k to the six nearest neighbors shown in Figure 3.2-3. For convevience, the subscript 1 referring to the gast group has been omitted. The notation is as follows:

Σ_{R_0} = removal cross section = $\Sigma_{s1}(1\to2) + \Sigma_{a_1}$

$S_o = \frac{1}{k_{eff}} (\nu\Sigma_{f_1} + \nu\Sigma_{f_2}\bar{\phi}_2/\bar{\phi}_1)$

V_o = volume of node

d_k = distance between mesh point k and mesh point 0

A_k = area o oundary mesh point k and mesh point 0

$\bar{D}_k$ = effective ffusion coefficient between mesh point k and mesh point 0

$$\bar{D}_k = \frac{D_0 D_k(\delta R_0 + \delta R_k)}{D_0\delta R_k + D_k\delta R_0} \qquad (3.2\text{-}6)$$

$\delta R_0, \delta Rk$ = node size in direction of calculation

If h_x, is the mesh spacing in both the X and Y directions and h_z is the mesh spacing in the z direction, the

$$\frac{A_k}{d_k} = h_z \text{ in x,y direction} \qquad (3.2\text{-}7)$$

$$\frac{A_k}{d_k} = \frac{h_x^2}{h_z} \text{ in z direction} \qquad (3.2\text{-}8)$$

$$\bar{D}_k = \frac{2D_0D_k}{D_0 + D_k} \tag{3.2-9}$$

$$V_0 = h_x^2 h_z \tag{3.2-10}$$

Equation (3.2-5) becomes

$$\sum_k \frac{2D_kD_0R_k}{D_k + D_0} (\phi_k - \phi_0) = -S_0 h_x^2 \bar{\phi}_0 + \Sigma_{R_0} h_x^2 \bar{\phi}_0 \tag{3.2-11}$$

where

$$R_k = 1 \text{ if k in x,y direction} \tag{3.2-12}$$

$$= \frac{h_x^2}{h_z^2} \text{ if k in z direction}$$

with minimal error, $\bar{D}_k$ can be approximated by

$$\frac{2D_kD_0}{D_k + D_0} = \sqrt{D_k}\sqrt{D_0} \tag{3.2-13}$$

with the additional definitions

$$\psi_j = \phi_j \sqrt{D_j} \qquad j=0,k \tag{3.2-14}$$

$$\bar{\psi}_0 = \bar{\phi}_0 \sqrt{D_0} \tag{3.2-15}$$

$$P_0 = \sum_k R_k \sqrt{D_k} / \sqrt{D_0} + \Sigma_{R_0} h_x^2/D_0 \tag{3.2-16}$$

and with some algebraic manipulation, Equation (3.2-11) can be written as

$$P_0\psi_0 + \sum_k R_k\psi_k = \frac{S_0}{D_0} h_x^2\bar{\psi}_0 - \frac{\Sigma R_0}{D_0} h_x 2(\bar{\psi}_0 - \psi_0) \tag{3.2-17}$$

$\bar{\phi}_0$ is a weighted average flux for node 0 calculated from the mid-point fluxes of node 0 plus the six surrounding k nodes. Specifically $\bar{\phi}_0$ is calculated from

$$\bar{\phi}_0 = b\phi_0 + 2c \sum_k R_k \phi_k^0 \qquad (3.2\text{-}18)$$

where

$$b = \frac{3 * AFA}{3 * AFA + (1 - AFA)(R + 2)} \qquad (3.2\text{-}19)$$

$$c = \frac{1 - AFA}{4 * (3 * AFA + (1 - AFA)(R + 2))} \qquad (3.2\text{-}20)$$

ϕ_k^0 = the flux on the interface between node 0 and node k and is derived using continuity of current

$$\phi_k^0 = \frac{\psi_0}{2\sqrt{D_k}} + \frac{\psi_k}{2\sqrt{D_0}} \qquad (3.2\text{-}21)$$

AFA = the weighting factor for the mid-point fast flux.

Using equations (3.2-18) and (3.2-21)

$$\bar{\psi}_0 = (b + c * r_0)\psi_0 + c \sum_k R_k \psi_k \qquad (3.2\text{-}22)$$

where

$$r_0 = \sqrt{D_0} \sum_k R_k / \sqrt{D_k} \qquad (3.2\text{-}23)$$

The numerical solution is obtained by rewriting equation (3.2-17)

$$\psi_0 = \left(\sum_k R_k \psi_k + \frac{\bar{S}_0}{D_0} h_{x^2} \bar{\psi}_0 \right) / P_0 \qquad (3.2\text{-}24)$$

where

$\bar{\psi}_0$ = average nodal ψ from previous iteration (3.2-25)

$$\bar{S}_0 = \frac{1}{k_{eff}} (\nu\Sigma_{f_1} + \nu\Sigma_{f_2} \bar{\phi}_2/\bar{\phi}_1) - \Sigma_{a_1} - \Sigma_{s1}(1\to2) \quad (3.2\text{-}26)$$

Equation (3.2-24) is used to iterate on the fast flux solution.

The thermal flux is calculated by assuming no thermal leakage among nodes. Equation (3.2-3) reduces to

$$\bar{\phi}_2 = \bar{\phi}_1 \cdot \frac{\Sigma_{s1}(1\to2)}{\Sigma_{a2}} \quad (3.2\text{-}27)$$

where $\bar{\phi}_1$ is calculated from Equation (3.2-18). $\bar{\phi}_2$ may then be calculated using the form of Equation (3.2-18) except that all parameters refer to the thermal group. An empirical correction factor is applied to the model for controlled nodes and is used to improve the prediction of the nodal powers.
[ ]

A new eigenvalue (k_{eff}) is calculated after each outer iteration. This eigenvalue and updated values of $\bar{\phi}_1$ and $\bar{\phi}_2$ are used to compute a source term and the inner iterations are repeated. After each ten or fewer outer iterations, the cross sections are updated to account for the power distribution effects of thermal hydraulic feedback, Doppler broadening and xenon. These changes to the cross sections are described under the respective headings in the following sections of this report. This procedure of inner and outer iterations and cross section updating continues until

convergence or the specified maximum iterations are reached, whichever is sooner. The power distribution in each node is calculated by:

$$P = (\kappa\Sigma_{f_1}\bar{\phi}_1 + \kappa\Sigma_{f_2}\bar{\phi}_2) \qquad (3.2\text{-}29)$$

3.2.3 Boundary Conditions

3.2.3.1 Outer Boundary

The outer boundary conditions determine the leakage from the core. XTGBWR utilizes an extrapolation distance at which the fast flux goes to zero to determine the flux profile and the leakage of fast neutrons from the nodes on the core-reflector interface. The extrapolation distance is calculated separately for each boundary node and is based on input "reflector" cross section data which represents the neutron diffusion (material) properties of reflector nodes found at the top, bottom, and periphery of the core boundary. [ ]

3.2.3.2 Reflected Boundary

The zero current boundary condition is achieved by simply setting $\phi_k = \phi_o$ in Equation (3.2-5) for a reflected node.

3.2.3.3 Periodic and Other Boundary Conditions

Periodic and other boundary conditions are achieved by setting the flux node value for node k in Equation (3.2-5) to the correct value when a node is a boundary node.

3.2.4 Exposure and Void Dependent Cross Sections

The XTGBWR code requires two group cross section sets as a function of exposure and voids to describe each material type. Cross sections

are input for zero void, near core average void, and near maximum void for each fuel type. A typical hot operating cross section set is input at voids of [ ] for each of the following exposures (GWD/MT): [ ] The cross sections are obtained for the actual void and exposure conditions of a node by linearly interpolating between or beyond the input values.

The base cross sections are calculated by burning the fuel at a given void fraction from zero exposure to the maximum exposure that any node of this fuel type is expected to achieve throughout the life of the fuel. At each calculational exposure increment the instantaneous void and the average void history is the same. The void history is defined by the following [

]

3.2.5 Control Rod Effects

[ ]

If a core model is set up such that a fuel node is partially controlled, the fully controlled cross sections are homogenized with the uncontrolled cross sections using the fraction of node height controlled as a mixing factor.

3.2.6 Equilibrium and Time Dependent Xenon

Xenon is calculated within XTGBWR by equations which are solutions to the differential equations for iodine and xenon. This allows the calculation of both time and equilibrium power dependent xenon. The

exposure and void dependent cross section data from the XFYRE code at exposures greater than zero include constant power equilibrium xenon absorption cross sections. The XTGBWR code calculates a base macroscopic xenon free absorption cross section from the input data by subtracting the constant power xenon absorption cross section. The xenon concentration used to calculate the magnitude of the xenon absorption cross section that is subtracted is obtained from the input constant power cross section parameters and the power that was assumed for the XFYRE calculations. The time and power dependent xenon concentration for the actual reactor operating conditions is calculated for each node. The xenon adjustment to the base macroscopic absorption cross section is calculated by multiplying the xenon concentration by a xenon microscopic absorption cross section which has been adjusted for actual void and void history effects via Equation 3.2-38. This delta cross section is then added to the macroscopic base thermal absorption cross section.

The differential equations which are used for the formation and decay of the iodine and xenon isotope are:

$$\frac{dI}{dt} = -\lambda_I I + \gamma_I \phi \Sigma_f \qquad (3.2\text{-}39)$$

$$\frac{dX}{dt} = -\lambda_X X - AX + \gamma_X \phi \Sigma_f + \lambda_I I \qquad (3.2\text{-}40)$$

The solution of the differential equations gives the following equations for the time dependent iodine I(t) and xenon X(t)

$$I(t) = I_0 \exp(-\lambda_I \Delta T) + \frac{\gamma_I}{\lambda_I}\left[1 - \exp(-\lambda T)\right] \phi \Sigma_f \qquad (3.2\text{-}41)$$

$$X(t) = \frac{(\gamma_I + \gamma_X)\,\phi\,\Sigma_f}{\lambda_X + A} + \left[X_0 - \frac{(\gamma_I + \gamma_X)\,\phi\,\Sigma_f}{\lambda_X + A} \right. \qquad (3.2\text{-}42)$$

$$\left. - \frac{\gamma_I I_0 - \gamma_I\,\phi\,\Sigma_f}{\lambda_X + A - \lambda_I} \right] * \exp(-(\lambda_X + A)\,\Delta T)$$

$$+ \frac{\lambda_I I_0 - \gamma_I\,\phi\,\Sigma_f}{\lambda_X + A - \lambda_I} * \exp(-\lambda_I \Delta T)$$

where

$\phi \Sigma_f = \phi_1 \Sigma_{f_1} + \phi_2 \Sigma_{f_2}$

Σ_{f_1} = fast macroscopic fission cross section

Σ_{f_2} = thermal macroscopic fission cross section

$A = \sigma^X_{a_1} \phi_1 + \sigma^X_{a_2} \phi_2$

$\sigma^X_{a_1}$ = fast microscopic cross section for xenon

$\sigma^X_{a_2}$ = thermal microscopic cross section for xenon

ϕ_1 = fast flux

ϕ_2 = thermal flux

λ_I = decay constant for iodine

λ_X = decay constant for xenon

γ_I = fission yield of iodine

γ_X = fission yield of xenon

ΔT = time since last time step

I_0 = iodine number density at the last time step

X_0 = xenon number density at the last time step

For equilibrium power conditions, the exponential terms in the above equation are zero and the xenon concentration (X) is given by the following formula:

$$X = \frac{(\gamma_I + \gamma_X)\ \phi\ \Sigma_f}{\lambda_X + A} \qquad (3.2\text{-}43)$$

where the terms in the equation are given above.

The thermal absorption cross section for each node of fuel is then adjusted to account for xenon thermal absorption by

$$\Sigma_{a_2} = \Sigma_{a_2}\ (\text{base}) + X(t) * \sigma^X_{a_2} \qquad (3.2\text{-}44)$$

where

Σ_{a_2}(base) = nodal cross section with constant power xenon subtracted.

3.2.7 Samarium Buildup

At exposures greater than zero, the base cross sections generated by the XFYRE code contain equilibrium samarium. For hot operating conditions where the reactor has operated for greater than 10 days, the samarium is at equilibrium and no correction to the absorption cross section for non-equilibrium samarium is necessary.

For startup conditions after shutdown the samarium buildup option in the XTGBWR program can be used to calculate time dependent samarium concentration. After the reactor has been shutdown for about 15 days, the promethium has decayed to samarium and the samarium concentration will be

$$Sm\ (shutdown) = Sm_0 + Pm_0 \tag{3.2-45}$$

where Sm_0 and Pm_0 are the equilibrium concentration of samarium and promethium. The equilibrium concentration of an isotope is

$$N_i = \frac{\gamma_i(\phi_1\Sigma_{f_1} + \phi_2\Sigma_{f_2})}{\lambda_i} \tag{3.2-46}$$

where

N_i = concentration of isotope i

γ_i = yield of isotope i

λ_i = decay constant of isotope i

ϕ_1 = fast flux

ϕ_2 = thermal flux

Σ_{f_1} = fast fission cross section

Σ_{f_2} = thermal fission cross section

After startup the excess Sm is burned out exponentially until equilibrium Sm is once again established. The equation for the time dependent added absorption cross section due to samarium depletion is

$$\Delta\Sigma_{a_2} = Pm_0 * \sigma_{a_2}^{Sm} * \exp(-\sigma_{a_2}^{Sm}\phi_2\Delta T) \qquad (3.2\text{-}47)$$

where

$\sigma_{a_2}^{Sm}$ = thermal samarium absorption equation

ϕ_2 = thermal flux

ΔT = time since startup.

3.2.8 Doppler Broadened Cross Sections

The base cross sections are calculated with the XFYRE code at a constant power and fuel temperature. For a given node of fuel in the core the fuel temperature depends on the power, exposure, void fraction, and fuel rod design. Since the Doppler broadening of the uranium and plutonium resonance absorption peaks is dependent on the fuel temperature, the XTGBWR code accounts for the Doppler effects by adjustment of the fast absorption cross section of each node when the cross sections are calculated. The adjustment is made by the following equation:

[ ]

3.2.9 Coolant Flow Distribution

The coolant flow distribution is calculated from a hydraulic model of the reactor core described in Reference 3-11. In this model, the core consists of a number of parallel flow paths between upper and lower plenums, with an equal pressure drops across all paths. Each assembly constitutes a separate path and the bypass flow region shared by all the assemblies is a flow path. For each flow path, the pressure drop is calculated by a channel flow model which includes frictional acceleration, and gravitational terms. The effects of orificing, lower and upper tie plates, grip spacers, and other frictional losses are modeled by flow dependent loss coefficients. The effects of power on the flow distribution are included by a void fraction model, described below, and by a two-phase friction multiplier. The coolant flow through each parallel path is adjusted iteratively until the pressure drops for all parallel flow paths are equal within a specified limit.

All assemblies with the same number of rods and the same set of loss coefficients comprise a hydraulic type. The results of the hydraulic model calculations can be used to obtain an empirical relationship between assembly flow and assembly power for each type which describes the flow versus power for the assembly to good accuracy. [ ] The flow distribution is redetermined and renormalized at each cross section update.

3.2.10 Steam Quality and Void Fraction

The coolant enthalpy (h_{ijk}) at each axial node k of a fuel assembly is calculated from the flow and power by integrating the heat deposited in the water up to the node midpoint using the following formula:

[ ]

The void fraction at each node is calculated from the coolant enthalpy. The void fraction correlation used in the XTGBWR program is based upon a mechanistic description of two-phase separated flow and incorporates the effects of integral and relative phase slip and is a function of the pressure, mass velocity, flow quality and rod surface heat flux within an assembly. A subcooled void model is included in the void fraction correlation to include the effects of thermal nonequilibrium. The void fraction model is described fully in Reference 3-11.

3.2.11 Thermal Limits Calculation

As an edit option, the XTGBWR code calculates the average planar linear heat generation rate (APLHGR), the linear heat generation rate (LHGR), and the critical power ratio (CPR) for each node of fuel in the core. The APLHGR is calculated from the relative nodal power P_{ijk} and the total reactor thermal power PTH converted to kw/ft as follows:

$$APLHGR_{ijk} = \frac{PTH * P_{ijk} * FPGIF * 12{,}000}{ND2D * NRODAS_{ij} * HEIGHT} \qquad (3.2\text{-}52)$$

where

PTH = core thermal power in MWth

P_{ijk} = relative nodal power

FPGIF = fraction of power deposited within fuel rods

ND2D = fuel assemblies in core

$NRODAS_{ij}$ = fuel rods per assembly at core locations

HEIGHT = core height in inches

The LHGR is the maximum rod power in a node of fuel and is calculated from the APLHGR and the relative local peaking factor (P_L).

$$LHGR = APLHGR*P_L \quad (3.2\text{-}53)$$

The local peaking factor is calculated by the XFYRE code and input into the XTGBWR program as a function of exposure, voids, fuel type, and control.

The CPR is calculated in the XTGBWR code for each fuel assembly using the Exxon Nuclear XN-3[3-12] critical power correlation. [ ].

3.2.12 Incore Detector Response Calculation

The XTGBWR code has the edit capability to calculate the relative incore detector response. The incore detector assembly consists of an outer stainless steel sheath, a stainless steel tube for the traveling incore probe (TIP), four fixed position local power rate monitors (LPRM's) and the signal cables to the LPRM's. A cross section of the BWR incore detector is shown in Figure 3.2-4.

The incore detector is physically located outside the channel in the water gap corner opposite the control rod. The location of an incore detector relative to the assembly is shown in Figure 3.1-1.

In the reactor core the incore detectors are placed in approximately one out of every four possible locations such that if the core is operated with quarter core mirror symmetry, all fuel assemblies excluding those on the core periphery are monitored by a traveling incore detector. A typical placement of the incore detectors in the core is shown on Figure 3.2-1.

The TIP and LPRM incore detectors are both miniature fission detectors usually containing uranium-235. The signal ouput from the detectors is proportional to the thermal neutron flux.

In the XTGBWR program, the detector response is calculated from the nodal power of each of the four fuel assemblies surrounding the detector. The relative detector response (TIP) at a given axial location is given by the following equation.

[ ]

Tables of basic T factors are input as a function of exposure and void history as part of each cross section set. These basic factors are corrected for each node to account for the effects of 1) difference between instantaneous voids and average void history, 2) axial variation of instantaneous void, and 3) presence of control rod. The correction factors are reactor

dependent, but not fuel type dependent. Specifically, for BWR's with asymmetric water gaps, the T factor for an uncontrolled node is [

]

For BWR's with symmetric water gaps, the T factor for an uncontrolled node is [

]

For either water gap, the T factor for a controlled node is given by [

]

The axial TIP correction factor (DC_N) is the ratio of the relative thermal fission density in the actual incore detector to the fission density in a dilute U-235 and water mixture at a specific axial core height. This factor is function of the axial position and the in-channel void fraction,

[ ]

3.2.13 Zero Power Critical Option

The XTGBWR code will perform zero power flux and eigenvalue solutions with no flow, void, or Doppler feedback. The nuclear parameters for the zero power solutions are calculated with the XFYRE code. Starting with void history and exposure dependent isotopics, the cross sections are calculated for each fuel type in the core at the desired fuel and moderator temperature. The calculations are performed both controlled and uncontrolled.

The zero power nuclear data are input into the XTGBWR code as the ratio of the zero power cross sections divided by the hot operating cross sections. The cross section ratio data are normally input into the

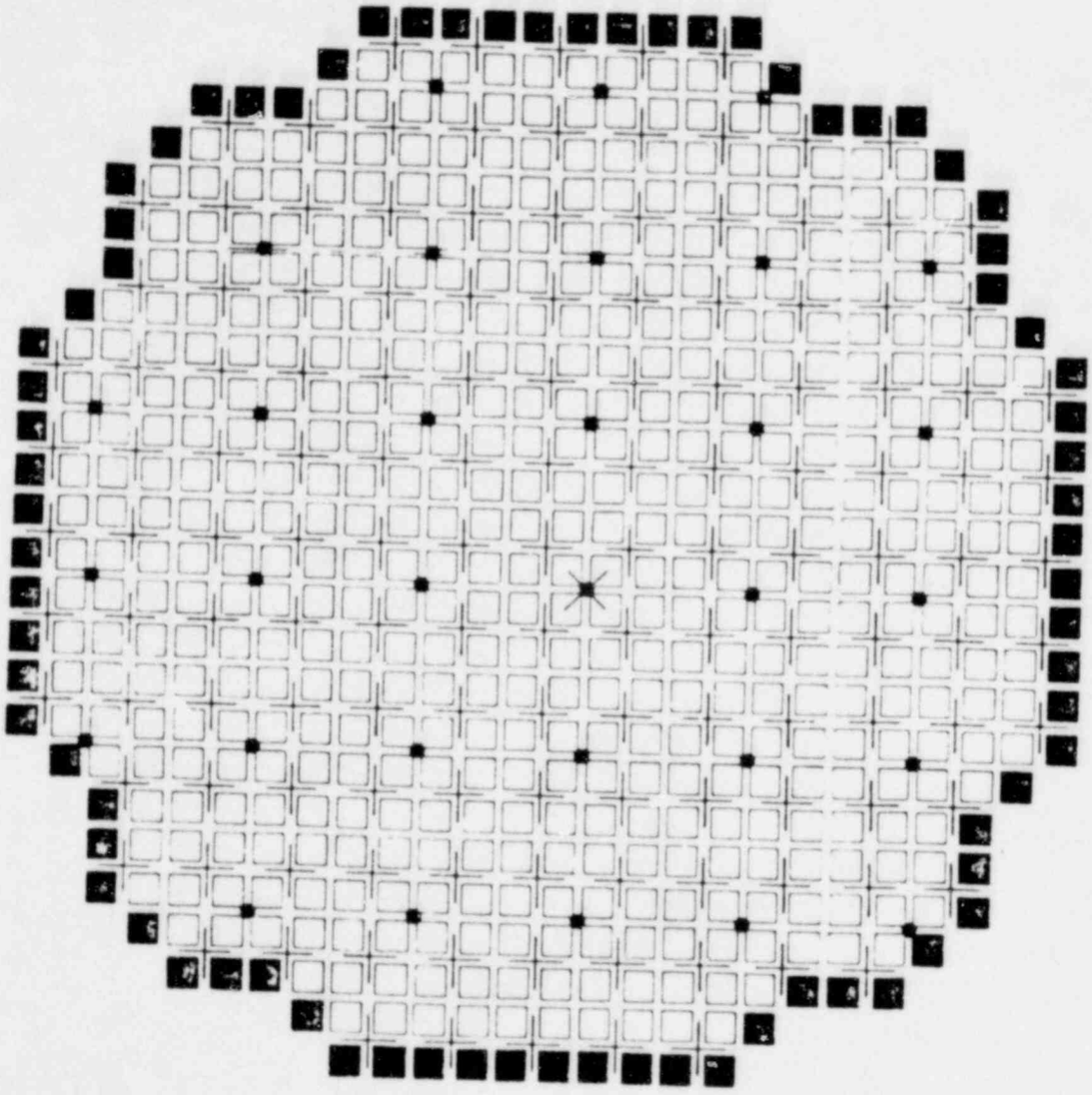

+ Control Rods

● TIP Instrument Assemblies

Common Position for all TIP Machines

Fuel Assemblies with Large Diameter Orifice

Fuel Assemblies with Small Diameter Orifice

Figure 3.2-1 Typical BWR Reactor Core Geometry

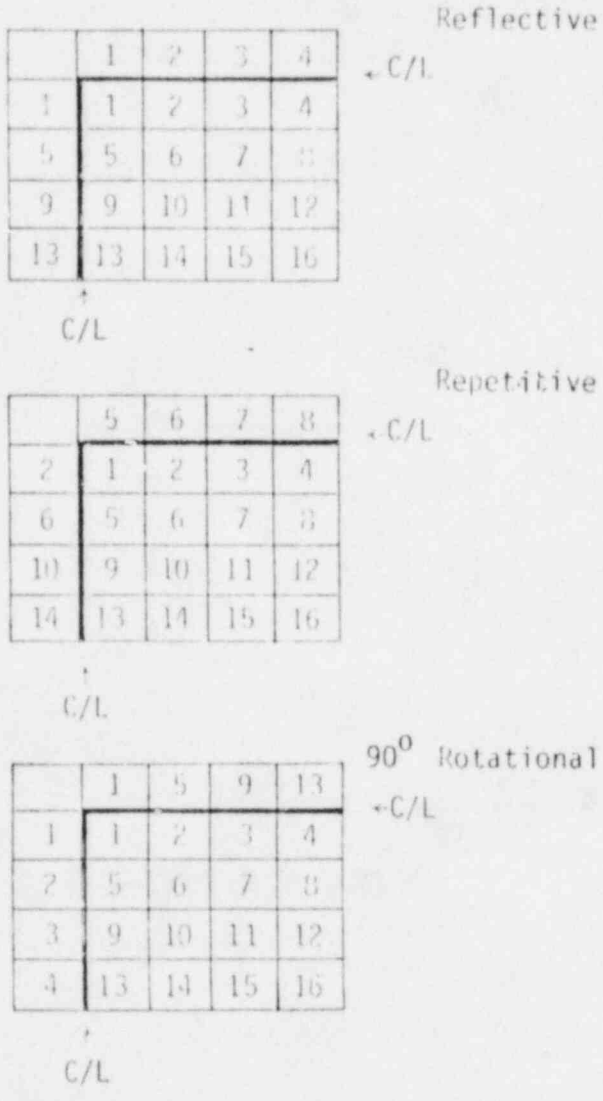

Figure 3.2-2 XTGBWR Quarter Core Symmetry Boundary Conditions

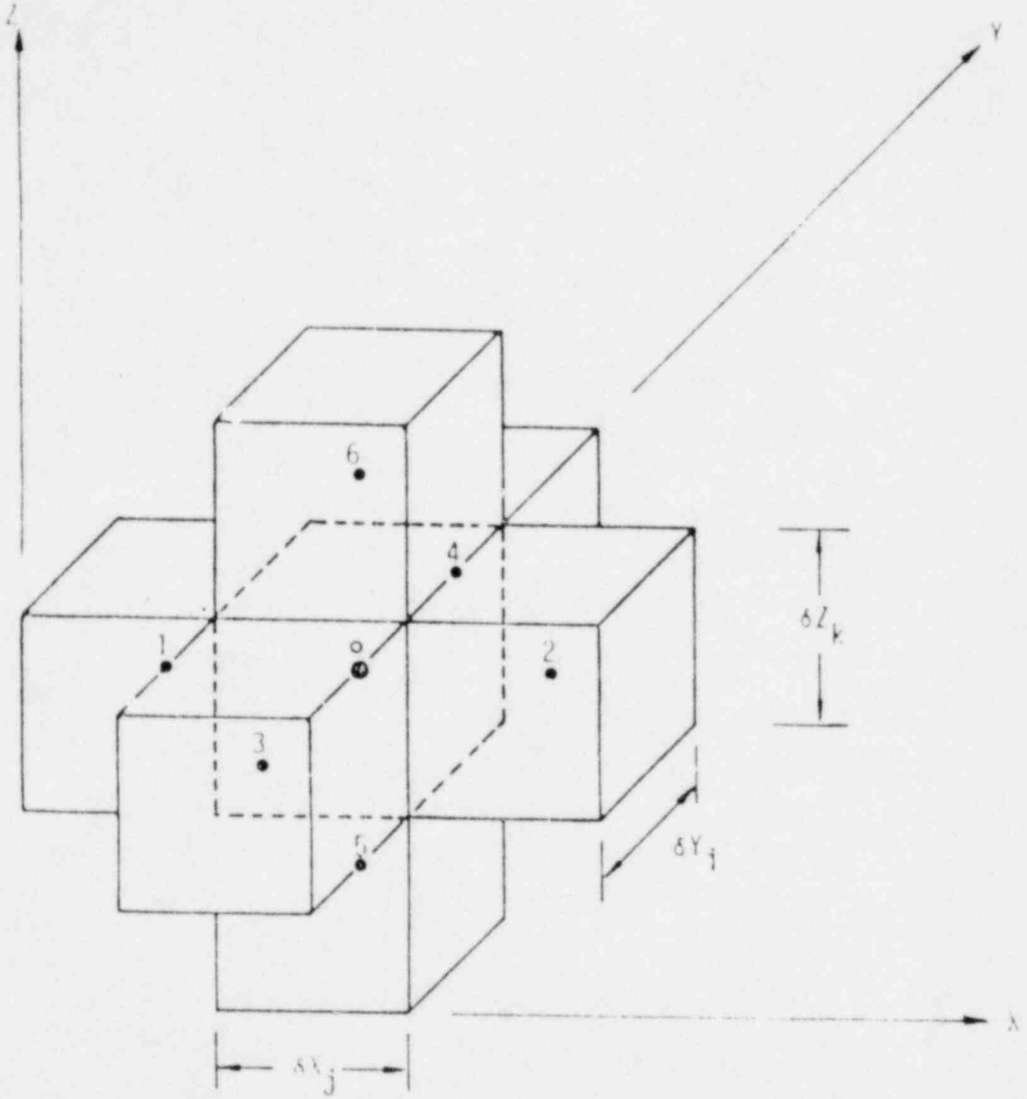

Figure 3.2-3 Three Dimensional Mesh Description in XYZ Geometry

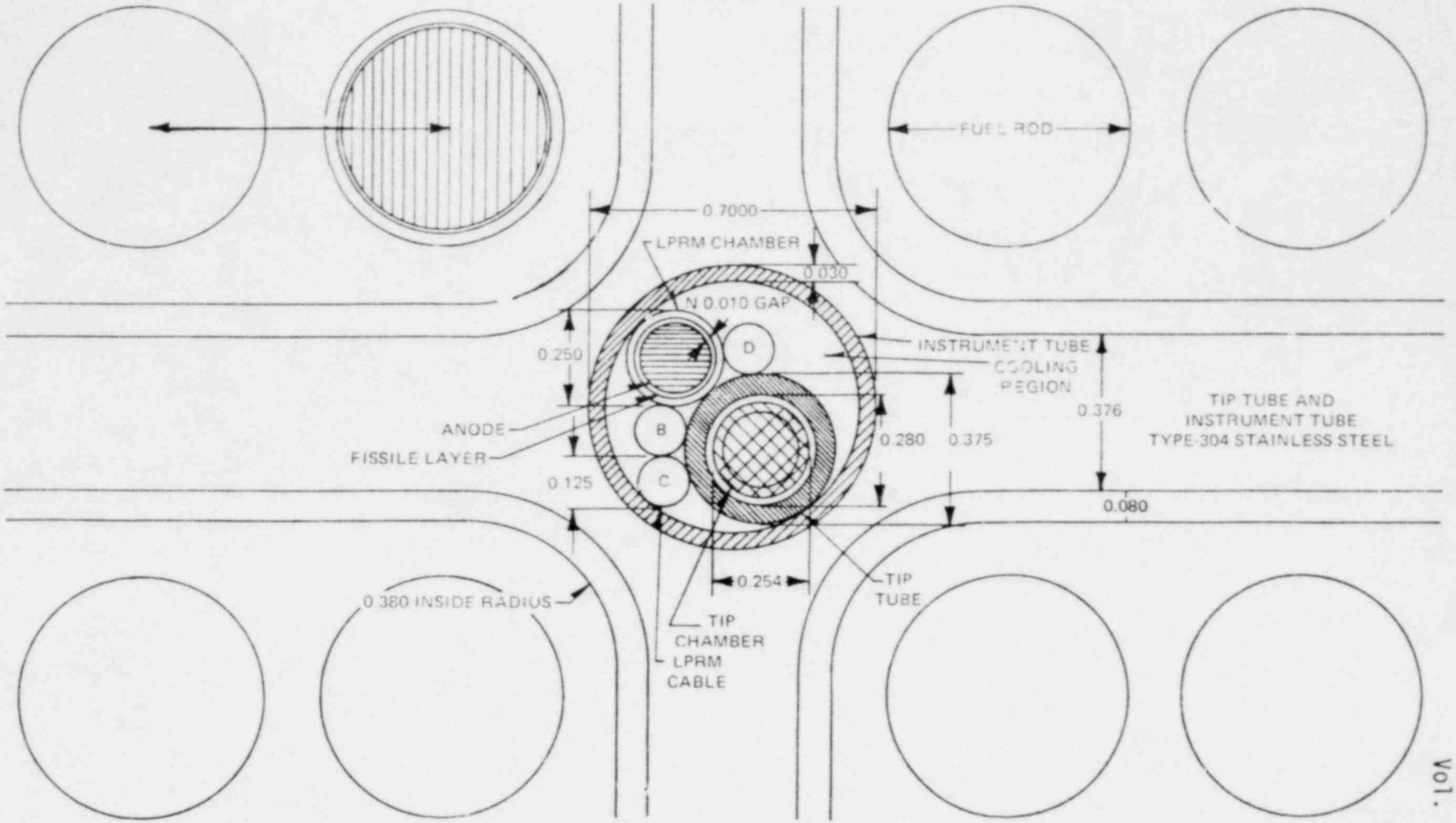

Figure 3.2-4 TIP/LPRM In-Core Assembly Cross Section

code at exposures of [ ]. The zero power cross sections for controlled fuel nodes are input as the ratio of controlled cross sections to uncontrolled cross sections. The controlled cross section data are input [ ]. Prior to performing a zero power calculation, the XTGBWR code determines the cross sections for each node of fuel in the core from the input data by interpolating on exposure and void history and considering control, xenon, and samarium. Since there is no thermal hydraulic or power feedback, the cross sections for a given node of fuel do not vary during the flux and eigenvalue calculation.

3.3 REACTOR KINETICS MODEL (COTRAN)

The ENC reactor kinetics model for the analysis of BWR reactor cores is the COTRAN code. COTRAN is a two dimensional (r-z) computer program which solves the space and time dependent one energy group neutron diffusion equation with one prompt and six delayed neutron groups. Fuel temperature and void reactivity feedback are determined from a solution of the equations of mass, energy and momentum for the coolant coupled with a fuel heat conduction model. The coolant model is a one-dimensional solution of the hydrodynamic equations assuming thermodynamic equilibrium between phases in the two-phase region. The fuel rod model is a two-dimensional solution of the heat conduction equation by the method of weighted residuals in the radial direction with finite differences used for time and axial space derivatives. Axial conduction and temperature dependent fuel thermal conductivity are included.

The COTRAN code integrates the two separate codes XTRAN[3-13] and COBRA IV.[3-14, 3-15] XTRAN supplies the neutronic solution and COBRA IV, reduced to one dimension by the elimination of cross flow, determines the thermal-hydraulic feedback.

The COTRAN code requires input from the XFYRE and XTGBWR codes including cross sections, rod worths, initial flux and power shapes, peaking factors and other initial condition parameters. The COTRAN code has the capability to accept forcing functions as a function of time for several system parameters. These forcing functions allow COTRAN to model the reactor while including input total system feedback.

3.3.1 COTRAN Neutronics Model

3.3.1.1 Space & Time Dependent Iterative Equation

The one neutron group, space and time dependent neutron diffusion equation with no external sources is:

$$\frac{1}{v(\vec{r},t)}\frac{d\phi(\vec{r},t)}{dt} = \left[(1-\beta)\nu\Sigma_f(\vec{r},t) - \Sigma_A(\vec{r},t)\right]\phi(\vec{r},t) + \nabla\cdot D(\vec{r},t)\nabla\phi(\vec{r},t) + \sum_{\ell}\lambda_\ell C_\ell(\vec{r},t) \tag{3.3-1}$$

Applying Ficks Law,

$J(\vec{r},t) = -D(\vec{r},t)\nabla\phi(\vec{r},t)$

Equation (3.3-1) becomes

$$\frac{1}{v(\vec{r},t)}\frac{d\phi(\vec{r},t)}{dt} = \left[(1-\beta)\nu\Sigma_f(\vec{r},t) - \Sigma_A(\vec{r},t)\right]\phi(\vec{r},t) - \nabla\cdot J(\vec{r},t) + \sum_{\ell}\lambda_\ell C_\ell(\vec{r},t) \tag{3.3-2}$$

Integrating Equation (3.3-2) over the volume (Vi) of some of node i, assuming the quantities being integrated are separable in space and time and constant over the node, and making use of Gauss' theorem yields.

$$\frac{V_i}{v_i(t)} \frac{d\phi_i(t)}{dt} = \left[(1-\beta)\nu\Sigma_{fi}(t) - \Sigma_{Ai}(t)\right] \phi_i(t)V_i - \int_{surface} J(\vec{r}_s)\cdot\bar{n}\cdot dr_s + V_i \sum_{\ell} \lambda_\ell C_{i\ell}(t) \quad (3.3\text{-}3)$$

where

$$\int_{surface} J(\vec{r}_s)\cdot\vec{n}\cdot d\vec{r}_s = \sum_i J_{ij}A_{ij}$$

and

J_{ij} = net current per unit area at the interface of nodes i and j.

A_{ij} = area of the interface of node i and j.

$\sum_i$ = summation over all nodes immediately adjacent to node i.

If the flux is assumed to have the following spatial dependence between nodes i and j.

$$\phi(r) = \phi_i \frac{1-r}{d_{ij}} + \phi_j \frac{r}{d_{ij}}$$

where

d_{ij} is the distance between the centroids of nodes i and j, then

$$J_{ij} = -D_{ij} \left.\frac{d\phi}{dr}\right|_{r=r_{ij}} = \frac{-D_{ij}}{d_{ij}} (\phi_j - \phi_i)^*$$

If it is now assumed that for a small time step

$(\Delta t = t_2 - t_1)$

$$\frac{\partial\phi(t)}{\partial t} = \frac{\phi(t_2)-\phi(t_1)}{\Delta t}$$

Then Equation (3.3-3) can be approximated by

$$\frac{1}{v\Delta t}\left[\phi_i(t_2) - \phi_i(t_i)\right] = \left(1 - \sum_{\ell} \beta_\ell\right) \nu\Sigma_{f_i}\, \phi_i(t_2) - \Sigma_{A_i}\, \phi_i(t_2)$$

$$+ \frac{1}{V_i} \sum_{j} \frac{A_{ij}D_{ij}}{d_{ij}} \left[\phi_j(t_2) - \phi_i(t_2)\right]$$

$$- \sum_{\ell} \lambda_{i\ell}\, C_{i\ell}(t_2)$$

---

* D_{ij}, the diffusion coefficient at the interface adjacent nodes, is approximated by: $D_{ij} = \sqrt{D_i}\sqrt{D_{ij}}$

This was shown by Borresen[3-16] to be a very good approixmation when the dimensions of node i are similar to node j.

Solving for $\phi_i(t_2)$, yields

$$\phi_i(t_2) = \frac{V_i\left[\frac{1}{v\Delta t}\,\phi_i(t_1) + \sum_{\ell} \lambda_{i_\ell}\, C_{i\ell}(t_2) + \right]\sum_j \frac{A_{ij}\,D_{ij}}{d_{ij}}\,\phi_j(t_2)}{V_i\left[\frac{1}{v\Delta t} - (1 - \sum_{\ell} \beta_\ell)\nu\,\Sigma_{f_i} + \Sigma_{A_i}\right] + \sum_j \frac{D_{ij}A_{ij}}{d_{ij}}} \qquad (3.3\text{-}4)$$

At this time it is necessary to solve for the precursor densities as a function of flux. Recall that the precursor density equation is of the form:

$$\frac{\partial C_\ell}{\partial t} = \beta_\ell\,\nu\,\Sigma_f\,\phi - \lambda_\ell C_\ell$$

Making use of the finite difference approximation and using the average value of the flux and precursor density during the time step leads to the following expression:

$$\frac{C_{i\ell}(t_2)-C_{i\ell}(t_1)}{\Delta t} = \beta_\ell\nu\,\Sigma_{fi}\,\frac{\phi_i(t_1)+\phi_1(t_2)}{2} - \frac{\lambda_\ell}{2}\left[C_{i\ell}(t_2)+C_{i\ell}(t_1)\right]$$

which can be solved for $C_{i\ell}(t_2)$ as:

$$C_{i\ell}(t_2) = \frac{C_{i\ell}(t_1)\,(2-\lambda_\ell\Delta t) + \beta_\ell\Delta t\,\nu\,\Sigma_{fi}\left[\phi_i(t_1)+\phi_i(t_2)\right]}{2+\lambda_\ell\Delta t}$$

substituting this expression for $C_{i\ell}(t_2)$ in Equation (3.3-4) yields:

$$\phi_i(t_2) = V_i\phi_i(t_1)\left[\frac{1}{v\Delta t} + \nu\,\Sigma_{Fi}\sum_{\ell}\frac{\beta_\ell\Delta t\lambda_\ell}{2+\lambda_\ell\Delta t}\right] + Vi\sum_{\ell}\left(\frac{2-\lambda_\ell\Delta t}{2+\lambda_\ell\Delta t}\right)\lambda\; C_{i\ell}(t_1) + \frac{\sum_j \frac{A_{ij}D_{ij}\phi_j(t_2)}{d_{ij}}}{V_i\left[\frac{1}{v\Delta t} - \nu\Sigma_{Fi}\left(1 - \sum_{\ell}\frac{2\beta_\ell}{2+\lambda_\ell\Delta t}\right) + \Sigma_{a_i}\right] + \sum_j \frac{A_{ij}D_{ij}}{D_{ij}}} \qquad (3.3\text{-}5)$$

This equation is the iterative equation solved at the end of each time step of length Δt.

3.3.1.2 Calculations at Core-Reflector Interface

COTRAN employs a very simplified technique to account for the effects of the reflector core interface. Infinite difference form, the net leakage (L) into a node i can be expressed as:

$$L_i = \sum_j \frac{D_{ij}A_{ij}}{d_{ij}}(\phi_j - \phi_i) \qquad (3.3\text{-}6)$$

where

D_{ij} = Effective diffusion coefficient at nodal surface = $\sqrt{D_iD_j}$

A_{ij} = Area of the interface between nodes i and j

d_{ij} = Distance between centroids of nodes i and j

ϕ_i = Flux of node i

ϕ_j = Flux of node j

The technique used in COTRAN if node j is the reflector is to assume that:

$$\phi_j = 0$$

and to adjust the value of the reflector diffusion coefficient (D_j) until realistic flux distrubitions are obtained when compared to a more sophisticated static calculation. It can be seen that reflector diffusion coefficients of 0.0 and ∞ yield reflecting and vacuum boundary conditions respectively.

3.3.2 COTRAN Thermal-Hydraulic Model

3.3.2.1 Transient Mixture Balance Laws

The integral balance laws which form the basis of COTRAN are formed on an Eulerion control volume, V, which is bounded by a fixed surface A. This surface may include solid interfaces, such as a fuel rod or structural wall, and fluid boundaries, but all solid material is outside V and composes the fuel thermal model in Section 3.3.2.4. The fluid in V is a single component, two phase mixture of liquid and vapor in thermodynamic equilibrium.

The integral balance on the control volume for the mixture properties* mas, energy and momentum are:

$$\frac{\partial}{\partial t}\int_V \rho dV + \int_A \rho(\vec{u}\cdot\vec{u})dA = 0 \qquad (3.3\text{-}7)$$

$$\frac{\partial}{\partial t}\int_V \rho e dV + \int_A \rho e(\vec{u}\cdot\vec{n})da = \int_V (\rho(\vec{f}\cdot\vec{u})+\rho r)dV + \int_A ((\vec{\vec{T}}\cdot\vec{u})-\vec{q})\cdot\vec{n}dA \qquad (3.3\text{-}8)$$

$$\frac{\partial}{\partial t}\int_V \rho\vec{u}dV + \int_A \rho\vec{u}(\vec{u}\cdot\vec{n})dA = \int_V \rho\vec{f}dV + \int_A (\vec{\vec{T}}\cdot\vec{n})dA \qquad (3.3\text{-}9)$$

respectively,** where

$\vec{u}$ = fluid velocity

$\vec{n}$ = unit outward normal

e = energy, internal thermal energy, i, and kinetic energy ($e = i+u^2/2$).

$\vec{f}$ = sum of all body forces acting on the fluid.

r = rate of internal heat generation/unit mass from all sources.

---

* It is assumed that the local composition of the mixture can be described by the space-time average vapor volume fraction, α. Any mixture variable, Q, can be expressed as the volume weighted sum of the individual phase variables $Q = \alpha Q_v + (1-\alpha) Q_\ell$.

** Note the integral balance laws are of the form

change of the total amount of Q in V + rate at which Q is transported across boundaries = sum of all sources and sinks of Q inside V

$\vec{\vec{T}}$ = surface stress tensor.

$\vec{q}$ = heat flux vector.

Only these three mixture conservation equations with one mixture equation of state and one relation specifying the relative velocity of one of the phases with respect to the other (or the mixture) are required to treat separated two-phase flow assuming thermal phase equilibrium.

The integral balance laws, Equations (3.3-7) through (3.3-9), have been written for a single component two-phase mixture with the phases in thermodynamic equilibrium. Since the intended applications of COTRAN are for BWR channels with low speed flow and significant surface heat transfer the following assumptions apply:

- Kinetic energy changes are small compared to internal thermal energy changes
- Work done by body forces and shear stress is considered to be insignificant
- Gravity is the only significant body force
- Internal heat generation in the fluid is ignored
- Fluid flow is one dimensional

Under these assumptions, the only surface integrals of interest, associated with the solid interfaces, are the heat transfer and surface forces.

The surface heat transfer integral will be modeled by the fourier law, for advection across the fluid boundary, and the product of an emperical surface heat transfer coefficient, H, and temperature difference for the solid interface. That is

$$\int_A (\vec{q}\cdot\vec{n})dA = -\int_F K(\vec{\nabla}T\cdot\vec{n})dA + \int_W H(T_W - T_F)dA \qquad (3.3\text{-}10)$$

where

k = Fluid thermal conductivity

T_f = Local fluid temperature

T_W = temperature of solid boundary

The stress tensor, $\vec{\vec{T}}$, can be written as the sum of a hydrostatic component, p, and a viscous stress tensor, Π, as follows

$$\int_A (\vec{\vec{T}}\cdot\vec{n})da = -\int_F p\vec{n}dA + \int_F (\vec{\vec{\Pi}}\cdot\vec{n})dA + \left\{ -\int_W p\vec{n}dA + \int_W (\vec{\vec{\Pi}}\cdot\vec{n})dA \right\} \qquad (3.3\text{-}11)$$

The wall component, in brackets, will be modeled in the momentum equation by empirical friction factor and drag coefficient correlations. For the energy equation, in which work done by shear stresses has been assumed negligible, Equation (3.3-11) reduces to,

$$\int_A \vec{\vec{T}}\cdot(\vec{u}\cdot\vec{n})dA = -\int_F \rho(\vec{u}\cdot\vec{n})dA \qquad (3.3\text{-}12)$$

Applying these definitions and assumptions to the original intergal balances, Equation (3.3-7) through (3.3-9), form the following equations.

Mass

$$\frac{\partial}{\partial t}\int_V \rho dV + \int_F \rho(\vec{u}\cdot\vec{n})dA = 0 \qquad (3.3\text{-}13)$$

Energy

$$\frac{\partial}{\partial t}\int_V \rho h dV + \int_F \rho h(\vec{u}\cdot\vec{n})dA = -\int_F K(\vec{\nabla}T\cdot\vec{n})dA + \int_W H(T_W - T_W)dA \qquad (3.3\text{-}14)$$

where

$\rho h = \rho i + p$ (The temporal derivative of pressure can be ignored for low-speed flow).

Momentum

$$\frac{\partial}{\partial T}\int_V \rho\vec{u}dV + \int_F \rho\vec{u}(\vec{u}\cdot\vec{n})dA = \int_V \rho\vec{g}dV - \int_F p\vec{n}dA + \int_F (\vec{\vec{\pi}}\cdot\vec{n})dA - \int_W p\vec{n}dA + \int_W (\vec{\vec{\pi}}\cdot\vec{n})dA \qquad (3.3\text{-}15)$$

3.3.2.2 Channel Equations

In order to consider the essential nature of two-phase flow, it is necessary to smooth out its chaotic nature. In deriving the integral balance laws of Section 3.3.2.1 it was assumed that the mixture variables are sufficiently space-time averaged to provide continuous derivatives inside the fixed volume and over its surface.

To solve the integral balance equations the following volume and surface averages are defined for an arbitrary mixture variable, Q,

$$\langle\langle Q\rangle\rangle_V = \frac{\int_V Q dV}{\int_V dv} \qquad \langle Qu\rangle_A = \frac{\int_A Q(\vec{u}\cdot\vec{n})dA}{\int_A dA}$$

Consider the channel section in Figure 3.3-1. The centroid is located at x and its length is Δx. Therefore, the upper and lower surfaces are at $x + \frac{(\Delta x)}{2}$ and $x - \frac{(\Delta x)}{2}$, respectively. The axial flow area is A and the axial velocity is u.

Mass Balance

The mass balance Equation (3.3-13) may be applied directly to the channel control volume.

$$V\frac{\partial}{\partial T}\langle\langle\rho\rangle\rangle_V + \langle\rho u\rangle_A A\Big|_{X+\frac{\Delta x}{2}} - \langle\rho u\rangle_A A\Big|_{X-\frac{\Delta x}{2}} = 0$$

The channel equation is formed by dividing through by Δx and taking the limit as Δx becomes small

$$A\frac{\partial}{\partial t}\langle\langle\rho\rangle\rangle_V + \frac{\partial}{\partial X}\langle\rho u\rangle_A A = 0 \qquad (3.3\text{-}16)$$

Energy Balance

Formal averaging of the surface heat fluxes will not be defined since commonly used surface heat transfer correlations already imply considerable surface averaging. Instead the average nuclear power in a radial region will be utilized such that the heat input to V from rods is

$$Q_r = \Delta x \left[P_r \phi H \right] \left[D_r \right] T + \Delta x \gamma$$

where

H = surface heat transfer coefficient

P_r = rod perimeter

ϕ = number of rods contained in V

$\left[D_r\right]T$ = difference between the rod surface temperature and bulk fluid temperature

γ = volumetric heat input from direct moderator heating

Applying this definition and the energy balance law in Equation (3.3-14) to the channel control volume yields:

$$V\frac{d}{dt} \langle\langle \rho h \rangle\rangle_V + \langle \rho u h \rangle_A^A \Big|_{x+\frac{\Delta x}{2}} - \langle \rho u h \rangle_A^A \Big|_{x-\frac{\Delta x}{2}} = \Delta x \left\{ \left[P_r \phi H \right] \left[D_r \right] T + \gamma \right\}$$

$$+ A \left\langle K \frac{dT}{dx} \right\rangle \Big|_{x+\frac{\Delta x}{2}} - A \left\langle K \frac{dT}{dx} \right\rangle_A \Big|_{x-\frac{\Delta x}{2}}$$

again dividing by Δx and taking the limit as Δx becomes small leads to:

$$A\frac{\partial}{\partial t} \langle\langle \rho h \rangle\rangle_V + \frac{\partial}{\partial X} \langle \rho u h \rangle_A^A = \left[P \phi H \right] \left[D_r \right] \left\langle T \right\rangle + \frac{\partial}{\partial X} A \left\langle K \frac{\partial T}{\partial X} \right\rangle_A + \gamma \qquad (3.3\text{-}17)$$

Axial Momentum Balance

Before the integral momentum balance Equation (3.3-15) can be applied to the channel control volume, descriptions for the pressure and shear forces on the volume must be derived.

Using an area average, the net axial pressure force acting on the ends of the channel segment can be written as:

$$F_p = - \langle p \rangle_A A\Big|_{x+\frac{\Delta x}{2}} + \langle p \rangle_A A\Big|_{x-\frac{\Delta x}{2}}$$

If, however, the area varies axially an additional force, Fw, is exerted by the side walls. If both the area and pressure variation are assumed linear within Δx, this additional force is:

$$Fw = \langle p \rangle_x \left(A\Big|_{x+\frac{\Delta X}{2}} - A\Big|_{x-\frac{\Delta x}{2}}\right)$$

the total pressure force is simply the sum that is,

$$F_p + Fw = -Ax\left[\langle p \rangle_{x+\frac{\Delta x}{2}} - \langle p \rangle_{x-\frac{\Delta x}{2}}\right]$$

As mentioned in Section 3.3.2.1 the rest of the solid interface stress integral is approximated by emperical wall friction correlations and form loss coefficients. The axial drag force is computed as:

$$F_D = 1/2\left[f\Delta x Pw + KA\right] \langle \rho u^2 \rangle_A$$

where

f = dimensionless friction factor determined by correlation

Pw = wetted perimeter of the channel

K = total form loss coefficient in Δx

applying the difinition of the hydraulic diameter, D_H,

$$Fd = 1/2\left(\frac{f'\Delta x}{D_h} + K\right)\langle\rho u^2\rangle_A A$$

where

$$f' = 4f$$

Using these defin'tions the channel equation becomes

$$V\frac{d}{dt}\langle\langle\rho u\rangle\rangle_V + \langle\rho u^2\rangle_A A\Big|_{x+\frac{\Delta x}{2}} - \langle\rho u^2\rangle_A A\Big|_{x-\frac{\Delta x}{2}} = -A_x\left(\langle p\rangle_{x+\frac{\Delta x}{2}} - \langle p\rangle_{x-\frac{\Delta x}{2}}\right)$$

$$- 1/2\left(\frac{f'\Delta x}{D_h} + K\right)\langle\rho u^2\rangle_A A - V\langle\langle\rho\rangle\rangle_V g\ \cos\theta$$

dividing by Δx and taking the limit produces:

$$\frac{\partial}{\partial T}\langle\langle\rho u\rangle\rangle_V A + \frac{\partial}{\partial X}\langle\rho u^2\rangle_A A = -A\frac{\partial}{\partial X}\langle p\rangle_A - 1/2\left(\frac{f'}{D_h} + \frac{K}{\Delta X}\right)\langle\rho u^2\rangle_A A$$

$$- A\langle\langle\rho\rangle\rangle_V g\cos\theta \qquad (3.3\text{-}18)$$

where

θ is the channel orientation angle measured from the vertical.

3.3.2.3 Numerical Solution Procedure

At present, there are two independent solution schemes for the thermal-hydraulic balance equations in COTRAN. One is the implicit technique which provides a direct steady state solution but is limited to positive axial flow rates. The other solution scheme removes the positive flow restriction but is limited to small time steps. The explicit solution is further limited to transient problems although it may be initialized by an implicit steady state calculation.

The implicit solution scheme includes options for two-phase slip models, void-quality relations and two-phase friction multipliers. The explicit procedure uses only the homogeneous equilibrium model for two-phase flow.

Both solution procedures employ the same fuel temperature model. This heat conduction model uses the method of weighted residuals by the orthogonal collocation technique. The model incorporates the Kirchoff transformation so that temperature-dependent thermal conductivity may be considered. The fuel is interfaced with the fluid thermal-hydraulics by means of a surface heat transfer correlation specified by code input. Further details of the fuel model are presented in Section 3.3.2.4.

The two COTRAN solution schemes employ the reference pressure approach. This is, the local fluid density is assumed to be a function of the local enthalpy and a spatially uniform reference pressure. The assumption is valid as long as spatial pressure variations are small compared to the system pressure.

In order to solve the three channel equations derived in Section 3.3.2.2, as well as the state equation, the area and volume averaged terms must be related so that the equations can be rewritten in terms of four primary variables. These are axial mass flow rate, M, mixture static enthalpy, h, or flowing enthalpy $\hat{h}$, mixture density, ρ, and pressure, P. The definitions required to form these variables are different between the two methods since the implicit solution is formed in terms of flowing quality and includes slip whereas the explicit method requires static quality and no slip between phases. Primary variables used in the solution are defined in Table 3.3-1.

Implicit Solution Scheme

If the implicit solution scheme is chosen in COTRAN, the problem is limited to positive flow rates. However, two phase slip flow can be considered with the assumption that the phases are in thermal equilibrium and that the phase velocities and volume fractions are uniformly distributed within the control volume.

Defining the flowing enthalpy and quality as:

$$\hat{h} = \frac{\langle \rho u h \rangle}{\langle \rho u \rangle} \qquad \text{and} \qquad \hat{x} = \frac{\langle \alpha \rho_v u_v \rangle}{\langle \rho u \rangle}$$

respectively, and realizing that the assumption of uniform phase distribution implies that:

$$m = A\langle \rho u \rangle = A\langle\langle \rho u \rangle\rangle$$

leads to the derivation of the continutiy equation from Equation (3.3-16) as:

$$A\frac{\partial}{\partial t}\rho + \frac{\partial}{\partial x} m = 0 \qquad (3.3\text{-}19)$$

Using the definition of flowing enthalpy, the energy equation, Equation (3.3-17) becomes:

$$A\frac{\partial}{\partial t}\rho h + \frac{\partial}{\partial x} m\hat{h} = Q$$

where Q = the terms on the right hand side of Equation (3.3-17) factoring yields,

$$A\frac{\partial}{\partial t}\rho h + m\frac{\partial}{\partial x}\hat{h} + \hat{h}\frac{\partial}{\partial x} m = Q \qquad (3.3\text{-}20)$$

at this point it is beneficial to define a new property, ψ, introduced by Tong in 1965[3-17], which is defined as

$$\psi = \rho(\hat{h}-h)/h_{fg}$$

which can be rearranged to

$$\rho h = \rho\hat{h}-h_{fg}\psi$$

substituting Equation (3.3-20) reduces to

$$A\left(\frac{\partial}{\partial t}\rho\hat{h} - h_{fg}\frac{\partial\psi}{\partial t}\right) + m\frac{\partial}{\partial x}\hat{h} + \hat{h}\frac{\partial}{\partial x} m = Q$$

introducing the continuity equation, Equation (3.3-19) for $\hat{h}\frac{\partial}{\partial x}m$ gives

$$A\left(\frac{\partial}{\partial t}\rho\hat{h} - \hat{h}\frac{\partial}{\partial t}\rho - h_{fg}\frac{\partial\psi}{\partial t}\right) + m\frac{\partial}{\partial x}h = Q$$

which is equivalent to

$$A\left(\rho - h_{fg}\frac{\partial\psi}{\partial\hat{h}}\right)\frac{\partial\hat{h}}{\partial t} + m\frac{\partial\hat{h}}{\partial x} = Q \qquad (3.3\text{-}21)$$

The axial momentum equation, Equation (3.3-18) is rewritten by use of the definitions of the mementum velocity, $\hat{u}$, and the assumption of uniform phase distribution:

$$\frac{\partial}{\partial t}m + \frac{\partial}{\partial x}m\hat{u} = F$$

where F contains all the terms on the right hand side of Equation (3.3-18), applying the definition of the specific volume for momentum, $\hat{v}$, and differentiating,

$$\frac{\partial m}{\partial t} + \frac{\hat{V}}{A}2m\frac{\partial m}{\partial X} + m^2\frac{\partial}{\partial X}\frac{\hat{V}}{A} = F \qquad (3.3\text{-}22)$$

applying the continuity equation yields

$$\frac{\partial m}{\partial t} - 2m\hat{v}\frac{\partial\rho}{\partial t} + m^2\frac{\partial\hat{v}/A}{\partial X} = F$$

Equations (3.3-19), (3.3-21) and (3.3-22) are the basic equations from which the implicit numerical scheme is derived. These partial differential equations are approximated by finite differences when

the channel is divided into a finite number of axial segments and the variables assigned positions on the computational mesh.

The computational mesh illustrated in Figure 3.3-2 leads to the following finite difference equations:

Fluid Continuity

$$\frac{1}{\Delta t}\bar{A}_i \left(\rho_i - \rho_i^n\right) + \frac{m_i - m_{i-1}}{\Delta X} = 0 \qquad (3.3\text{-}23)$$

Energy

$$\frac{1}{\Delta t}\bar{A}_i \left(p_i^n - h_{fg}\frac{\partial \psi}{\partial \hat{h}}\right)\left(\hat{h}_i - \hat{h}_i^n\right) + m_{i-1}\left(\hat{h}_i - \hat{h}_{i-1}\right) = p\phi\bar{H}\left[D_r\right]\left\{\begin{matrix} T \\ T_r \end{matrix}\right\}_i \qquad (3.3\text{-}24)$$

$$+ \gamma_i + \frac{1}{\Delta x^2}\left(kAi\left(\tilde{T}_{i+1} - \tilde{T}_i\right) - KAi\text{-}1\left(\tilde{T}_i - \tilde{T}_{i-1}\right)\right)$$

Axial Momentum

$$\frac{m_i - m^n_i}{\Delta t} - 2\bar{m}\frac{\hat{v}_i}{}\left(\frac{\rho_i - \rho_i^n}{\Delta t}\right) + m^2_{i-1}\left(\frac{(v/A)_i - (\hat{v}/A)_{i-1}}{\Delta X}\right) = -\bar{A}\left(\frac{p_i - p_{i-1}}{\Delta X}\right) \qquad (3.3\text{-}25)$$

$$\bar{A}_i K_L m_i^2 - \bar{A}p_i g\cos\theta$$

where

$\bar{A}_i$ = average flow area = $0.5(A_i + A_{i-1})$

$$K_L = \frac{v\ell f\phi}{2D_h A_i^2} + \frac{K\hat{v}}{2\Delta X A_i^2}$$

T = channel temperature

Tr = rod surface temperature

$\bar{m} = 0.5\ (m_i + m_{i-1})$

and the superscripts are defined as

n = previous time step (no superscript implies present time)

$\sim$ = present time but previous iteration.

Equations (3.3-23), (3.3-24) and (3.3-25) are the iterative equations used in the implicit solution scheme of COMMIX.

Explicit Solution Scheme

Unlike the finite difference technique employed by the implicit solution the explicit solution scheme solves the cell balance equations directly. To solve the cell balance equations, two-phase flow is assumed to be completely homogeneous with the phases in thermal equilibrium. This restriction on fluid modeling is compensated, however, by the capability of addressing reverse flow conditions.

The homogeneous assumption implies that both phase velocities are equal (no slip) and that the phase distribution is uniform throughout the control volume. These assumptions lead to the following definitions:

- $\langle \rho u \rangle = \langle\langle \rho \rangle\rangle u$
- $\langle \rho h u \rangle = \langle\langle \rho h \rangle\rangle u = h \langle\langle \rho \rangle\rangle u$
  where h = average enthalpy = $\frac{\langle\langle \rho h \rangle\rangle}{\langle\langle \rho \rangle\rangle}$

- $x = \frac{\alpha\rho v}{\langle\langle\rho\rangle\rangle}$ = static quality
- $h = xh_v + (1-x)\, h_\ell$

To form the difference equations requires the formulation of a computational cell and the assignment of primary variables to the computational mesh. The cell used in the explicit solution is shown in Figure 3.3-3. A cell balance leads to the following equations for mass, energy and momentum conservation+.

Mass

$$\hat{A}_i\, \Delta x\, \frac{d}{dt}\, \rho_i + m_i - m_{i-1} = 0 \tag{3.3-26}$$

Energy

$$\hat{A}_i\, \Delta x\, \frac{d}{dt}\, \rho_i h_i + m_i h_i - m_{i-1} h^*_{i-1} = \Delta x \left\{ P_r \phi H \right\} \left[D_r \right] \left\{ T_i \right\} + \gamma_i$$

$$+ \frac{1}{\Delta x} \left\{ Ak_i\, (T_{i+1} - T_i) - \hat{Ak}_{i-1} \left(T_i - T_{i-1} \right) \right\} \tag{3.3-27}$$

Momentum

$$\frac{d}{dt}\, m_i + \hat{A}_i\, \frac{1}{\Delta x}\, (p_{i+1} - p_i) + \frac{1}{2} \left(\frac{f}{D_H} + \frac{k}{\Delta x} \right) \left(\frac{m^2}{\rho^* A} \right)_i$$

$$- \frac{1}{\Delta x} \left(\hat{u}_{i+1} m^*_{i+1} - \hat{u}_i m^*_i \right) = -\hat{A}_i \hat{\rho}_i\, g \cos\theta \tag{3.3-28}$$

+ All terms on the right hand side of the equals sign are computed from the previous time step information.

Where the superscript * denotes convected quantities. That is, the enthalpy convected by m_i in the energy equation is denoted by h* and is defined as:

$$h_i^* = h_i \quad \text{if } m_i > 0$$

$$h_i^* = h_{i+1} \quad \text{if } m_i < 0$$

The basis of the explicit solution is an explicit energy equation using flows and energies from the previous time step to form the convective terms. Consider the abgreviated forms of the cell balance equations:

Mass

$$\hat{A}_i \frac{\Delta x}{\Delta t} (\rho_i - \rho_i^n) + m_i - m_{i-1} = 0 \qquad (3.3\text{-}29)$$

Energy

$$\hat{A}_i \frac{\Delta x}{\Delta t} (\rho_i h_i - \rho_i h_i^n) + m_i h_i^* - m_{i-1} h^*_{i-1} = Q_i^n \qquad (3.3\text{-}30)$$

Momentum

$$m_i - m_i^n - \Delta t \frac{\hat{A}i}{\Delta x} (p_{i+1} - p_i) - t F_i^n \qquad (3.3\text{-}31)$$

where the superscript n denotes previous time step

By inverting the state equation, enthalpies can be expressed in terms of specific volumes, v, i.e.,[++]

$$h_i^* = h_o + \left.\frac{\partial h}{\partial v}\right|_p (v_i^* - v_o)$$

apply this equation to the energy balance yields:

$$m_i v_i^* - m_{i-1} v_{i-1}^* - \left.\frac{\partial v}{\partial h}\right|_p Q_i^n = \left(v_o - \left.\frac{\partial v}{\partial h}\right|_p h_o\right)\left(\hat{A}_i \frac{\partial x}{\partial t}(\rho_i - \rho_i^n) + m_i - m_{i-1}\right) \quad (3.3\text{-}32)$$

by continuity the right hand side equals zero.

The left side of Equation (3.3-32) is the basis of the explicit solution scheme. At the beginning of a time step the fuel model is evaluated and the explicit terms Q and F are determined. An initial estimate of $\tilde{m}$ is obtained from the momentum equation based on pressures and flows from the previous time step. When this value is used in Equation (3.3-32) there will be a residual error, E_i, that is:

$$\tilde{m}_i v_i^* - \tilde{m}_{i-1} v_{i-1}^* - \left.\frac{\partial v}{\partial h}\right|_p Q_i^n = E_i \quad (3.3\text{-}33)$$

++ h_o and v_o define a reference state close enough to h^* and v^* so that $\partial h/\partial v$ can be assumed constant between the two states.

This residual error is reduced to near zero in all computational cells by adjusting the pressure and flows in each cell in an iterative loop. The pressure change, Δp_i, needed to reduce E_i to zero in any cell is computed from $\partial E/\partial p$.

$$\Delta p_i = \frac{-E_i}{\partial E/\partial p} \tag{3.3-34}$$

The total derivative is formed by holding the specific volume constant:

$$\frac{\partial E}{\partial p_i} = \frac{\partial E}{\partial \tilde{m}_i} \frac{\partial \tilde{m}_i}{\partial p_i} + \frac{\partial E}{\partial \tilde{m}_{i-1}} \frac{\partial \tilde{m}_{i-1}}{\partial p_i}$$

The flow differentials are formed from Equation (3.3-31).

$$\frac{\partial \tilde{m}_i}{\partial p_i} = \frac{\Delta t \, \hat{\hat{A}}_i}{\Delta x} \tag{3.3-35}$$

$$\frac{\partial \tilde{m}_{i-1}}{\partial p_i} = \frac{\Delta t \, \hat{\hat{A}}_{i-1}}{\Delta x} \tag{3.3-36}$$

from Equation (3.3-33).

$$\frac{\partial E}{\partial \tilde{m}_i} = v_i^*$$

and

$$\frac{\partial E}{\partial \tilde{m}_{i-1}} = v^*_{i-1}$$

therefore

$$\frac{\partial E}{\partial p_i} = \frac{\Delta t}{\Delta x}\left[v^*_i \hat{A}_i + v^*_{i-1} A^*_{i-1}\right] \qquad (3.3\text{-}37)$$

The pressure change is computed from Equation (3.3-34) and then used to update the cell flow and density. Flows are updated by the momentum derivatives Equations (3.3-35) and (3.3-36). These updated flows are then used in the continuity equation to determine the new density and specific volume. This procedure is repeated over all cells until the maximum error, E, is less than a specified value. The solution is then considered converged.

3.3.2.4 COTRAN Fuel Model

The conductive heat transfer model used in COTRAN calculates the internal temperature distribution of the fuel rod and the surface heat flux to the adjacent fluid channel. The model[3-18], which is a combination of the Method of Weighted Residuals (MWR) in the radial coordinate and finite differences in time and the axial coordinate, can include options for axial conduction and temperature dependent fuel thermal conductivity.

Fuel Interior

The fundamental heat conduction equation is:

$$\rho c \frac{\partial T}{\partial t} = \nabla \cdot (K \nabla T) + q''' \qquad (3.3\text{-}38)$$

where

K = local thermal conductivity and

q''' = volumetric rate of heat generation in the fuel rod.

We can write this equation in cylindrical coordinates as:

$$\rho c \frac{\partial T}{\partial t} = \frac{1}{R^2 r} \frac{\partial}{\partial r} rK(T) \frac{\partial T}{\partial r} + \frac{\partial}{\partial x} K(T) \frac{\partial T}{\partial x} + q''' \qquad (3.3\text{-}39)$$

where

$r = r^1/R$

r^1 = radial coordinate

R = fuel radius

Making use of Kircoffs Transformation,

$$\theta = \frac{1}{K_o} \int_{T_o}^{T} K(T)\, dT = G(T) \qquad (3.3\text{-}40)$$

where ko is the conductivity at the reference temperature To, allows Equation (3.3-39) to be written as:

$$\rho c \frac{Ko}{K(T)} \frac{\partial \theta}{\partial t} = \frac{Ko}{R^2 r} \frac{\partial}{\partial r} r \frac{\partial \theta}{\theta r} + \frac{\partial}{\partial x} K(T) \frac{\partial T}{\partial x} + q''' \qquad (3.3\text{-}41)$$

If the radial coordinate is approximated by the symmetric polynomial of the form:

$$\theta(r) = d_1 + d_2 r^2 + d_3 r^4 + \cdots + d_n r^{2n-2} = \sum_{i=1}^{N} (r^{2i-2}) di$$

and evaluated at the N radial positions, yields,

$$\theta(r_j) = \sum_{i=1}^{N} (r_j^{2i-2}) di \qquad (3.3\text{-}42)$$

or, rewritten in matrix notation

$$\left\{\theta\right\} = \left[Q\right] \left\{d\right\}$$

where

$$Q_{ji} = r_j^{2i-2}$$

In COTRAN the radial positions (r_j) are taken to be the roots of orthogonal polynomials as defined by Finlayson (1974)[3-19]. From Equation (3.3-42) the first and second radial derivatives can be derived:

$$\frac{\partial \theta}{\partial}\bigg|_{r_j} = \sum_{i-1}^{N} (2i-2)\, r_j^{(2i-3)}\, d_i \qquad (3.3\text{-}43)$$

and

$$\frac{1}{r}\,\frac{\partial}{\partial r}\,r\,\frac{\partial \theta}{\partial r} = \sum_{i-1}^{N} (2i-2)\,(2i-2)\, r_j^{(2i-4)} d_i \qquad (3.3\text{-}44)$$

which may be written in matrix notation as:

$$\frac{\partial}{\partial r} \left\{\theta\right\} = \left[C\right]\left[Q\right]^{-1} \left\{\theta\right\} \tag{3.3-45}$$

and

$$\frac{1}{r} \frac{\partial}{\partial r} r \frac{\partial}{\partial r} \left\{\theta\right\} = \left[D\right]\left[Q\right]^{-1} \left\{\theta\right\} \tag{3.3-46}$$

where

$\left\{d\right\}$ has been replaced by $\left[Q\right]^{-1} \left\{\theta\right\}$

$C_{ji} = (2i-2)\, r_j^{2i-3}$

$D_{ji} = (2i-2)^2\, r_j^{2i-4}$

substituting Equation (3.3-46) into Equation (3.3-41 yields)

$$\rho c \frac{Ko}{K(T)} \frac{\partial \theta}{\partial t} = \frac{Ko}{R^2} \left[B\right] \left\{\theta\right\} + \frac{\partial}{\partial x} K(T) \frac{\partial T}{\partial x} + q''' \tag{3.3-47}$$

where

$$\left[B\right] = \left[D\right]\left[Q\right]^{-1}$$

Approximating the axial conduction term by a central finite difference and the time derivative by a forward finite derivative yields the heat conduction model at N-1 interior nodel positions.

$$\frac{\rho c Ko\ \theta}{\Delta t Ki} - \frac{Ko}{R^2} \sum_{1-1}^{N} B_{il}\, \theta_l = \frac{\rho c Ko}{\Delta t Ki}\, \theta_i^n + q''' \tag{3.3-48}$$

$$+ \frac{2}{\Delta x^2} \left[\frac{\tilde{T}_{j-1} - \tilde{T}_i}{\frac{1}{K_{j-1}} + \frac{1}{Ki}} + \frac{\tilde{T}_{j+1} - \tilde{T}_i}{\frac{1}{K_{j+1}} + \frac{1}{Ki}} \right]$$

Fuel Clad Interface

The boundary condition at the fuel surface is handled by a lumped resistance technique. The equation is:

$$\frac{-Ko}{R} \frac{\partial\theta}{\partial r} = H_g (T_N - T_{N+1}) \qquad (3.3\text{-}49)$$

where

T_N = fuel exterior surface temperature

T_{N+1} = clad exterior surface temperature

$$\frac{1}{H_g} = \frac{1}{H_c} + \frac{Yc}{Kc}$$

Hc = Fuel-clad gap conductance

Yc = Clad thickness

Kc = Clad conductivity

applying Equation (3.3-45) produces:

$$\frac{-Ko}{R} \sum_{1=1}^{N} A_{N_1} \theta_1 = H_g (T_N - T_{N+1}) \qquad (3.3\text{-}50)$$

where

$$[A] = [C] [Q]^{-1}$$

Cladding

A transient energy balance for the lumped clad is:

$$\rho c \frac{\partial T_{N+1}}{\partial t} = \frac{Hg}{Yc} \left(\frac{r_N}{r_{N+1}} \right) \left(T_N - T_{N+1} \right) - \frac{Hs}{Yc} \left(T_{N+1} - \tilde{T}_F \right) + Kc \frac{\partial^2 \tilde{T}_{N+1}}{\partial x^2} \qquad (3.3\text{-}51)$$

where Hs is the clad surface heat transfer coefficient and T_F is the fluid temperature. Using Kircoffs transformation, an implicit time derviative, and an explicit axial conduction term gives:

$$\frac{(\rho c)_c}{\Delta t}\ \frac{Ko}{K_{N+1}}\ \theta N+1 = \frac{(\rho c)_c}{\Delta t}\ \frac{Ko}{K_i}\ \theta^n_{N+1} + \frac{Kc}{\Delta x^2}\left(\tilde{T}_{1+1} - 2T_{N+1} + \tilde{T}_{1-1}\right) \tag{3.3-52}$$

$$+ \frac{Hg}{Yc}\left(\frac{r_N}{r_{N+1}}\right)\left(T_N - T_{N+1}\right) - \frac{Hs}{Yc}\left(T_{N+1} - \tilde{T}_F\right)$$

The implicit temperature T_N and T_{N+1} appearing in Equations (3.3-50) and 3.3-52) are evaluated by a truncated Taylor series as:

$$T = T^n - \frac{G(T^n) - \theta(T)}{G'(T^n)} \tag{3.3-53}$$

where G is defined in Equation (3.3-40) and G´ is the derivative of G with respect to T.

Solution Scheme

The boundary conditions at the fuel-clad interface Equation (3.3-50) and the clad surface Equation (3.3-52) are combined with the differential heat conduction Equation (3.3-48) to yield a matrix equation of the form

$$\left[a\right]\left\{\theta\right\} = \left[Q\right]$$

for the transformed temperatures at one axial level. These matricies (shown) in Figure 3.3-4 for a third order orthogonal collocation are solved by an iterative Gauss-Siedel procedure. Once θ is determined, the temperature solution is evaluated by Equation (3.3-53). This temperature solution is then utilized to determine a rod average fuel temperature for Doppler Feedback.

3.3.3 Description of Code Mechanics and Output Features

COTRAN will initially determine the static flux, power and hydraulic distribution corresponding to the input it has received. This includes a user specified option for an input axial power profile. When this option is selected the code will iterate on control density in each node until the desired power shape is achieved. If no transient calculations are to be performed the code will edit the results, punch out control densities and fluxes for a restart if so desired, and exit. If transient calculations are to be made, equilibrium precursor concentrations will be determined and all production corss sections will be divided by the calculated K_{eff} to insure $K_{eff} = 1.000$ at the beginning of the transient.

The initial time step size is 0.0001 seconds for the explicit solution (0.005 seconds for the implicit solution). The forcing functions are updated and the new thermal-hydraulic solution determined. This solution is used to update the cross sections and a new flux calculation is made. At the end of each time step the precursor densities are

updated for the next time period. The input variable LATCH is used to control the time step size and thus relieve the user of choosing time step sizes. The time step size is doubled after LATCH time steps have been taken consecutively during which the number of flux iterations to achieve convergence has not exceeded 25. If at any time more than 60 iterations are required, the time step is halved. This scheme permits small time steps during times of large changes in power level and inversely, large time steps during periods of slow change.

3.3.4 Input and Use of Cross Sections

COTRAN requires two sets of two group macroscopic cross sections for each fuel type in the problem. These cross section sets describe the material in its entirely uncontrolled and completely controlled states [ ]. A control density array can then be input by the user or calculated by the code to describe the initial conditions of the core. Linear interpolation is utilized to determine the cross sections for each fuel node at a given control density and void fraction. [

]. The bases for requiring two group cross sections as input is that normally only

the fast neutron group cross sections vary with fuel temperature.[3-20,3-21] Primarily the fast absorption and slowing down cross sections are affected by fuel temperature. COTRAN, therefore, allows the two group cross section values to change with fuel temperature (based on the average nodal fuel temperature at each time step) and then collapses to new one group values for the next solution. This feature allows a COTRAN calculation to exhibit many of the characteristics of a two group solution at the much reduced computer time of a one group neutron diffusion theory code.

It has been found that the fast neutron cross sections affected by fuel temperature vary linearly as the square root of the fuel temperature (^{o}K).[3-21] These rates of change cross sections with fuel temperature are input for each material type.

[

].

The input cross section tables for COTRAN are calculated using XTGBWR. [

]

3.4 MULTIGROUP DIFFUSION THEORY MODEL (XDT)

The Exxon Nuclear model used to perform multigroup diffusion theory calculations for BWR fuel assemblies is the XDT code. The XDT code was developed from the 2DB[3-22] code that was written for fast reactor multigroup calculations.

Table 3.3.1 Definitions of Variables for Thermal-Hydraulic Solutions

Symbol	Description and Units	Definition
m	Axial mass flow rate, (lb/sec)	$m = \langle \rho u \rangle A$
ρ	Mixture density, (lb/ft^3)	$\rho = \langle\langle \rho \rangle\rangle_v + (1-\alpha)\rho_\ell$
$\hat{\rho}$	Two-phase momentum density, (lb/ft^3)	$\hat{\rho} = \frac{\langle \rho u \rangle^2}{\langle \rho u^2 \rangle}$
	In terms of void-quality	$\frac{1}{\rho} = \frac{(1-x)^2}{\rho_\ell (1-\alpha)} + \frac{x^2}{\rho_v \alpha}$
$\hat{v}$	Momentum specific volume, (ft^3/lb)	$\hat{v} = \frac{1}{\hat{\rho}}$
v	Mixture specific volume, (ft^3/lb)	$v = 1/\rho$
	In terms of static quality	$v = xv_v + (1-x)v_\ell$
h	Mixture enthalpy, (Btu/lb)	$h = \frac{\langle\langle \rho h \rangle\rangle}{\langle\langle \rho \rangle\rangle}$
	In terms of static quality	$h = xh_v + (1-x)h_\ell$
$\hat{h}$	Flowing enthalpy, (Btu/lb)	$\hat{h} \simeq \langle \rho u h \rangle / \langle \rho u \rangle$
	In terms of flowing quality	$\hat{h} = \hat{x}h_v + (1-\hat{x})h_\ell$
$\hat{x}$	Flowing quality	$\hat{x} = \langle \alpha \rho_v u_v \rangle / m$
x	Static qualtiy (vapor mass fraction)	$x = \langle\langle \alpha \rho_v \rangle\rangle / \rho$
ψ	Function defining relationship between h and $\hat{h}$, (lb/ft^3)	$\psi = \rho_\ell x(1-\alpha) - \rho_v \alpha (1-x)$
α	Vapor volume fraction	$\alpha = (\rho_\ell - \rho)/(\rho_\ell - \rho_v)$
u	Axial velocity, (ft/sec)	$u = \langle \rho u \rangle / \rho = m/\rho A$
P	Pressure, (lb_f/ft^2)	$P = P_v = P_\ell$
A	Subchannel flow area, (ft^2)	

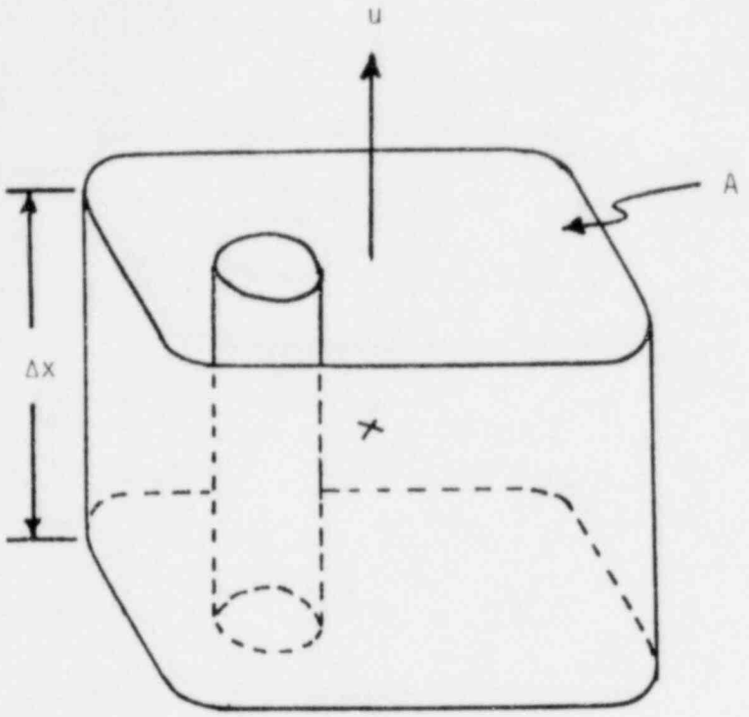

Figure 3.3-1 Channel Control Volume for Thermal-Hydraulic Balance Equations

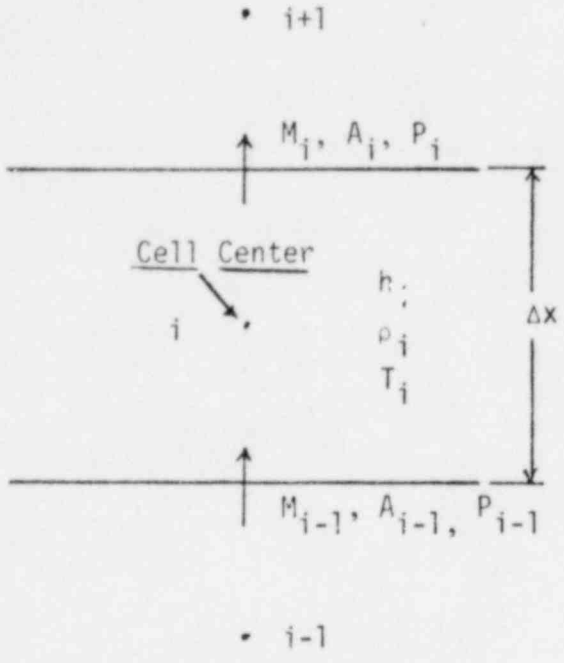

Figure 3.3-2 Placement of Variables for Implicit Solution

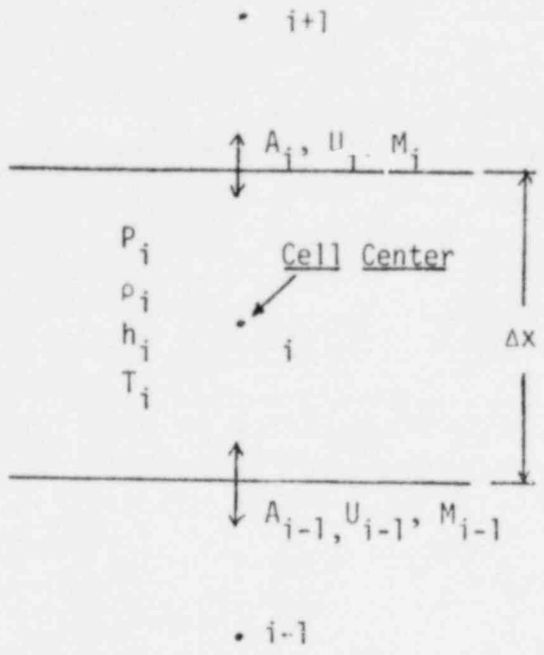

Figure 3.3-3 Placement of Variables for Explicit Solution

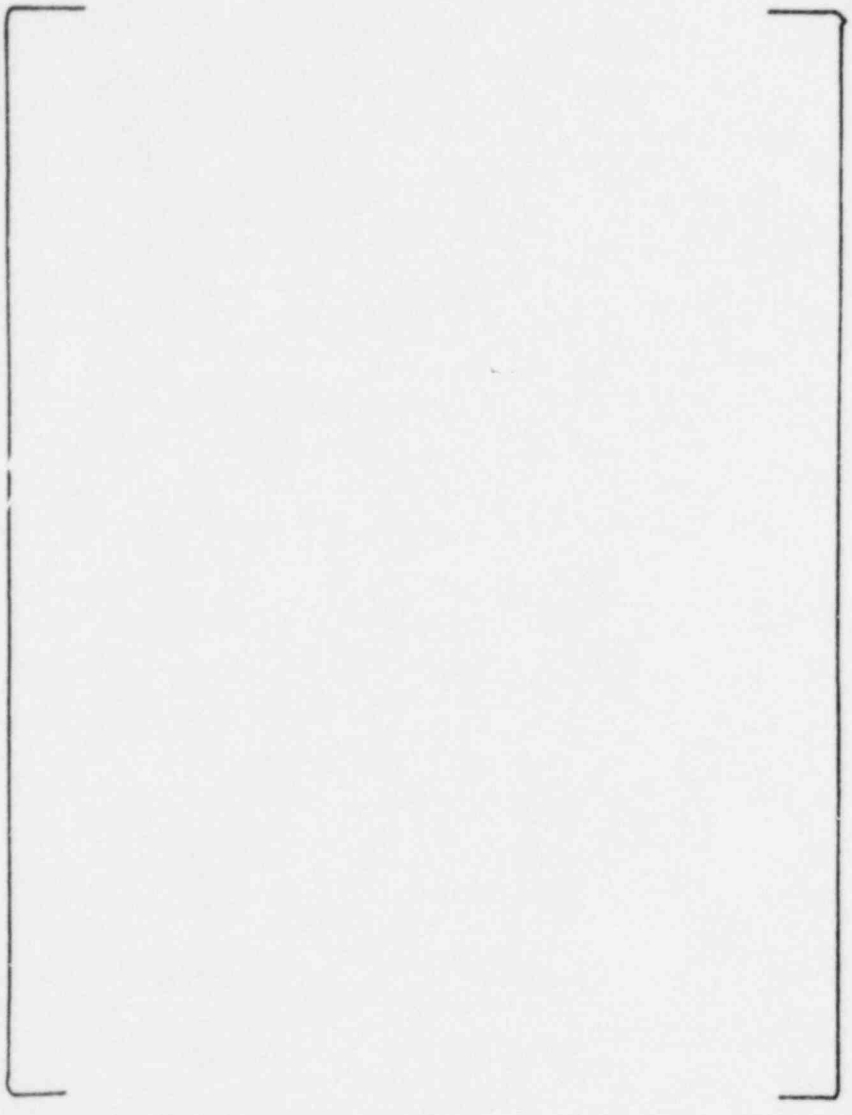

Figure 3.3-4 Matrix Elements for Third Order Collocation

The XDT code is used to perform special diffusion theory calculations such as four and sixteen bundle calculations, fuel misloading calculations, and incore detector calculations. The cross sections for the XDT code are generated by the XFYRE depletion model.

The XDT code calculates the eigenvalue, relative powers, multigroup neutron fluxes, and flux and volume weighted cross sections.

Eigenvalues are computed in XDT by standard source-iteration techniques. Group rebalancing and successive over-relaxation with line inverson are used to accelerate convergence. Adjoint solutions are obtained by inverting the input data and redefining the source terms.

Variable dimensioning is used to make maximum use of the available fast memory. Since only one energy group is in the fast memory at any given time, the storage requirements are insensitive to the number of energy groups.

Neutron Balance Equations

The multigroup diffusion equations can be written in the form

$$D_g \nabla^2 \phi g - \Sigma_g^r \phi_g + S_g = 0, \; g = 1, \ldots N \qquad (3.4\text{-}1)$$

where

$$S_g = \frac{\chi_g}{k_{eff}} \sum_{g'=1}^{N} (\nu\Sigma_f)_{g'} \phi_{g'} + \sum_{g'=1}^{g-1} \Sigma(g' \rightarrow g) \; \phi_{g'} \qquad (3.4\text{-}2)$$

and:

N = number of energy groups,

g = energy group index,

ϕg = flux in group g,

S_g = source in group g,

D_g = diffusion constant for gourp g (= $1/3\ \Sigma_g^{tr}$),

$(\nu\Sigma_f)_g$ = fission source cross section for group g,

$\Sigma(g' \rightarrow g)$ = group transfer cross section from g′ to g,

Σ_g^r = removal cross section from group g

$$= \left[\Sigma_g^a + \sum_{g'=g+1}^{N} \Sigma(g \rightarrow g') \right],$$

x_g = fission source fraction in group g,

K_{eff} = effective multiplication constant.

The mesh points in the XTD code are located in the center of the homogeneous mesh interval (see Figure 3.4-1). This choise leads to a more clean-out calculation and interpretation of all reaction rates.

The spatical difference equations are obtained by integrating Equations (3.4-1) and (3.4-2) over the volume associated with each mesh point. For the (i,j) mesh point shown in Figure 3.4-1, the radial integration would be from $(R_i - \frac{\delta R_i}{2})$ to $(R_i + \frac{\delta R_i}{2})$, and the axial integration would be from $(Z_j - \frac{\delta Z_j}{2})$ to $(Z_j + \frac{\delta Z_j}{2})$.

The leakage terms are obtained by first transforming the volume integral over the Laplacian to a surface integral using Green's theorem,

$$\int DA^2\phi dV = \int D\vec{\nabla}\phi \cdot d\vec{A} . \tag{3.4-3}$$

The flux gradients at the mesh boundary are obtained by interpolating the two contiguous flux values, Thus, volume integration of Equation (3.4-1) for mesh point o (see Figure 3.4-1) leads to the expression

$$\sum_{k=1}^{4} \frac{\bar{D}_k A_k}{\ell_k} (\phi_k - \phi_o) - \Sigma_o^r \phi_o V_o + S_o V_o = 0, \tag{3.4-4}$$

where, for simplicity, the gourp indices have been omitted, and

Σ_o^r = removal cross section associated with mesh point o,

S_o = source rate associated with mesh point o,

V_o = volume associated with mesh point o,

ϕ_k = flux associated with mesh point k,

ℓ_k = distance between mesh point k and mesh point o,

A_k = area of boundary between mesh point k and mesh point o,

$\bar{D}_k$ = effective diffusion constant between mesh point k and mesh point o

$$\bar{D}_k = \frac{D_o D_k (\delta R_o + \delta R_k)}{D_o \delta R_k + D_k \delta R_o} . \tag{3.4-5}$$

Finally, Equation (3.4-4) can be recase into a form more convenient for performing flux iterations. That is

$$\phi_o = \frac{S_o V_o + \sum_{k=1}^{4} C_k \phi_k}{C_5} \quad , \tag{3.4-6}$$

where

$$C_k = \frac{\bar{D}_k A_k}{\ell_k} \quad k=1, \ldots 4 \quad , \tag{3.4-7}$$

and

$$C_5 = \Sigma_o^r V_o + \sum_{k=1}^{4} C_k \quad . \tag{3.4-8}$$

Discussion of Boundary Conditions

Three standard conditions are available in XDT: $\vec{\nabla}\phi = 0$, $\phi = 0$, and periodic. These are described below using a slight modification to the nomenclature developed in the foregoing sections.

Zero Flux Gradient

Consider the left hand boundary of the one-dimensional reactor shown in Figure 3.4-2. Let us now imagine that a pseudo mesh interval, interval o, has been added on the left hand side of the boundary with the same composition and thickness of interval 1. Clearly, then if $\vec{\nabla}\phi = 0$ at the boundary, $\phi_o = \phi_1$. Therefore, since $(\phi_o - \phi)$ vanishes, the coefficient of $\phi_o - \phi_1$, C_1 (see Equation (3.4-4)), is immaterial--hence C_1 can be set equal to zero. The calculation is performed assuming that ϕ_o does not exist and $C_1 = 0$.

Zero Flux

Again, imagine that a pseudo mesh interval with the same composition as interval IM has been added to the right hand side of the right boundary. Now, since $\phi_{IM} \neq 0$ and $\phi_{IM+1} = 0$, the coefficient of $(\phi_{IM}-\phi_{IM+1})$ in Equation 3.4-4 cannot be disregarded. In fact, from Equation (3.4-7), it is clear that

$$C_K = \frac{D_K A_K}{.5\ \delta R_{IM} + .71\ \lambda_{tr}} \tag{3.4-9}$$

where λ_{tr} is assumed to equal $1/\Sigma_{tr}$.

Note, as in the $\vec{\nabla}\phi = 0$ case, that there is no contribution of the pseudo flux in Equation (3.46). For a zero flux gradient, $C_K = 0$; whereas for a zero flux, $\phi_K = 0$.

Periodic Flux

Period boundary conditions are available for the top, bottom, left and right boundaries. In this option,

$$\phi_o = \phi_{IM} \tag{3.4-10}$$

$$\phi_1 = \phi_{IM+1} \tag{3.4-11}$$

and

$$C_K(1\text{-}IM) \quad \frac{\bar{D}_K A_K}{.5(\delta R_1 + \delta R_{IM})} \tag{3.4-12}$$

It should be stressed that the pseudo mesh intervals discussed above are not in any way a part of the code. They are mentioned here only for heuristic purposes.

Solution of Different Equations

The eignvalue and flux profiles are computed by standard source-iteration techniques, i.e., by using an initial fission source distribution, the flux profiles in each gorup are sequentially computed beginning in the top (highest energy) group. After the new fluxes for all groups have been calculated, a new fission source distribution is computed from the new flux profiles. The mulitplication ratio, λ, is then obtained by simply taking the ratio of the new fission source rate to the old (previous iteration) fission source rate. The above sequence of events is called an outer iteration.

Before each new outer iteration, the fission spectrum is multiplied by $1/\lambda$, so that λ approaches unity as the iteration proceeds. The effective multiplication constant is simply the product of the successive λ's. Convergence is assumed when $|1-\lambda| < \varepsilon$, where ε is an input parameter.

Fission source over-relaxation is employed in XDT to accelerate convergence. The procedure is as follows: After the new fission source rate profile, $F_1^{\nu+1}$, is calculated, a second "new" value, $F_2^{\nu+1}$, is computed by magnifying the difference between the new fission source rate and the old fission source rate. Thus,

$$F_2^{\nu+1} = F^{\nu} + \beta(F_1^{\nu+1} - F^{\nu}) , \qquad (3.4\text{-}13)$$

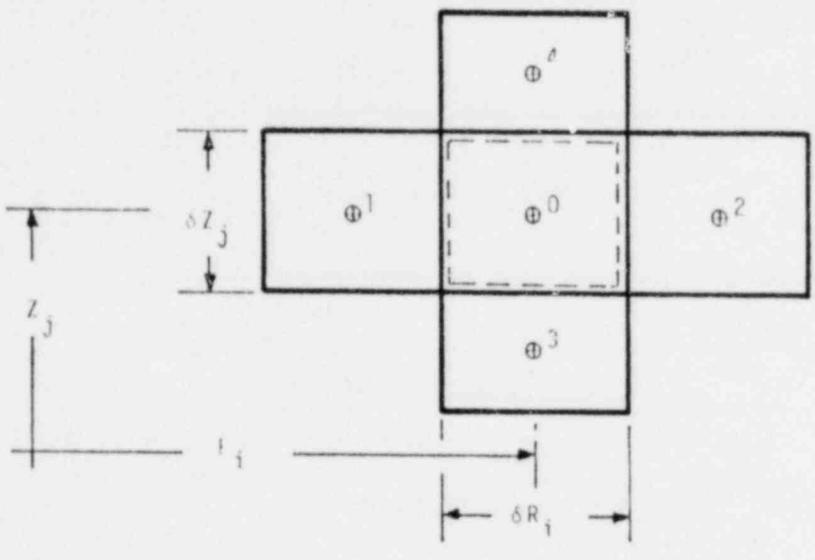

Figure 3.4-1 Mesh Description

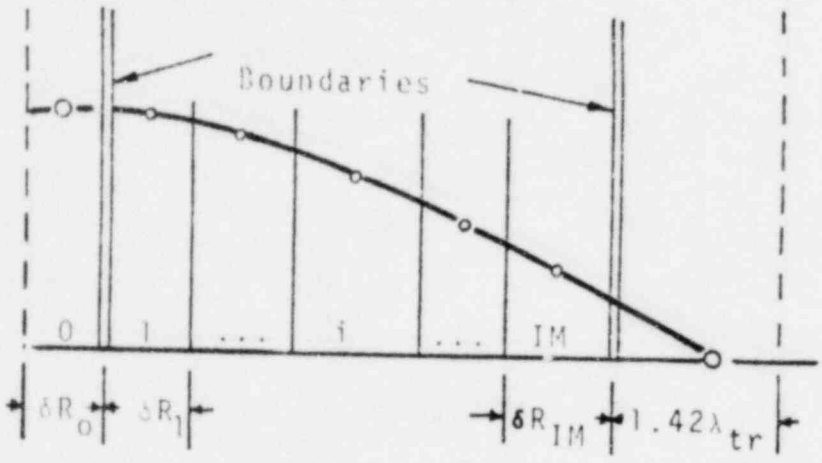

Figure 3.4-2 Schematic Diagram of 1-D Reactor

where β' is the fission source over-relaxation factor. $F_2^{\nu+1}$ is then normalized to give the same total source as $F_1^{\nu+1}$.

The group-fluxes are computed using successive line over-relaxaton (SLOR). That is, the fluxes on each vertical (or horizontal) line are simultaneously computer (by the familiar Crout reduction technique) and then over relazed using the algorithm

$$\phi^{\nu+1} = \phi^{\nu} + \beta(\phi^{\nu+1}-\phi^{\nu}) \quad , \tag{3.4-14}$$

where β is the over-relaxation factor. In R-θ problems or problems involving periodic boundary conditions, direct inversion is performed on veritical lines beginning at the left boundary and proceeding by column to the right boundary. In triangular problems, direct inversion is performed along horizontal lines beginning at the bottom boundary and proceeding by row to the top boundary. In all other situations, direct inversion is used along the dimension with the most mesh points. One mesh sweep is defined as one inner iteration.

The flux over-relaxation factor, β, is an input parameter. The fission source over-relaxation factor, β', is computed internally from the ad hoc expression

$$\beta' = 1.0 + .6(\beta-1) \ . \tag{3.4-15}$$

The flux in each group is normalized (by balancing the total source and loss rate) immediately before each group-flux calculation. Thus, one-region problem with zero-gradient boundary conditions would be solved exactly in one outer iteration.

It should be mentioned that an altering direction SLOR scheme (single line inversion for rows and then columns in alternation) is included as an option to enhance convergence for problems involving tight mesh spacing in both dimensions.

3.5 MONTE CARLO MODEL (XMC)

The Exxon Monte Carlo Code (XMC) is a general purpose Monte Carlo code developed from the Battelle Monte Carlo Code (BMC)[3-23]. XMC was designed to calculate thermal reactor benchmark problems. XMC is capable of describing the exact geometrical description of a light water fuel assembly. This geometrical capability and a coupled space-energy solution of the transport equation makes the Monte Carlo method in XMC a highly accurate method for evaluating key nuclear parameters and the effects of water gaps, control blades and burnable poison rods in light water reactor fuel bundle.

XMC uses basic cross section and neutron scattering data to calculate the various neutronic events. Thus, its accuracy is limited only by the accuracy of the basic cross sections and the number of neutron histories which are run for each problem.

The neutron flux, reaction rates by isotope and region, group-averaged cross sections, neutron leakage rates, and the standard deviation for each of these parameters are calculated in three dimensional space over the energy range from 0 to 10 MeV. The reaction types included are fission, capture, inelastic scattering, n-2n scattering, elastic scattering with

isotropic or anisotropic angular distributions, and thermal scattering based on a scattering law generated using the Haywood[3-3] representation of the phonon spectrum for water. The energy distribution of the neutrons is continuous. However, the cross sections are averaged over 190 microscopic energy groups. Resolved resonance cross sections are calculated by the code for each neutron energy using the Doppler-broadened Breit-Wigner single-level formula.

The isotopic material cross sections are processed from the ENDF/B format[3-2]. The data can be provided either from the Battelle Master Library[3-1], from the ENDF/B Library, or from any source which can be put into the ENDF/B format.

The XMC code geometry routines can handle any region that can be enclosed by a set of boundaries of the general form

$$A(x-x_0)^2+B(y-y_0)^2 + C(z-z_0)^2-K = 0.$$

Provisions are included for several special forms of the above equations including planes, cylinders and spheres. Also, there is a special region geometry routine for a rectangular lattice of clad fuel rods.

Statistics for the values calculated are obtained by making a series of calculations on equal sized sets of neutron histories called "batches" and averaging the results from each batch. The initial space-velocity-angle coordinates for each neutron of a batch are either picked from a random source distribution or from the fission particles produced by the previous batch.

Neutron absorption is accounted for by reducing the weight of the neutron at each collision. When the weight has been reduced sufficiently the neutron are terminated by a Russian Roulette process.

3.5.1 The XMC Code Package

The XMC code package consists of two parts: the Monte Carlo code and the cross-section data library with the processing support codes, XMCLIB and LIBR. The general flow diagram for the XMC code package is shown in Figure 3.5-1. The XMCLIB code uses isotopic or material cross sections and reaction rates data to prepare a cumulative cross section library (CCT). The data is obtained from a library tape which is written in the ENDF/B format. The CCT library tape is saved between problems. New isotopes can be added to an old CCT tape. Changes to the CCT tape are made using the LIBR code. A list of the isotopes available in XMC is given in Table 3.5-1.

The XMC code consists of three segments or overlays comprised of the input routines, the Monte Carlo routines and the output routines. The input routines use card input and the CCT library tape to prepare the data needed by the Monte Carlo and output routines. The Monte Carlo routines are then loaded and the Monte Carlo calculation performed. The output routines are used to process, print, and/or plot the Monte Carlo output. Statistics are calculated for the various output values.

The next section describes the theory and techniques which are used in the Monte Carlo calculation. Following this, some of the major Monte Carlo routines are described along with the input-output, and the XMC loader routine.

3.5.2 The XMC Monte Carlo Routines

The flow diagram shown in Figure 3.5-2 describes the sequence of events to follow the histories of a "batch" of neutrons. This figure describes the path followed if importance weighting is not being used. The XMC code uses a "beam" type Monte Carlo technique instead of a "particle" method. It starts each track with a beam of neutrons. The beam is used for tallying the flux, leakage, and reaction rates. The beam strength is reduced by the negative exponential of the mean free path traveled between each collision. A beam is followed until it is terminated either by leakage or by Russian Roulette.

The neutron history is initiated by generating a starting location for the neutron beam. The region, the distance to the next boundary, the material type, the mean free path for the material and the region tally number are determined for this location. If a resonance calculation is required the resonance routines are called and the cross section value is added to the total cross section. The distance-to-collision is compared to the number of mean free paths to the boundary. Neutrons are either moved to the collision point or the region boundary which ever is nearer. If a

collision occurs the collision routine checks to see if a fission occurred and stores the fission neutrons in the fission bank. The collision routine uses the probability of nonabsorption to reduce the beam weight and determine if the beam is to be tracked further. It then determines the scattering nuclide and scattering event. A new direction and velocity are calculated and the scattered neutrons are stored. As the Monte Carlo calculation progresses, the flux, leakage, and reaction rates are tallied.

The flow of the calculation is altered slightly if region importance weighting is being used. The main difference is that the calculation-of-distance-to-collision is made after the mean free path is obtained and must be made again in each region.

3.5.3 Treatment of Neutron Absorption

Neutron absorption is accounted for by reducing the importance weighting of a neutron by the absorption probability at each collision. The reduction is done by multiplying the weight before the collision by the non-absorption probability (P_{na}) for the collision. This process can be written as $Wt' = Wt \times P_{na}$. The non-absorption probability can be defined as the total scattering neutron production divided by the total cross section or

$$P_{na} = \frac{\sum_s + \sum_{in} + 2\sum_{n-2n}}{\sum_T}$$

For a n-2n scattering event the extra neutron is treated as negative absorption. Since the weight will never become zero, the code terminates neutrons using the method previously stated. These are Russion Roulette and "weight ratioing".

Russian Roulette.

Russion Roulette, as the name implies, uses chance to determine if a neutron survives. The Russion Roulette routine is only used if the importance weighting of a neutron has been reduced below the minimum weight. Given a minimum weight (Wt_{min}) and a survival weight (Wt_s), Russian Roulette is performed by picking a random number (ξ) between 0 and 1. If the ratio of the neutron weight to the survival weight is greater than the random number, then the neutron is given the survival weight, otherwise the weight is set to zero and the tracking is terminated. This can be written as

$$\text{if } Wt < Wt_{min} \text{ and if } \xi \leq \frac{Wt}{Wt_s} \text{ then set } Wt = Wt_s$$

$$\text{but if } \xi > \frac{Wt}{Wt_s} \text{ then set } Wt = 0 \text{ and terminates the neutron.}$$

On the average, with a large number of samples, the weight will be preserved by this method.

Weight Ratioing

For systems which are very thermal it may take a very large number of collisions to terminate neutrons by using Russian Roulette. This

is because the weight reduction at each collision is very small; i.e., $P_{na} \simeq 1$. Often this results in obtaining answers concerning thermal parameters that which are statistically very accurate while the accuracy of the epithermal parameters is very poor. A method called "weight ratioing" was devised to allow control of the time spent in the thermal range compared to the epithermal range.

Weight ratioing uses two flux tally sets: one tally set for neutrons slowing down and one for neutrons that have been slowed down past an entry energy (E_{th}). The neutrons reaching the thermal tally range (second tally set) can have their energy increased above E_{th} but the results are still tallied into the thermal tally set.

The weight ratioing method tallies the results of a neutron history into tally set 1 until it is slowed down past the energy E_{th}. Russian Roulette is then played with each neutron so that R_{th} neutrons entering the thermal tally set are rejected for each one entering the thermal tally range. The ones that survive are followed and the results tallied into a second tally set. The final tallies are the sums of the values from the first tally set plus the values from the second tally set times a weight ratio. This ratio is the weight entering the thermal tally range divided by the weight lost by neutrons followed in the thermal tally range or approximately $1/(1-R_{th})$. This method statistically conserves the neutron absorption and allows a way of controlling the statistics obtained for epithermal parameters relative to those obtained for thermal parameters.

3.5.4 The Neutron Flux and the Neutron Beam

The neutron flux at energy E integrated over volume and energy is the total neutron track length in the volume, or

$$\phi_{if} = \int_{V_f}\int_{E_i} \phi(E,V)dEdV = \sum_{n=1}^{N} \ell_n Wt_n$$

where V_f is the volume of region f, ℓ_n is the track length and Wt_n is the weight of the n'th neutron in region f and energy group i. Note that the reaction rate for the k'th event is $R_{i,f,k} = \Sigma_{i,f,k}\phi_{if}$ where $\Sigma_{i,f,k}$ is the macroscopic cross section.

Instead of tallying the track length of individual neutrons the XMC code tallies the estimated track length for a beam of neutrons going in the same direction as the individual neutron. The flux contribution to a region and energy group can be written as

$$\phi_{if} = \sum_{n=1}^{N} \lambda_{if}\, I_n(1-\exp(-S_{bn}/\lambda_{if}))$$

where λ_{if} is the mean free path in the i'th energy group of region f, S_{bn} is the distance to the outside boundary of the region for the n'th beam, and I_n is the beam strength at the beginning of the n'th flight of the beam. The beam strength is set equal to the weight of the neutron at the start of the neutron path. It is then diminished by the factor $\exp(-S_{bn}/\lambda_{if})$ at each boundary crossing. Note that the neutron is followed until it has a collision.

or leaks from the cell while the beam is followed even after the collision. If the neutron leaks then the beam is also terminated; otherwise the beam is tracked until terminated by Russian Roulette.

The leakage tallied by the beam crossing a boundary is just the beam strength, I, at the boundary. The leakage is tallied as a function of the broad-energy groups.

The XMC code has provisions for zone importance weighting. Zone importance weighting provides a method for spending more time in regions (zones) of greater importance while reducing the time spent in regions of low importance. When importance weighting is used the number of neutrons in the beam and the weight of each neutron is modified when the beam passes between regions of different importance.

The XMC code can be used in two problem modes. One mode, the fission descendant problem, allows fission neutrons to be born as a result of collisions. These fission progeny are stored and used as starting neutrons for the next batch. The other mode, called the direct source problem, obtains all starting neutrons from the source routine. In this case, there is no need to save the fission neutrons, so the fission reaction is not sampled.

Associated with each neutron is a set of parameters which describe its position, direction, and velocity. The position is described by the position vector x,y,z where the units are in centimeters and an index

which tells which geometrical region the neutron is in. The direction is defined by the three normalized direction cosines α, β, and γ. The velocity is defined by the microscopic energy-velocity group which the velocity falls into. The velocity units are centimeters per micro second.

3.5.5 Energy Group Structures

The energy range for XMC is from 0 to 10 MeV or any part of this energy range. The neutron energy-velocity distribution is continuous in the XMC calculation; however, the energy dependent input is divided into energy groups. There are two different energy group structures; these are the micro-groups, and broad-groups.

The micro-group is the smallest energy group structure. The cross sections and reaction probabilities are group-averaged over each micro-group. The code uses the micro-averaged values for any velocity which falls within the velocity limits of the micro-group. The fluxes are also tallied for each micro-group.

Most calculations with the XMC code use 190 energy groups with 60 groups below 1 ev. Above 1 ev the groups are equally spaced in lethargy.

The broad-groups are the energy groups used for output. The boundaries of the broad-groups must coincide with those of the micro-groups but each broad-group may contain one or more micro-groups. The

broad-group structure is usually picked to coincide with a group structure used by typical multi-group reactor cell codes. The leakage and reaction rate tallies are made by broad-group.

3.5.6 Code Check Tallies

A set of values are tallied as the Monte Carlo calculation is being made which serve as code check tallies. They are a set of values which are not needed as output, but serve as a means of checking the performance and characteristics of the Monte Carlo code. The code check tallies are obtained directly from the neutron histories and are not results obtained using the flux estimator. The answers obtained using the code check tallies are usually not as accurate as those obtained using the flux estimators.

The code check tallies include such things as the number of initial fission or source neutrons, the number and weight of neutrons to and from collision, the number of neutrons leaking from the system, the loss of beam strength and weight by application of Russian Roulette, and the number and weight of neutrons entering, and leaving the thermal tally range, etc.

The code check tallies are written out at the completion of each Monte Carlo batch. Average values with associated statistical errors are also written by the output routines.

3.5.7 The Source Routine

The source routine is used to pick the initial parameters for the neutron histories. If the calculation is a fission descendant problem, the source routine will only be used for the first batch and only the

spatial parameters will be picked. For a direct source problem, all the parameters are generated by the source routine.

The source routine in the XMC code is very versatile. It allows the selection of the neutron spatial distribution using combinations of point, equal volume, cosine $\frac{\pi}{2}\frac{r}{R}$, J_o (2.405 r/R), and $(\sin\pi r)/\pi r$ distributions. The velocities can be picked using combinations of point, fission, Maxwellian, and/or slowing down distributions. The angular distribution is either isotopic or mono-directional.

3.5.8 The XMC Geometry Routines

The geometry routine determines the region that the neutron-beam is in and calculates the distance to the nearest boundary. This routine also contains the boundary conditions. The routine follows source, fission or collision neutrons and determines if these neutrons collide in the region, leave the region, or encounter a boundary. If a boundary is encountered the neutron can leak or be reflected isotropically or with a mirror image reflection.

There are geometrically eight types of boundarys which can be used. Table 3.5-2 lists these boundary functions.

3.5.9 Path Length Calculation

The distance from one collision to the next collision is determined by randomly sampling from the distribution $P(\lambda)d\lambda = \exp(-\lambda)\, d\lambda$ where λ is the mean free path for the appropriate region and energy.

The mean free path (λ) is stored for each material and micro group. If the material contains resonances and the energy is in the resonance region, the values of the resonance cross sections are calculated. The resonance cross sections are then combined with the micro group cross sections to obtain the mean free path. The equations explicitly include the Doppler broadening of both absorption and scattering. The values of the cross sections are calculated at the neutron energy on a point basis (ie, not at the micro-group energy).

In the unresolved resonance region, the cross section for a given energy is obtained from the contribution of the two nearest resonances. In this region the value of Γ_n is found from a Porter-Thomas distribution while Γ_f is taken from an exponential distribution. The nearest resonances to a given energy are found from the level spacing.

3.5.10 The XMC Collision Routines

When a collision occurs the code considers the following events: absorption, fission, inelastic scattering, and elastic scattering. The elastic scattering can be treated as isotropic or anisotropic slowing down scattering. Thermal scattering is treated by ENDF/B kernels.

Neutron Absorption and Fission

XMC first reduces the neutron weight to account for absorption. Then the code checks to see if a scattered neutron is to be produced. The fission probability is checked to see if any fission neutrons were produced. N fission neutrons are produced if $wt.P_f+\xi \geq N$ where ξ is a

random number and P_f is the ratio of the neutron fission production rate ($\nu\Sigma_f$) to the total reaction rate (Σ_T) in the material. Note that N will seldom be greater than 1. The fission neutrons are stored in the fission bank.

Selection of Scatterer

If the neutron survived absorption then the scattering isotope is selected. To save computer space and time use is made of a "heavy scatterer." More than one isotope in a material can be specified as heavy isotopes. All of the heavy isotopes elastic scattering cross sections are combined to form one elastic scatterer. A mass for the heavy scatterer is also specified. Scattering from a heavy scatterer is treated as if the scattering mass were infinite (no energy change) unless the neutron is in a region having an isotope with resonance parameters and the neutron has a velocity such that a resonance calculation was made. Then the mass of the special heavy scatterer will be used.

The scatterer is picked by selecting a random number ξ and comparing it to the cumulative scattering probabilities.

Inelastic Scattering

Inelastic scattering is treated in two ways and the n-2n scattering is combined with it. The two models used for inelastic scattering are discrete level energy loss and the evaporation model. Both models assume that scattering is isotropic in the center of mass system.

Inelastic Spectrum Table

The inelastic spectrum table (discrete energy loss) uses a table of the inelastic excitation level energies along with a probability for each one. If the neutron energy is below a certain excitation energy that level can not be excited. An approximation is made in that it is assumed that cross section for excitation of a certain level is a constant in energy above the level energy.

Evaporation Model

The evaporation model is used to select the emergent energy from the Maxwellian distribution

$$P(E') = \frac{E'}{T_n^2} e^{-E'/T_n}.$$

Actually $(V')^2 = 1.91322\ E'$ is selected. T_n is the nuclear temperature and is calculated by $T_n = a_0 + a_1V + a_2V^2 + a_3V^3$. The coefficients a_0, a_1, a_2, a_3 are fitted by least squares to the data on the ENDF/B library for T_n. The new velocity is then calculated as

$$V' = \left[T_n(\phi_1 + \phi_2)\right]^{1/2}$$

where ϕ_1 and ϕ_2 are random numbers selected from an exponential distribution. It is also required that $V' \leq V$. The Maxwellian is sampled correctly as shown in the equation

$$P(x) = \int_0^x e^{-y} e^{-(x-y)} dy = xe^{-x}.$$

It is assumed that the evaporation model is used only for heavy nuclei and so the conversion from the C.M. to the lab system is not made.

Nonthermal Elastic Scattering

Nonthermal elastic scattering can be treated as isotropic or anisotropic. If the scattering is isotropic, a random set of direction cosines are used as the new direction cosines in the center of mass. For anisotropic scattering the cosine of the scattering angle, μ is selected by making use of the sample rejection technique.

Once the new scattering cosine μ is selected, the new velocity and the direction cosines are selected. If the isotope is a heavy scatterer the velocity is not changed.

Thermal Elastic Scattering

The thermal elastic scattering cross sections are processed from the ENDF/D data files using the FLANGE[3-4] code. In particular, data for neutron scattering by hydrogen in water has been tabulated at temperatures from 273^{o}K to 800^{o}K based on the Haywood model of the phonon spectrum. The Haywood model takes into account the effects of the vibrational and rotational modes of hydrogen atoms bound in the water molecule.

The scattering kernel calculated from $S(\alpha, \beta, T)$ is too large to use directly in the Monte Carlo calculation. Thus, the scattering kernel is divided into downscattering and upscattering components. Then, the two dimensional array based on $S(\alpha, \beta)$ is used to determine the scattering angle. The upscattering, downscattering, and angular components were

calculated at a number of points using a modified version of FLANGE. Data points were then picked so that an accurate linear interpolation could be used. The base data was calculated at 276^{o}K. Correction factors are used for higher temperatures. The FLANGE calculations were made at the ENDF/B data temperatures.

3.5.11 The XMC Output Routines

The XMC output routines prepare the output and print it and/or plot it. The two main tasks in preparing the output are preparing averaged values of fluxes, cross sections, reaction rates,and leakages along with some other cell parameters and obtaining statistics for the values which are calculated.

Statistics

Statistics are obtained by processing a series of equal sized batches and averaging the results for the batches. It is possible to leave some of the first batches out of the average. This might be done to damp out the effects of the source distribution. There are two common types of average values obtained from the Monte Carlo calculation. One type is a direct answer such as flux or reaction rate and the other type is a ratio such as flux averaged cross sections. The statistical error for a single averaged value $\bar{a}$ is $S_{\bar{a}}$ where $S_{\bar{a}}$ is the error for one standard deviation. Let N be the number of equal sized batches and a_n be the value of a for the n^{th} batch. The values of $\bar{a}$ and $S_{\bar{a}}$ then become:

$$\bar{a} = \frac{1}{N} \sum_{n=1}^{N} a_n$$

and

$$S_{\bar{a}} = \left[\left\{ \sum_{n=1}^{N} a_n^2 - N\,(\bar{a})^2 \right\} / N\,(N-1) \right]^{1/2}$$

$$= \left[\left\{ \sum_{n=1}^{N} a_n^2 - \left(\sum_{n=1}^{N} a_n \right)^2 / N \right\} / N(N-1) \right]^{1/2}$$

The statistical error for a ratio R is

$$S_R = \left[\sum_{n=1}^{N} a_n^2 - 2R \sum_{n=1}^{N} a_n b_n + R^2 \sum_{n=1}^{N} b_n^2 \right]^{1/2} / \sum_{n=1}^{N} b_n,$$

where

$$R = \sum_{n=1}^{N} a_n / \sum_{n=1}^{N} b_n.$$

Note that for a ratio the values of a and of b may have large statistical errors and the statistical error of the ratio can be very small or even zero. This is accounted for by the correlation term

$$\left(-2R \sum_{n=1}^{N} a_n b_n\right).$$

The statistical error is written out in a way which reduces the printing space. The statistical error is forced to have the same exponent as the value. If a value and its error were $1.0685 \times 10^4 \pm 5.2 \times 10^2$ then the numbers would be printed out as 1.0685+04 0.052.

Broad Energy Averaging Groups

The output routines tally over broad groups. These broad group energy boundaries must coincide with the micro-group boundaries. However, the broad groups do not need to cover the entire energy range or to have joining boundaries. In fact, the boundaries can overlap.

The broad groups are used for flux and reaction rate integrals. These broad group fluxes are also used to obtain statistics on the ratios between different energy broad groups or between regions for a given broad group.

Printed Output

The output code prints the results of the Monte Carlo calculation. First the averaged code check tallies are printed. Next the broad-group fluxes and leakages are printed. Then, the broad-group average cross sections and reaction rates for each isotope in each region are printed along with the reaction rates for the region. The reaction rates for the entire cell along with an infinite and effective multiplication constant follow. Finally the micro-group fluxes for each region are printed and/or plotted.

3.5.12 Cross Section Library

The cross sections in the current XMC library were derived from the Battelle Northwest Master Library (BNML); except for the hydrogen thermal scattering kernal (which is from ENDF/B).

The resonance cross sections can either be group averaged and placed in with the smooth cross sections or they can be placed in a resonance parameter table with a "floor" being placed in with the smooth cross sections. The "floor" accounts for the resonances and resonances contributions not included in the resonance parameter table. The resonance parameter table contains resolved and unresolved resonance parameters.

The resonance parameter table preparation routine determines what energy width around each resonance will be accounted for by the resonance parameter table. The resonance contribution outside of this energy width will be added to the smooth cross sections as a "floor". The potential scattering cross section is also included in the "floor".

The resolved resonance contribution to the average group cross section is determined in one of two ways. If the resonance energy is more than 250 half widths outside the group, the contribution is integrated analytically. Otherwise, the resonance contribution is calculated for a number of points and numerical integration is made.

The analytical integration* assumes that the flux is 1/E and that the resonance equations are not Doppler broadened.

The numerical integration is made by calculating the Doppler broadened resonance cross sections at a number of points using the resonances within 250 half widths of the micro-group boundaries. The point cross sections are then multiplied by the correct weighting function and numerically integrated.

---

*Derived by Dr. J. L. Carter, Jr., while at Battelle-Northwest Laboratories.

The points are selected so that they are optimumly placed for an integration of $(1 + X^2)^{-1}$ using logarithmic interpolation. Additional points are then added as needed so that the maximum energy spread between points is less than $\Delta Ei/Np$ where $Np = A + B \cdot Emin_i$. The i is the group number and A and B are input numbers.

The weighting functions which are used are either 1/E or $1/E \cdot \sigma_T(E)$ where $\sigma_T(E) = \sigma_{Tp}(E) + \sigma_{T_{In}} + \sigma_{T_A}$ and $\sigma_{T_P}(E)$ is the total cross section at each point. $\sigma_{T_{In}}$ is the total cross section of the other isotopes in the material per atom of this isotope (an input number), and σ_{T_A} is the analytical contribution from the other resonances of this isotope. The point values are multiplied by unity or $1/\sigma_T(E)$ and the 1/E weighting is accounted for in the numerical integration. The integration assumes that the logarithm of the cross section varies linearly with the logarithm of the energy.

The unresolved resonance contribution is caluclated at a number of points using the equations as derived in the ETOE[3-24] and MC2[3-25] codes. The point values are then integrated numerically using linear log-log interpolation and assuming a 1/E flux. The point calculations account for Doppler broadening and use the narrow resonance approximation. The scattering from other isotopes in the material is again an input number.

The XMCLIB code first processes the anisotropic scattering data into group averaged Legendre coefficients in the center of mass system. The a's as used by the XMC code are then obtained by matrix multiplication

and normalized. The normalization is the maximum value of P(u) for $-1 \leq u \leq 1$ and is found by examining P(u) at 101 equally spaced values of u. The a's are also adjusted so that P(u) is never negative and so that the number of random selections of u per acceptance will not average more than 20.

The XMC code uses the same energy distribution data for inelastic and n-2n scattering. However, the information for both inelastic and n-2n scattering are placed on the CCT tape by the XMCLIB code.

It is assumed that the energy distribution from inelastic scattering will be of two forms. The two forms are discrete excitation level and the evaporation model. One isotope can have both forms. The evaporation model is used above the energy range covered by the discrete energy level model.

The temperature coefficients for the evaporation model are calculated by fitting a cubic in velocity to the ENDF/B library values. The probabiltiy of exciting a discrete level is calculated by the XMCLIB code by integrating over energy the probability times the product of the inelastic scattering cross section and the flux weighting function.

3.5.13 The XMC Loader

In order to simplify the data preparation for XMC, a special input routine was written. This routine, called the XMC LOADER, requires less than a dozen cards to prepare all the input to run an XMC case. The use of the XMC LOADER greatly reduces the time to prepare input and the chances of user errors.

The LOADER will prepare input for controlled and uncontrolled BWR fuel bundles, as well as PWR bundles. Additionally, several types of pin-cell geometries are treated by the LOADER.

The output of the LOADER is a file or card deck from which XMC runs. Since XMC plots the geometry of the problem run, a comparison to the actual desired input is easily made.

Some of the available geometry options are shown in Figures 3.5-3, 3.5-4, 3.5-5, and 3.5-6. Figures 3.5-3 and 3.5-4 show BWR and PWR fuel bundles, while Figure 3.5-5 shows some of the pin-cell "box types". These box types may also be placed in a bundle as shown in Figure 3.5-6.

Table 3.5-1 Isotopes in the XMC Cross Section Library

Hydrogen (in water)	Zirconium
Boron (natural)	Silver-107
Boron-10	Silver-109
Boron-11	Cadmium-112
B_4C	Indium-115
Carbon	Gadolinium-155
Nitrogen	Gadolinium-157
Oxygen	Uranium-235
Aluminum	Uranium-236
Silicon	Uranium-238
Chromium	Plutonium-238
Manganese	Plutonium-239
Iron	Plutonium-240
Nickel	Plutonium-241
304 Stainless Steel	Plutonium-242
Cobalt	

Table 3.5-2 XMC Code Boundary Functions

Boundary Function	Description
$r = x - x_o$	Plane at $X = x_o$
$r = y - y_o$	Plane at $y = y_o$
$r = z - z_o$	Plane at $z = z_o$
$r = y - ax - b$	Plane on $y = ax + b$
$r = x^2 + y^2 - R^2$	Cylinder of radius R centered on z axis
$r = (x-x_o)^2 + (y-y_o)^2 - R^2$	Cylinder of radius R centered at x_o, y_o
$r = x^2 + y^2 + z^2 - R^2$	Sphere of radius R centered at the origin
$r = A(x-x_o)^2 + B(y-y_o)^2 + C(z-z_o)^2 - K$	General boundary function

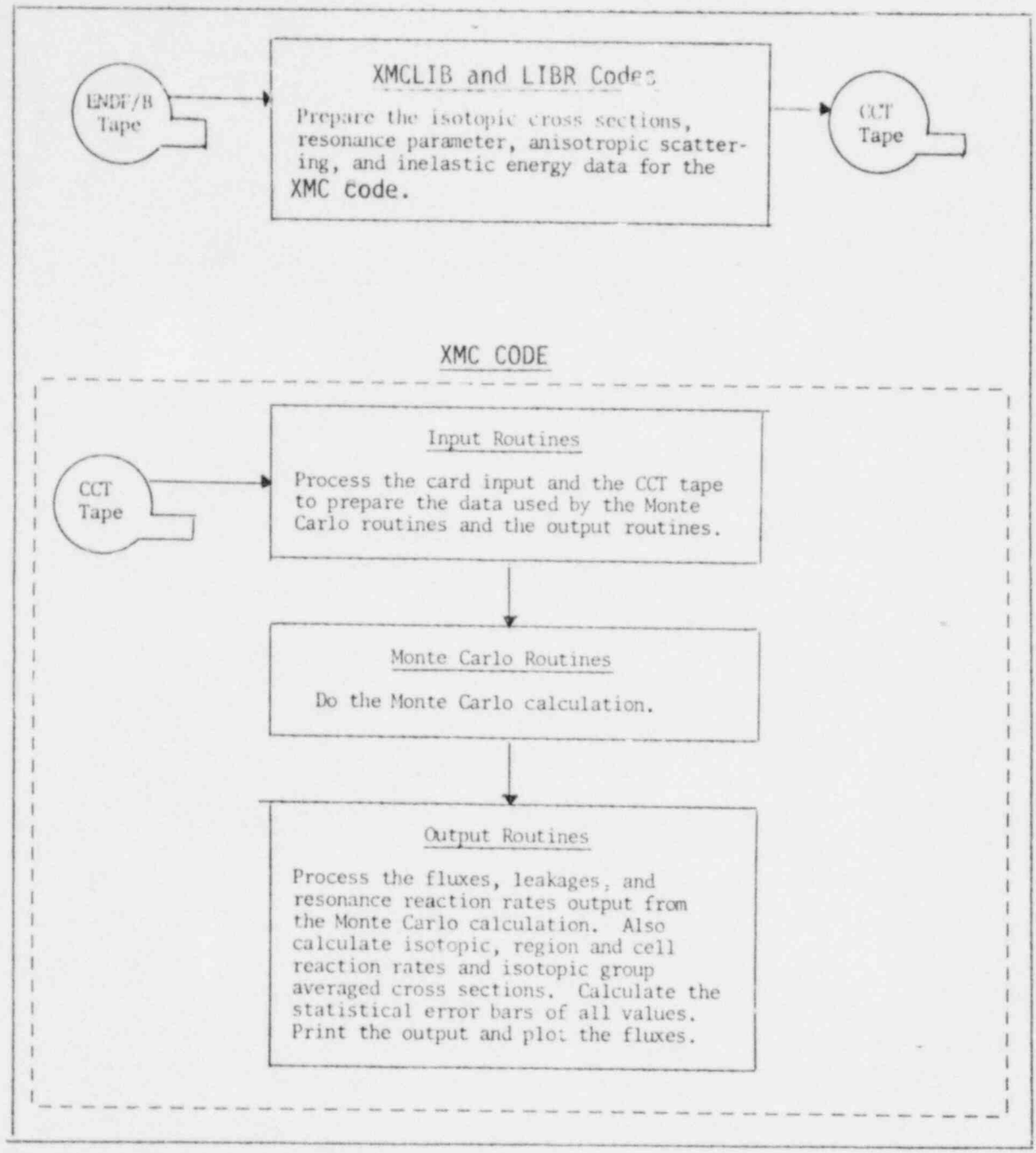

Figure 3.5-1 The XMC Code Package

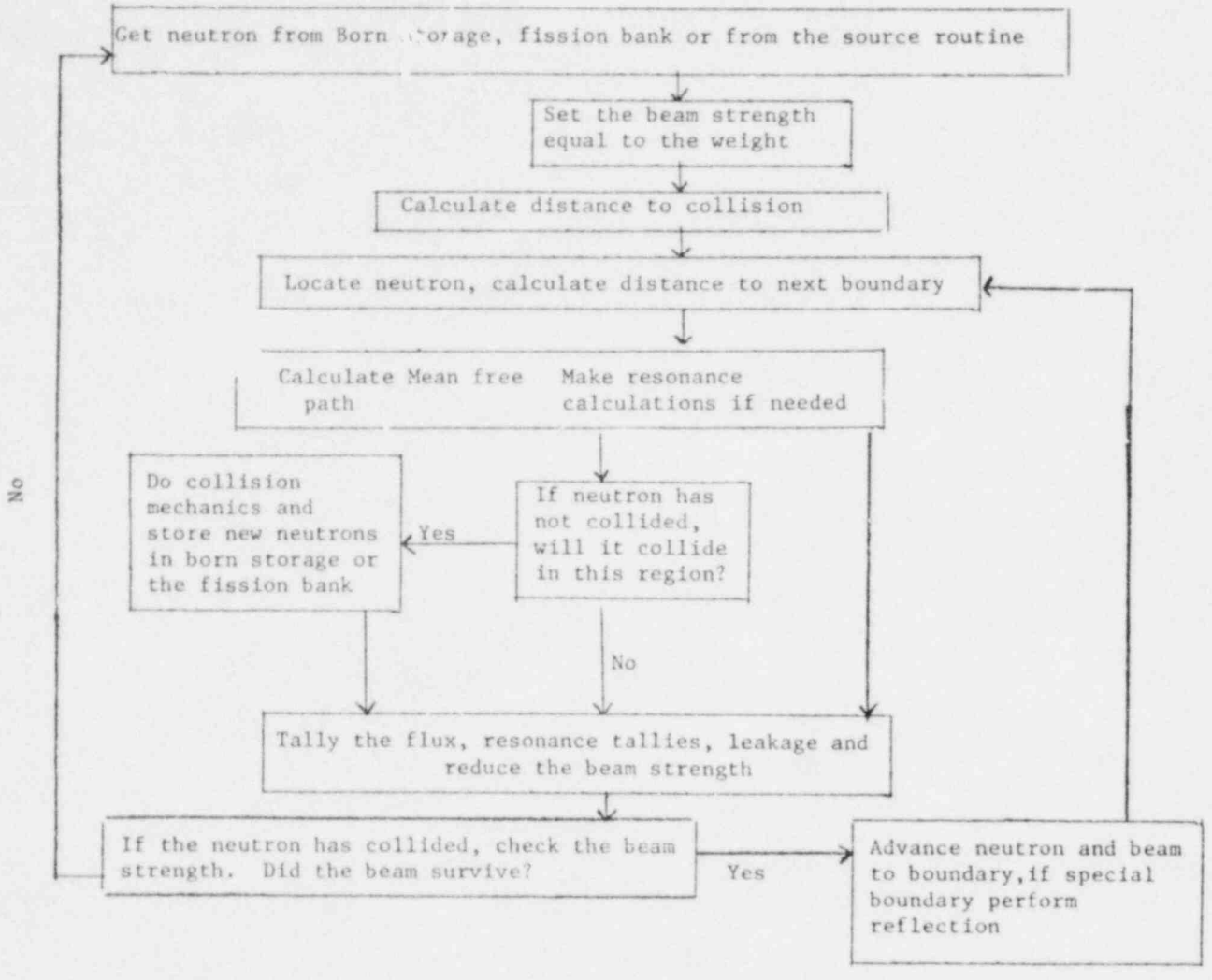

Figure 3.5-2 General Flow Diagram of the Monte Carlo Code Neutrons Importance Weighting not Being Used

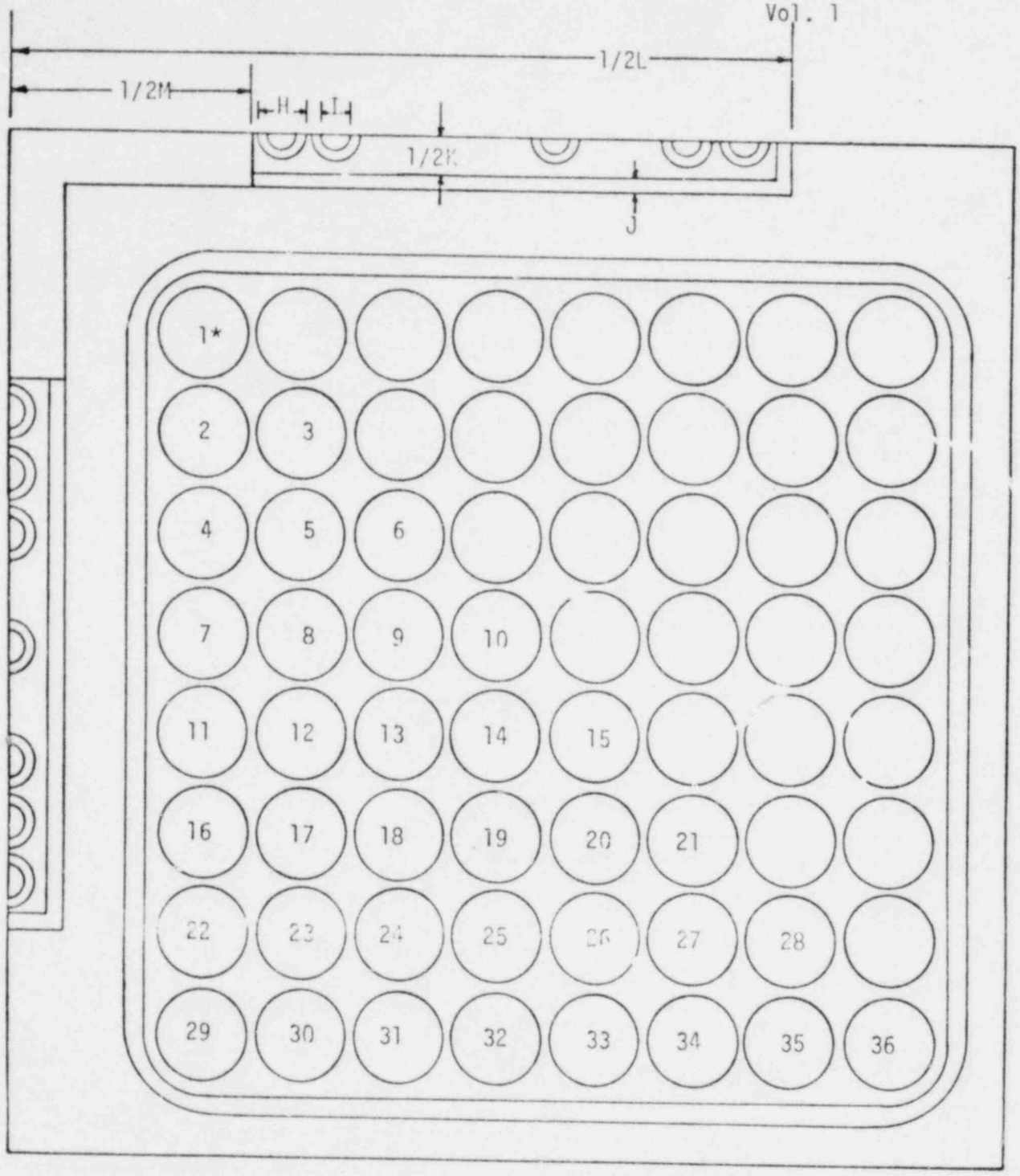

Figure 3.5-3 BWR Fuel Assembly Geometry

* Rod position numbers

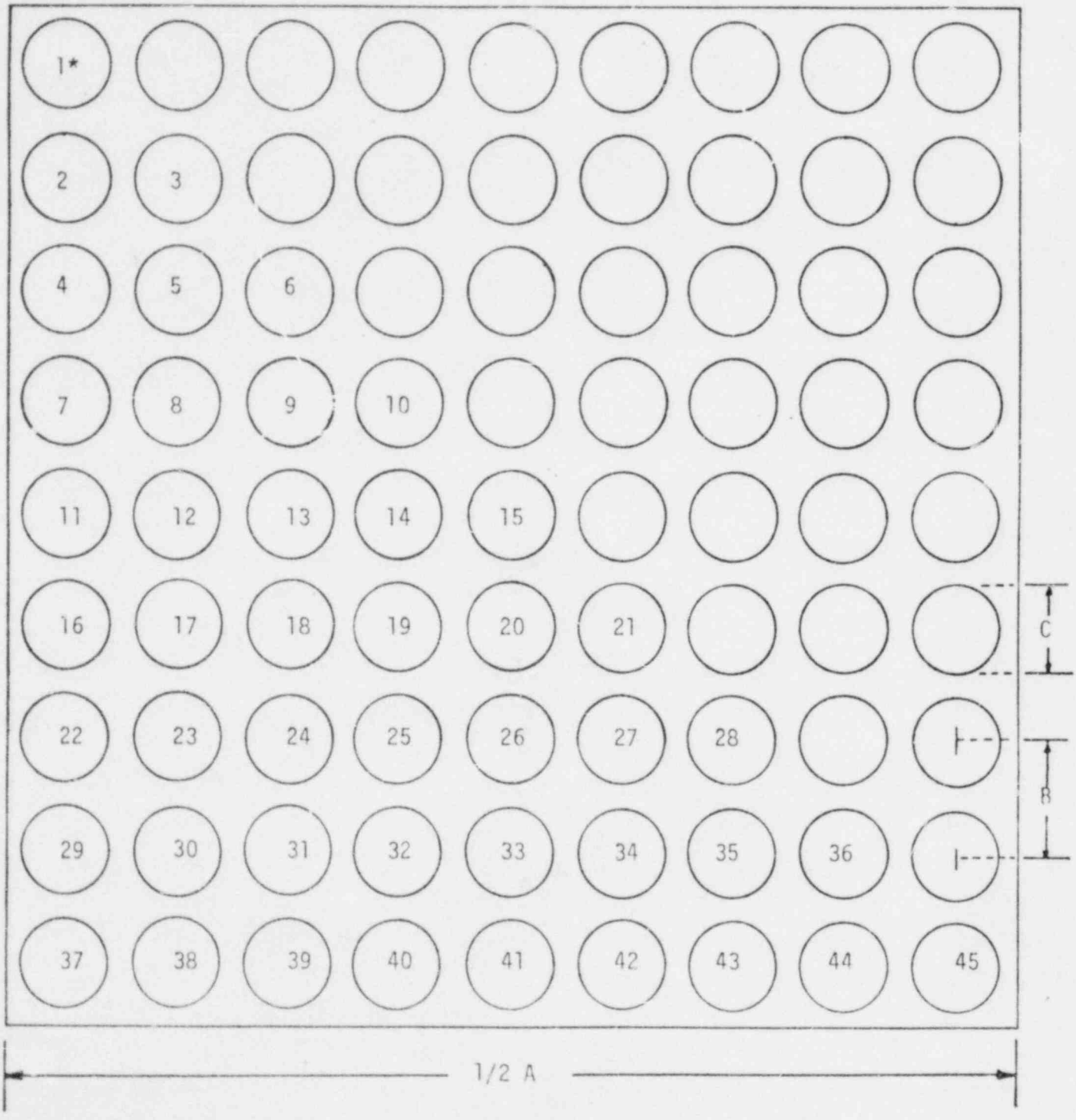

Figure 3.5-4 BWR Quarter Bundle Geometry

* Rod position numbers

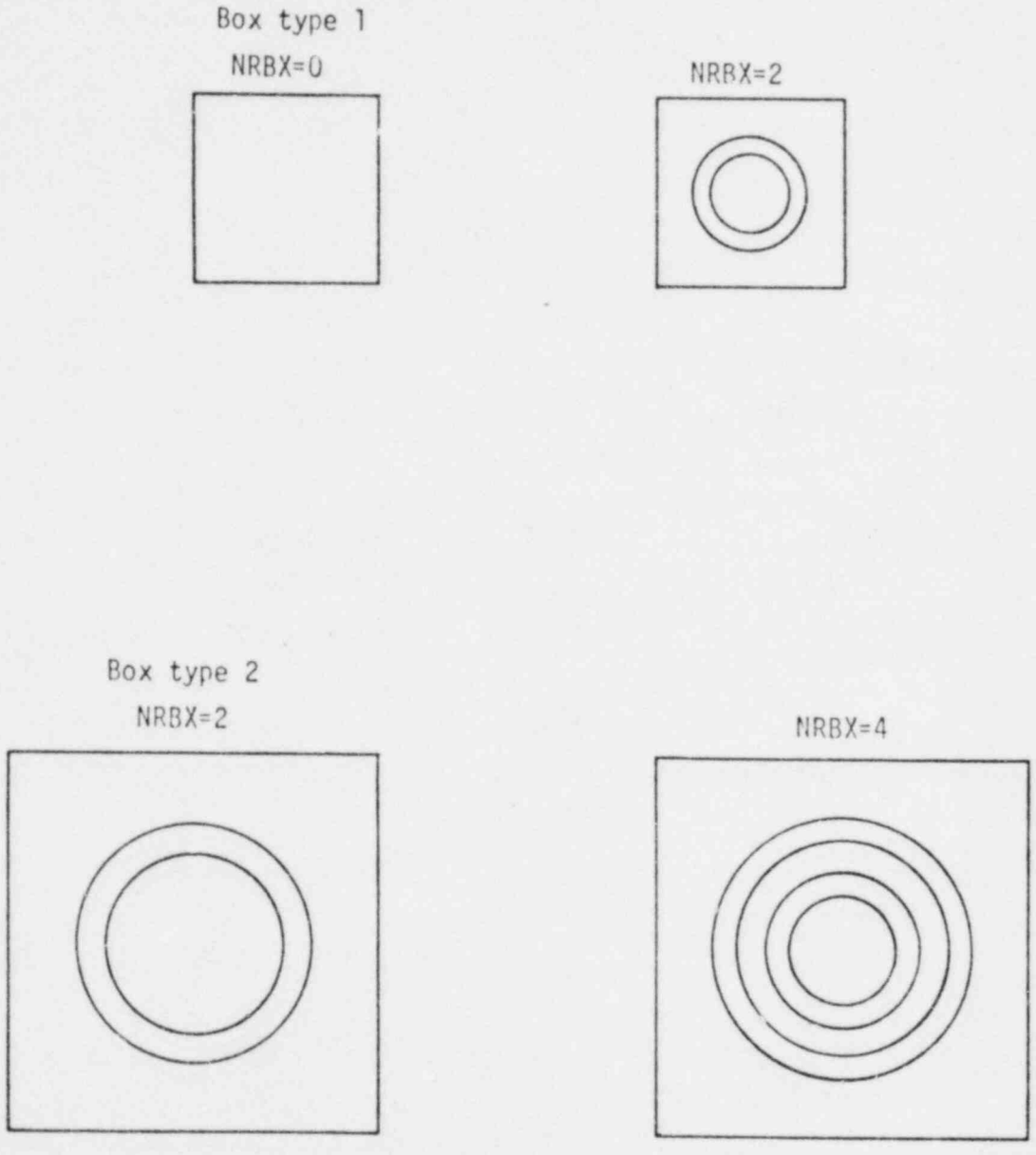

Figure 3.5-5 Box Types with Different Numbers of Internal Regions

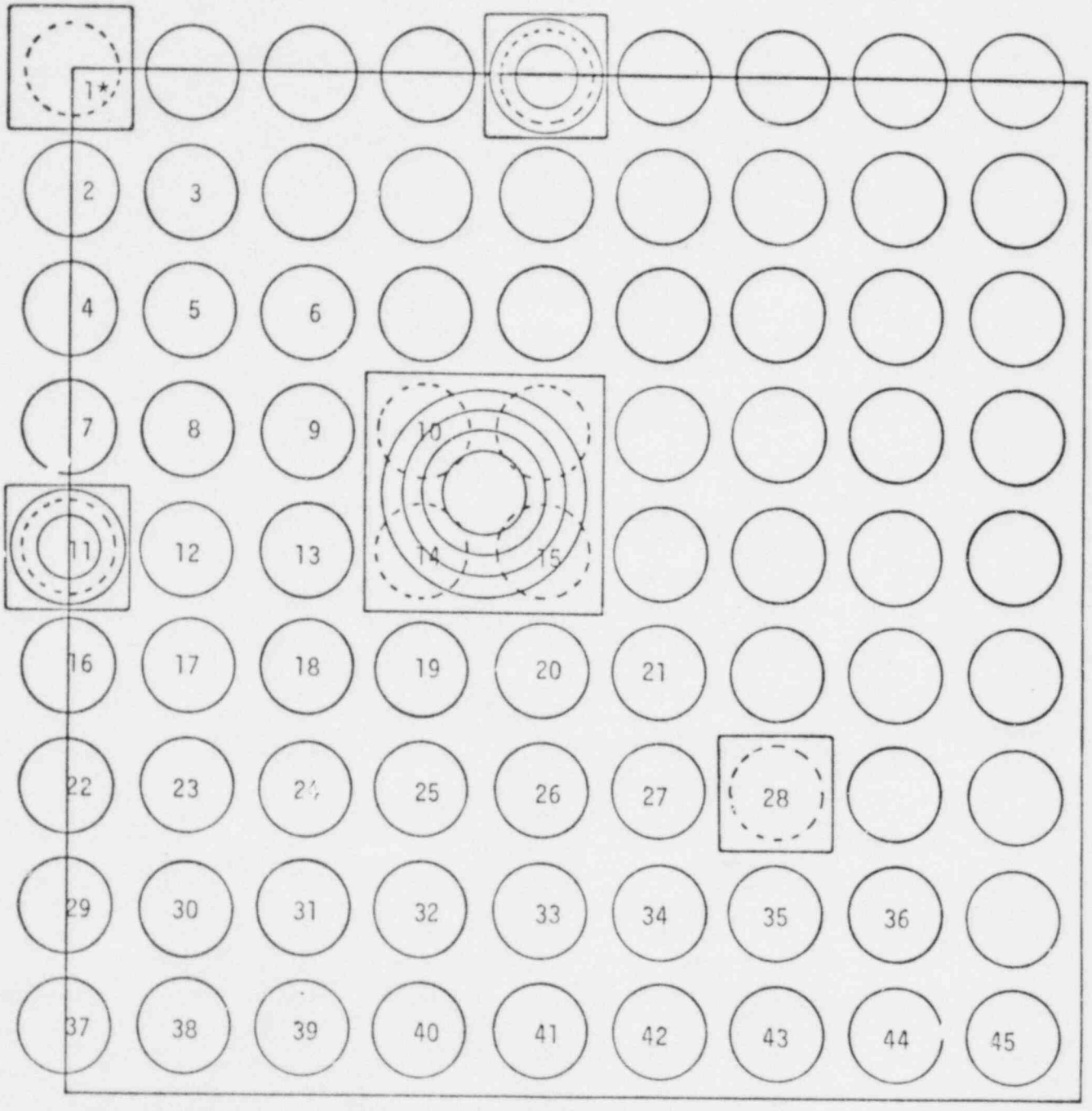

Figure 3.5-6 Examples of Boxes of Type 1 at Rod Position 1, 11, and 28, and a Box of Type 2 at Rod Position 15. Note that Insertion of a Box at an Off Diagonal Position Actually Inserts Two Boxes such as the Box at Rod Position 11.

*Rod position number

3.6 REFERENCES

3-1 K. B. Stewart, "BNW Master Library", BNWL-CC-325, Pacific Northwest Laboratory, September, 1965 and Subsequent Revisions.

3-2 H. C. Honeck, "ENDF/B, Specifications for an Evaluated Nuclear Data File for Reactor Applications, BNL-50066(T-467)", Brookhaven National Laboratory, Upton, New York, (May, 1966 Revised July, 1967).

3-3 B. C. Haywood, "The Spectral Density of Hydrogen in Water", Journal of Nuclear Energy, Vol. 21, pp. 249-262, 1967.

3-4 D. R. Skeen, "THERMOS: A Thermalization Transport Theory Code for Reactor Lattice Calculations", JN-CC-10, December, 1971.

3-5 H. C. Honeck, Y. David Naliboff, and Dale Houston, "FLANGE-II, A Code to Process Thermal Neutron Scattering Data from an ENDF/B Tape", Preliminary, December, 1968.

3-6 J. L. Carter, Jr., "HRG3: A Code for Calculating the Slowing Down Spectrum in the P_1 or B_1 Approximation", BNWL-1432, June, 1970.

3-7 I. Carlvik, "The Dancoff Correction in Square and Hexagonal Lattices", Nuclear Science and Engineering, 29, 325-326 (1967).

3-8 F. T. Alder, G. W. Hinman, and L. W. Hordheim, "The Quantitative Evaluation of Resonance Integrals", paper no. P/1988, "Proceedings of the Second United Nations International Conference on the Peaceful Uses of Atomic Energy", Vol. 16, pp 155-171, (1958).

3-9 E. A. Nephew, "Thermal and Resonance Absorption Cross Sections of the U-233, U-235, and Pu-239 Fission Products", ORNL-2869, March, 1960.

3-10 R. B. Stout, "XTG: A Two-Group Three-Dimensional Reactor Simulator Utilizing Coarse Mesh Spacing", XN-CC-28, January, 1975.

3-11 T. W. Patten and F. T. Adams, "Methodology for Calculation of Pressure Drop in BWR Fuel Assemblies", XN-NF-79-59, October, 1979.

3-12 T. W. Patten and J. L. Jaech, "XN-3 Critical Power Correlation", XN-NF-512, June, 1979.

3-13 J. N. Morgan, "XTRAN-PWR: A Computer Code for the Calculation of Rapid Transients in Pressurized Water Reactors with Moderator and Fuel Temperature Feedback", XN-CC-32, September, 1975.

3-14 C. W. Stewart, C. L. Wheeler, et. al., "COBRA-IV: The Model and the Method", BNWL-2214, July, 1977.

3-15 C. L. Wheeler, et. al., "COBRA-IV-I: An Interim Version of COBRA for Thermal-Hydraulic Analysis of Rod Bundle Nuclear Fuel Elements and Cores", BNWL-1962, March, 1976.

3-16 S. Borresen, "A Simplified, Coarse Mesh, Three-Dimensional Diffusion Scheme for Calculating the Gross Power Distribution in a Boiling Water Reactor", Nuc. Sci. and Engr., 44-37-43, 1971.

3-17 L. S. Tong, "Boiling Heat Transfer and Two Phase Flow", John F. Wiley and Sons, New York, New York, 1965.

3-18 R. J. Cena, N. F. Sather, and D. S. Rowe, "Predicting Fuel Rod Temperature Responses by Orthogonal Collocation", ANS Transactions, 21:205-206, June, 1975.

3-19 B. Finlayson, "The Method of Weighted Residuals and Variational Principles", Mathematics in Science and Engineering Series, Vol. 87, Acadamic Press, New York, New York, 1972.

3-20 A. R. Vernon, "Calculation of the Effective Resonance Integral of U-238", Nuclear Science Engineering, 7, 252, 1960.

3-21 L. W. Nordheim, "The Technology of Nuclear Reactor Safety", Vol. 7, Chapter 4.

3-22 W. W. Little, Jr., and R. W. Hardie, "2DB User's Manual". BNWL-831, Pacific Northwest Laboratory, Richland, WA, 1968.

3-23 D. H. Thomsen and T. M. Traver, "BMC-1: The Battelle Monte Carlo Code", BNWL-1433, June, 1970.

3-24 D. M. Green and T. A. Pitterle, "ETOE, A Program for ENDF/B to MC^2 Date Conversion", Technical Memorandum No. 44, Atomic Power Development Associates, Inc., March, 1967.

3-25 B. J. Toppel, A. L. Rago and D. M. O'Shea, "MC^2, A Code to Calculate Multigroup Cross Sections", June, 1967 (ANL-7318).

4.0 NEUTRONICS CORE ANALYSIS METHODOLOGY

This section covers the special methods for analyzing the control rod drop accident, the fuel misloading incident, reactor core and channel hydrodynamic stability, the control rod withdrawal incident, and the methods for calculating the neutronics parameters which are input to the plant transient and loss of coolant accident analyses.

4.1 CONTROL ROD DROP ACCIDENT

The control rod drop accident assumes a control rod becomes uncoupled from the drive and remains stuck fully inserted in the reactor core as the control rod drive is withdrawn. The uncoupled control rod is then assumed to drop out of the core.

The primary reactivity feedback mechanism that limits the power during a rod drop accident is the Doppler reactivity. The control rod scram ensures a final reactor shutdown state.

The limiting criteria for the control rod drop accident analysis are the following:

1. The maximum deposited enthalpy during the accident in a fuel rod at any axial location shall not exceed 280 calories per gram.
2. The maximum reactor pressure during the accident shall not cause reactor pressure vessel stresses to exceed the "Service Limit C" as defined in the ASME Code.[4-1]

The reactor neutronic parameters which significantly affect the rod drop analysis include the Doppler reactivity coefficient, the maximum control rod worth, the power peaking (peaking with control rod removed from core) and the delayed neutron fraction. For a given type of reactor, the maximum deposited enthalpy is parameterized as a function of the above variables.

For maximum deposited enthalpies less than 280 calories per gram, prompt fuel rupture does not occur and the heat transfer from the fuel to the coolant is by convection. The reactor coolant pressure is calculated for limiting values of Doppler, rod worth, power peaking, delayed neutron fraction, and scram bank reactivity worth.

Rod Drop Analysis Method - The rod drop calculations are performed with the COTRAN computer code described in Section 3.3. The COTRAN code solves the space and time dependent neutron diffusion equation in two-dimensional (r-z) geometry with fuel temperature and moderator density reactivity feedbacks. COTRAN employs a nodal method based directly on a one-group finite difference technique for the solution of the time dependent neutron diffusion equation. The one-group cross-sections used in the iterative flux solution are determined from input two-group values and modified at each time step by thermal feedback. The input two-group cross sections for COTRAN are calculated using the XTGBWR code following the procedure outlined in Section 3.3.

The space and time dependent COTRAN neutronic model is capable of computing a rapid reactor transient initiated by a reactivity insertion caused by a control rod being removed from the core. Since the model utilizes the two-dimensional (r-z) geometry, the code can calculate the rapidly changing flux distribution as a control rod leaves the core and the scram rod bank simultaneouly enters the core.

COTRAN initially determines the static flux and power distribution corresponding to the problem input. The initial time step for the rod drop analysis is 0.0001 seconds. The code then automatically determines the time step interval based on the number of iterations necessary to achieve convergence. This method permits small time steps during times of large changes in power level, and inversely, large time steps during periods of slow perturbation. Therefore, the code efficiently solves the transient problems without the user choosing time step sizes. Six groups of delayed neutron precursors are employed in the transient analysis.

The following is a step-by-step description of the procedure employed to perform the control rod drop accident analysis.

[ ]

4.2 FUEL MISLOADING ANALYSIS

At the present time two separate incidents are analyzed as part of the fuel misloading analysis. The first incident which is termed the fuel misorientation error assumes that a fuel assembly is misoriented by rotation

through 90^{o} or 180^{o} from the correct orientation when loaded into the reactor core. The second incident, the fuel mislocation error, assumes a fuel assembly is placed in the wrong core location during refueling. For both the fuel misorientation error and the fuel mislocation error, the assumption is made that the error is not discovered during the core verification and the reactor is operated during the cycle with a fuel assembly misloaded.

The limiting parameter of interest for the fuel misloading error is the MCPR in the misloaded fuel assembly. The fuel misloading analysis determines the difference between the MCPR for the correctly loaded core and the MCPR for the core with a fuel assembly misloaded. The resulting ΔMCPR for the misloading error is then compared with the ΔMCPR determined from the transient analysis for the cycle. The largest ΔMCPR is then added to the transient MCPR safety limity to determine the operating MCPR limit.

4.2.1 Fuel Misorientation Error

For the fuel misorientation error analysis, a limiting fuel assembly in the reactor core is assumed to be rotated 90^{o} or 180^{o} from the normal orientation. The fuel misorientation error is important for the fuel assemblies in the BWR/2, BWR/3 and BWR/4 reactor cores. In these cores the fuel assemblies are offset in the core lattice to provided a wider gap between the fuel channels where the control rods are inserted. To account for the moderating effects of the water in the wider gap, the fuel assemblies are designed with lower enrichment fuel rods next to the wide water gaps.

If a fuel assembly is charged into the reactor core in the rotated orientation, higher enrichment fuel rod powers higher than design values. The misoriented analysis is performed for the most severe case of the MCPR limiting fuel assembly being rotated 180 degrees. Four bundle calculations are performed to demonstrate that the 180 degree rotation is the most limiting case. The procedure used to calculate the power in a misorientated fuel assembly and the resulting MCPR consists of the following five steps:

[ ]

4.2.2 Fuel Mislocation Error

For the fuel mislocation error an incorrect fuel assembly is assumed to be loaded in one of the core locations during refueling. The limiting case is the loading of a high reactivity fuel assembly in place of a low reactivity fuel assembly. A misloading error in one of the inner core modules will produce a localized area of higher reactivity resulting in higher power and lower CPR than planned. The following procedure is used to find the lowest CPR that would result from a fuel mislocation. The CPR for the misloaded assembly compared to the CPR for the core with no assembly misloaded gives the ΔMCPR for the mislocation error.

[ ]

When the reactor is operating, the ENC core monitoring method will use all measured data including the local power range monitor (LPRM) data to determine the power of each node of fuel in the core. If a

high reactivity fuel assembly is mislocated in the core, the misloaded assembly will cause that area of the core to be higher in power than planned. The higher power will be detected by the LPRM detectors resulting in the measured operating MCPR being lower than the operating MCPR predicted by the XTGBWR core simulator code in the above procedure. The more accurate fuel mislocation analysis that will be performed when required includes the following additional calculations:

[ ]

4.3 STABILITY ANALYSIS

Stability can be defined for an operating system as follows: a system is stable if, following an input perturbation, the transient returns to a steady, non-cyclic state. Stability analysis is concerned with two basic phenomenon, reactor core (reactivity) stability and channel hydrodynamic stability. Reactor core instability is when the reactivity feedback of the entire core drives the reactor into power oscillations. Channel hydrodynamic instability is flow oscillations which may impede heat transfer to the moderator resulting in localized power osciallations. Stability is analytically demonstrated if no divergent oscillations develop as a result of perturbations of any critical variable, such as core pressure, control rod position, and recirculation flow.

The criterion to be evaluated is the decay ratio X_2/X_0, designated as the ratio of the magnitude of the second over shoot to the first overshoot resulting from a step perturbation. For a time domain analysis, the

decay ratio is determined from the time response containing several oscillations by averaging the decay ratios determined from each successive overshoot. When the decay ratio X_2/X_0 is less than 1.0, the reactor core is stable. Thus, the ultimate performance criteria for the stability analysis is specified in terms of the decay ratio as:

Reactor Core (reactivity) stability $X_2/X_0 < 1.0$

Channel hydrodynamic stability $X_2/X_0 < 1.0$

These criteria are demonstrated for all usual and unusal operating conditions of the reactor that may occur during the course of the fuel in-core lifetime. For stability purposes, the most severe conditions to which these conditions will be applied are:

1. Natural circulation flow at a power corresponding to the rod block power limit condition, and
2. End of cycle power distributions at low power operation.

Although the ultimate performance criteria ensure absolute reactor stability, an operational design guide is applied for all expected power and flow conditions encountered in normal operation. The most limiting condition expected corresponds to minimum normal flow.

Stability analysis is performed with the COTRAN computer code described in Section 3.3. The COTRAN code solves the space and time dependent neutron diffusion equation in two-dimensional (r-z) geometry with fuel temperature and moderator density reactivity feedback. These reactivity

feedbacks are determined from a solution of the equations of mass, energy and momentum for the hydrodynamic channels coupled with a fuel conduction model. As such, the COTRAN code provides the time response of important core parameters following a system perturbation. The calculational method for the reactor core (reactivity) stability analysis is as follows:

[ ]

The hydrodynamic and core reactivity decay ratios determined by the above procedures are then compared to the operational design criteria. If the criteria is met for all usual and unusual operating conditions of the reactor that may occur during the reload cycle then the core is stable.

4.4 NEUTRONIC REACTIVITY PARAMETERS

The neutronics models used in the plant transient and loss of coolant analyses require several neutronic input parameters which characterize the reactor core at a particular operating state. These parameters are:

1. Void reactivity coefficient,
2. Doppler reactivity coefficient,
3. Scram reactivity,
4. Delayed neutron fraction, and
5. Prompt neutron lifetime.

These parameters which vary with cycle exposure and core average void fraction are determined for each reactor condition to be analyzed. The neutronic parameters and their calculational methodology are discussed in the following sub-sections.

4.4.1 Void Reactivity Coefficient

The void coefficient of reactivity is the fractional change in core reactivity produced by a change in the core average void fraction. The void coefficient is dependent on the specific operating state and core average void level.

The void coefficient of reactivity is calculated with the reactor simulator code, XTGBWR. The calculational method for an operating state is as follows:

[ ]

4.4.2 Doppler Reactivity Coefficient

The Doppler coefficient of reactivity is the fractional change in core reactivity produced by a change in the core average fuel temperature. The Doppler coefficients for each fuel type in the core are determined with the XFYRE computer code described in Section 3.1. The calculational procedure for determining the core average Doppler coefficient is as follows:

[ ]

4.4.3 Scram Reactivity

The scram reactivity is defined as the core reactivity change as a function of the scram bank insertion. The total scram reactivity is calculated with the reactor kinetics model COTRAN as follows:

[ ]

4.4.4 Delayed Neutron Fraction

The delayed neutron fraction is calculated for each fuel type by the XFYRE code described in Section 3.1 as a function of exposure. For the plant transient analysis, a core average delayed neutron fraction (β_{eff}) is determined by exposure and volume weighting the fuel type dependent delayed neutron fraction.

4.4.5 Prompt Neutron Lifetime

The prompt neutron lifetime is calculated with the XFYRE code for each fuel type in the core. The calculations are performed at core average voids as a function of exposure. The core average prompt neutron lifetime is calculated by exposure and volume weighting the fuel type dependent neutron lifetimes.

4.5 CONTROL ROD WITHDRAWAL

The control rod withdrawal error is the withdrawal of a control rod by the reactor operator from a fully inserted position until the control rod motion is stopped by the rod block. For the analysis, the reactor is assumed to be in a normal mode of operation with the control rods being withdrawn in the proper sequence and all reactor parameters within the

Technical Specification limits and requirements. The most limiting case is when the reactor is operating at power with a high reactivity worth control rod fully inserted. To maximize the worth of the control rod, the reactor is assumed to be xenon free and the control rod with the maximum rod worth is selected as the rod to be withdrawn. When necessary, the partially withdrawn control rods in the core are adjusted slightly to place the fuel near the inserted control rod on thermal limits.

During the control rod withdrawal transient the reactor operator is assumed to ignore the local power range monitor (LPRM) alarms and the rod block monitor (RBM) alarms and continue to withdraw the control rod until the control rod motion is stopped by the control rod block.

While the control rod is being withdrawn, the reactor power and the local power in the area of the rod which is being withdrawn will increase. The reactor thermal limit of concern as the power increases is the transient minimum critical power ratio (MCPR) limit which protects against critical heat flux. The control rod withdrawal analysis will determine the ΔMCPR during the transient as a function of the rod block setpoint. The ΔMCPR values for the control rod withdrawal are compared to the ΔMCPR values for the other transients to determine the operating MCPR limit and rod block set point that will protect the MCPR safety limit of the reactor.

The control rod withdrawal incident is analyzed as a series of steady state calculations since the rate of power increase is slow compared to the time constants for heat transfer and delayed neutrons. The calculations are performed with Exxon Nuclear Company's reactor core simulator code, XTGBWR. The calculational method for the control rod withdrawal is as follows:

[ ]

4.6 REFERENCE

4-1 ASME Boiler and Pressure Vessel Code, Section III, "Nuclear Power Plant Components", American Society of Mechanical Engineers.

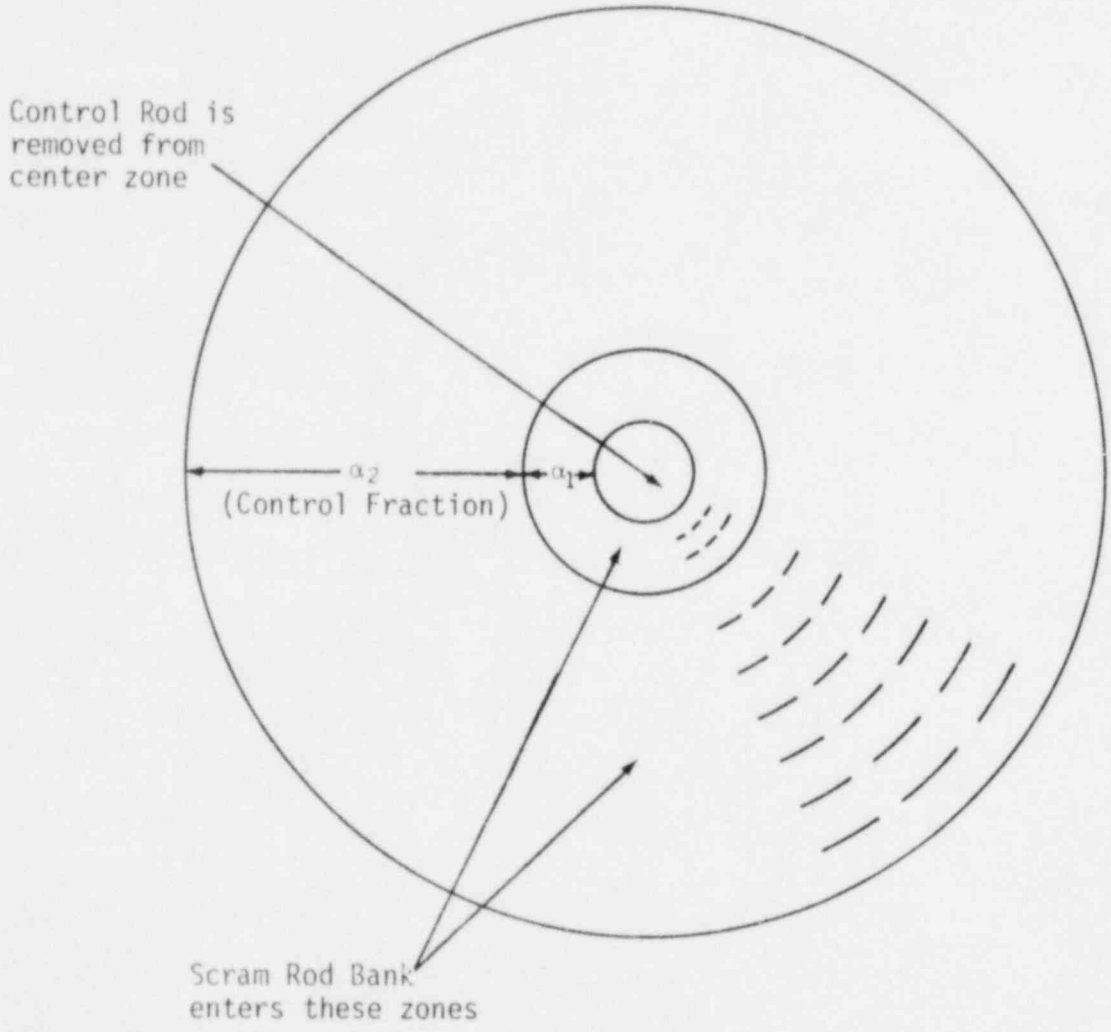

Figure 4.1-1 Cylindrical Geometry for Control Rod Drop Analysis

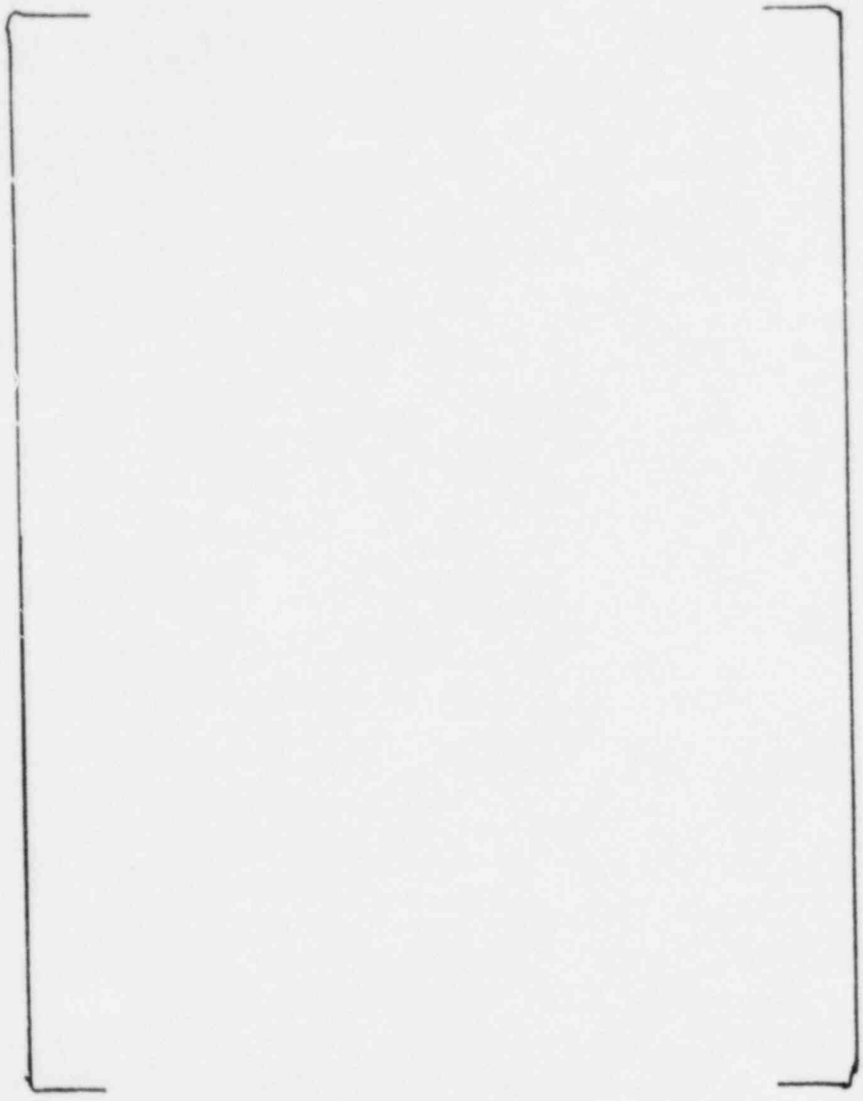

Figure 4.1-2 Typical Control Fractions α_1 vs α_2 for Central Rod Full In or Full Out

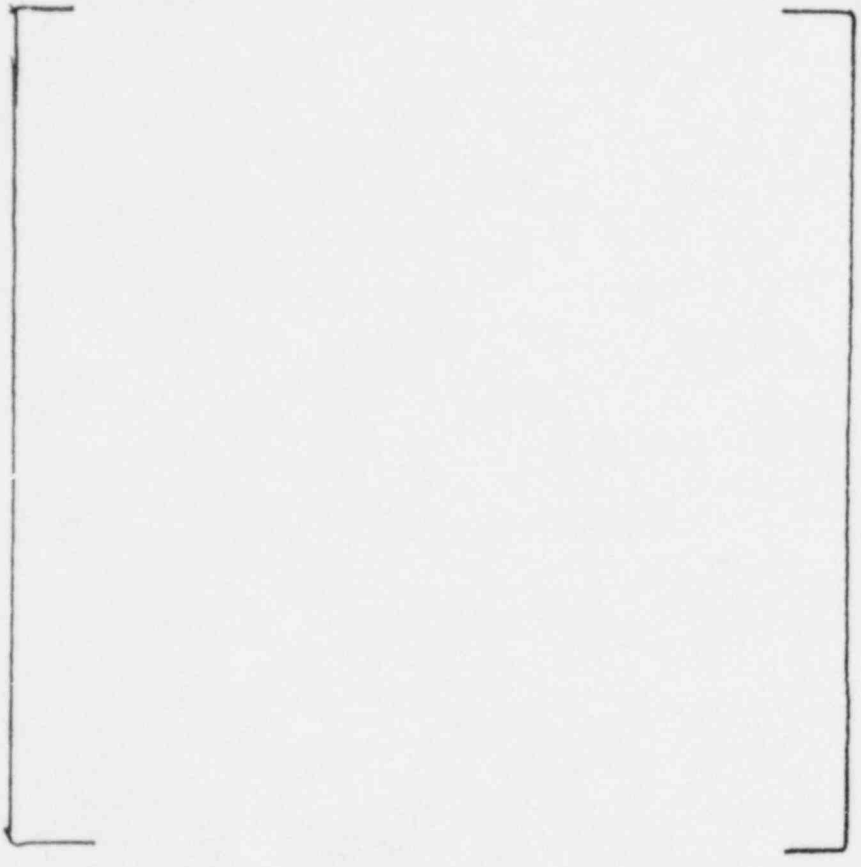

Figure 4.1-3 Typical Scram Bank Reactivity Worth Curve

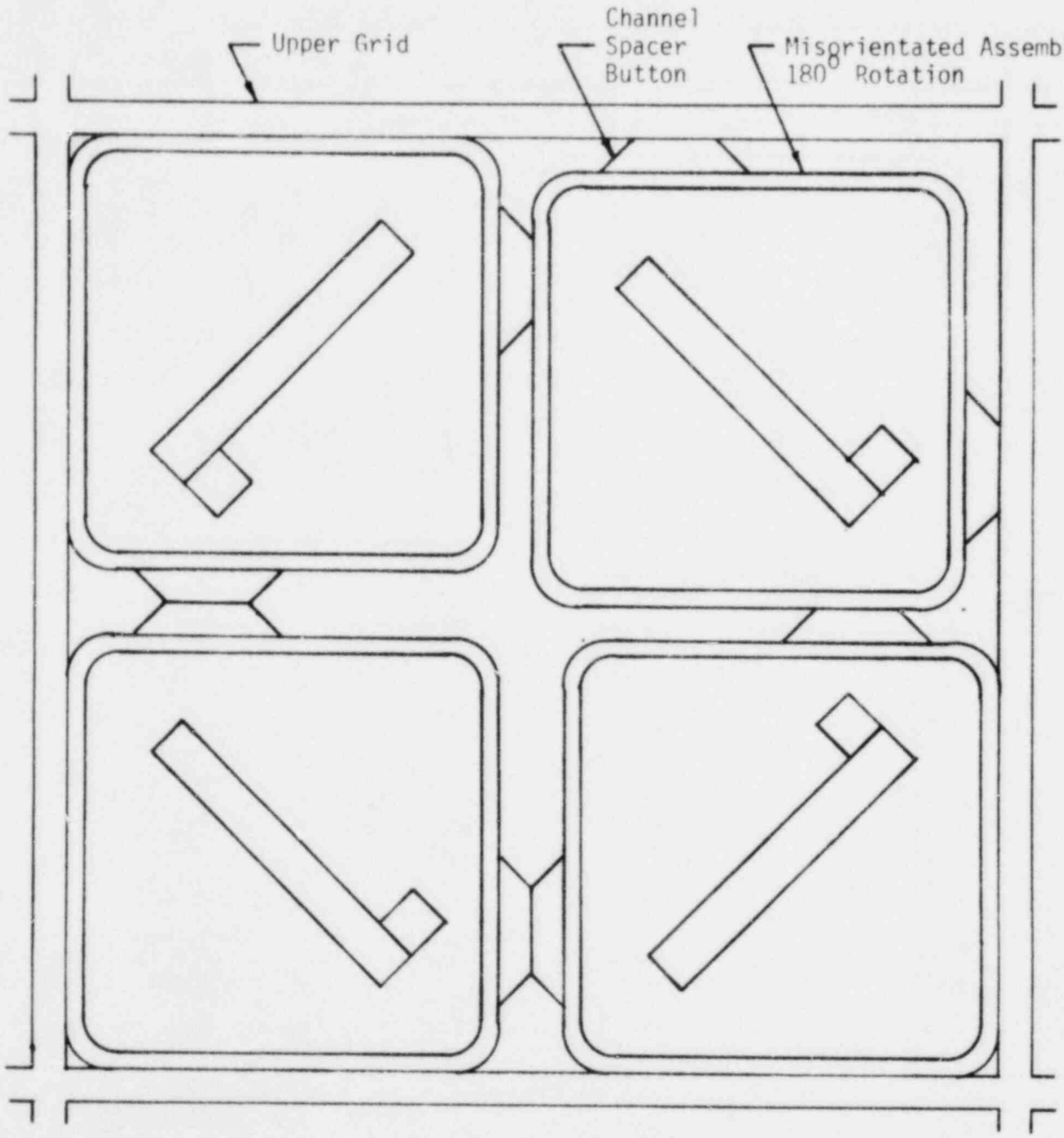

Figure 4.2-1 Four Bundle Module with Misorientated Fuel Assembly, 180° Rotation

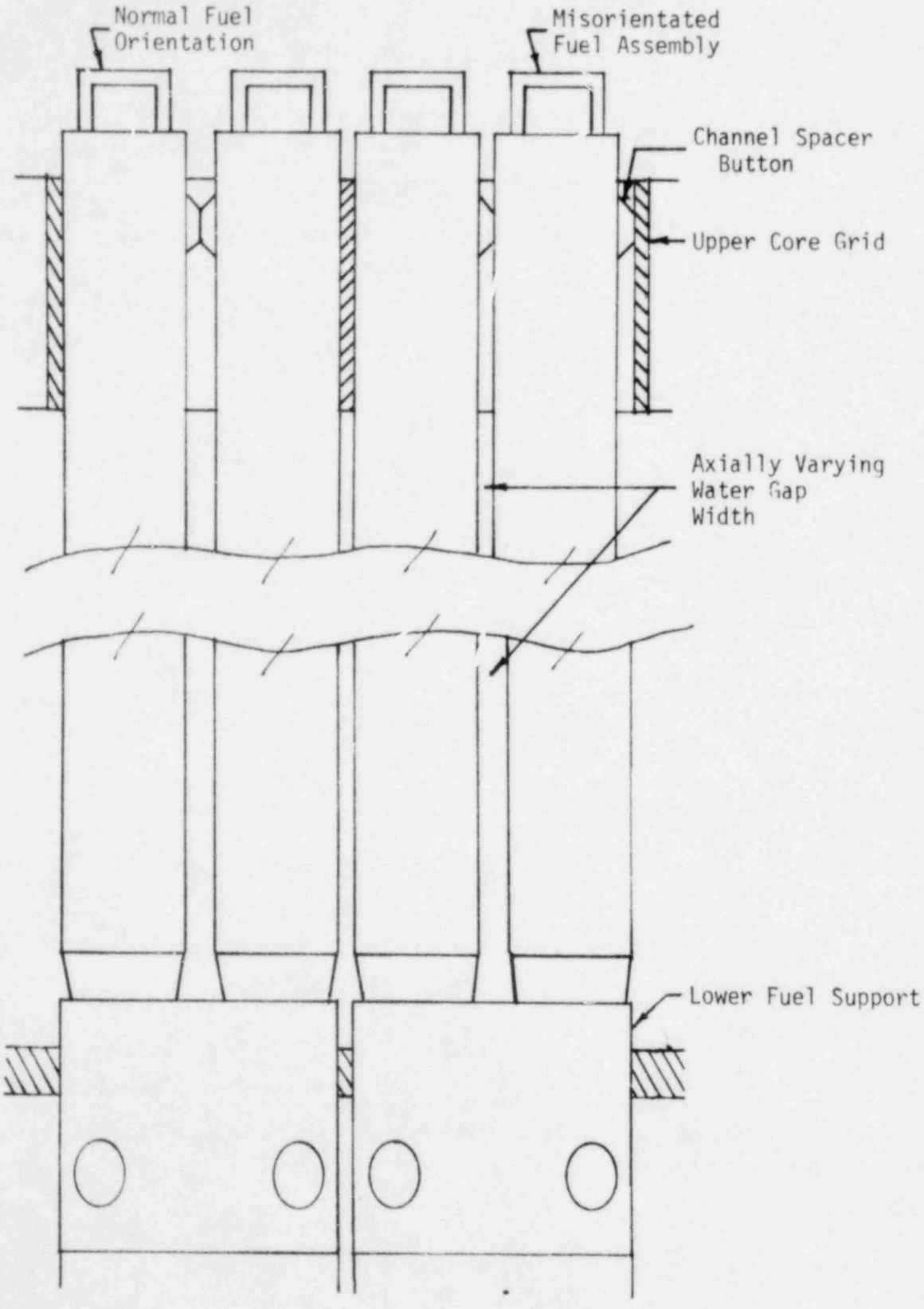

Figure 4.2-2 Elevation View of Misorientated Fuel Assembly

5.0 NEUTRONICS METHODS VERIFICATION

The ENC neutronics methods are verified by comparing calculations to measured reactor data and to calculations made by higher order methods. Methods verification for the XFYRE, XTGBWR, and COTRAN codes is presented in this section.

5.1 XFYRE VERIFICATION

The local power distributions calculated by the XFYRE code are verified by comparison to fuel rod gamma scan measurements. Comparisons of the calculated and measured local power distributions are shown in Figure 5.1-1 through 5.1-5. The measurements were performed by removing the fuel rods from the fuel assembly and measuring the La-140 activity at a given core height. The measured data shown in Figures 5.1-1 through 5.1-5 have not been corrected for core flux tilt effects caused by control rod and fuel exposure.

In addition to comparison to gamma scan results, the accuracy of the XFYRE calculational model for the microscopic depletion of a BWR fuel assembly has been verified by comparison with measured isotopics from a Garigliano fuel assembly[5-1]. Figure 5.1-6 is a representation of the Garigliano BWR fuel assembly for which the measurements were made. Table 5.1-1 shows the comparison between the measured and XFYRE calculated isotopics.

The XFYRE code has been benchmarked with the higher order XMC code described in Section 3.5. A series of XMC calculations have been performed to evaluate the effects of in-channel voids, control, gadolinia, and temperature on the BWR fuel assembly reactivity and local power distribution. A comparison of k_∞ calculated with the XMC and XFYRE codes is shown in Table 5.1-2. The local power distributions calculated with the XMC and XFYRE codes are shown in Figures 5.1-7 though 5.1-11.

The XFYRE calculations were performed with the standard x-y geometry described in Section 3.1. The XMC calculations were performed using an exact geometrical representation for the fuel, clad, channel, and control rod blade. The cross section library was identical for the XFYRE and XMC calculations.

5.2 XTGBWR VERIFICATION

The XTGBWR reactor core simulator code is verified by comparing the calculated and measured reactor parameters. The reactor core follow data for the Oyster Creek, Dresden-3, and Quad Cities reactors are listed in Tables 5.2-1 through 5.2-6. The k_{eff} values calculated by XTGBWR for the critical reactor condition are plotted as a function of cycle exposure on Figure 5.2-1. The k_{eff} data are corrected for known reactivity biases including the effects of "crud", incore instruments, sources, and fuel assembly spacers.

A comparison of measured and calculated traveling in-core probe (TIP) data for the Oyster Creek and Dresden-3 reactors is presented in Figures 5.2-2 through 5.2-12. All XTGBWR calculations were performed with a full core model using 24 axial nodes.

The fuel assembly gamma scan measurements made at the Quad Cities 1 reactor at the end of Cycle 2[5-2] are compared to the XTGBWR calculation results in Figure 5.2-13. The measured data are La-140 activity which is proportional to the power generation in the last few weeks of the reactor operation. The calculated La-140 activity is determined from the XTGBWR power distribution.

5.3 COTRAN VERIFICATION

The reactor kinetics calculations performed by the COTRAN code are compared to the Peach Bottom-2 transient measurements.[5-3] A comparison of the measured and calculated relative power response for the periodic step change in the pressure regulator setpoint is shown in Figure 5.3-1. The measured and calculated data for the random pressure regulator setpoints changes are shown in Figure 5.3-2. For both of the comparisons, the measured reactor pressure response was input into the COTRAN calculations as a forcing function.

Table 5.1-1 Garigliano Isotopic Comparison Measured/Calculated Data

Rod Position	1A	2B	3C	4D	5E	7G	8H	9J	9A
EXPOSURE MWD/MTU	10355	10060	8939	8653	8736	10309	12424	14180	13785
	10395	9807	8699	8344	8471	10337	12741	14336	13615
U-235 Kg/MTU	7.67	12.16	13.31	13.16	13.18	11.84	10.23	5.34	5.48
	7.93	12.50	13.38	13.67	13.58	12.15	10.34	5.55	5.92
U-236 Kg/MTU	1.60	1.87	1.67	1.71	1.63	1.81	1.98	1.89	1.82
	1.38	1.53	1.41	1.38	1.39	1.59	1.83	1.70	1.65
U-238 Kg/MTU	974.1	969.9	970.0	970.4	970.4	969.6	968.8	971.6	972.2
	975.0	970.7	970.9	970.8	970.6	969.9	969.1	972.4	973.0
Pu-239 Kg/MTU	3.741	3.874	4.167	4.200	4.240	4.186	3.872	3.534	3.504
	3.248	3.674	4.040	4.257	4.341	4.052	3.605	3.082	3.090
Pu-240 Kg/MTU	1.127	.887	.814	.771	.777	.949	1.143	1.487	1.432
	1.213	.931	.812	.767	.775	.967	1.181	1.567	1.505
Pu-241 Kg/MTU	.445	.365	.340	.335	.338	.394	.442	.591	.557
	.365	.325	.289	.281	.291	.371	.462	.540	.507
Pu-242 Kg/MTU	.088	.060	.039	.037	.036	.055	.064	.185	.168
	.077	.047	.033	.029	.031	.053	.094	.181	.158

Table 5.1-2 XMC (Monte Carlo)/XFYRE K∞ Comparisons for BWR Reload Fuel Assemblies

Case	K∞ XMC	K∞ XFYRE
OC 0% V, No Gd, No Control	1.3073 ± .0018	1.305
OC 32% V, No Gd, No Control	1.2889 ± .0018	1.289
OC 32% V, No Gd, Control	0.970 ± .0024	0.970
OC 32% V, 1.0 w/o Gd_2O_3, No Control	1.2111 ± .0010	1.212
OC 64% V, No Gd, No Control	1.2590 ± .0017	1.256
OC Cold, No Gd, No Control	1.289 ± .0023	1.296
OC Cold, No Gd, Control	1.100 ± .0030	1.108

Table 5.2-1 XTGBWR Calculated K_{eff} and Average Voids for Dresden-3 Cycle 5

Cycle Exposure MWD/MTU	K_{eff}	Average Voids	Power MWt	10^6 Flow lb/hr
195.6	1.003	.33	2339	97.8
663.2	1.003	.37	2400	94.4
782.9	1.002	.37	2475	97.8
1660.0	1.002	.34	2386	98.2
2377.6	1.002	.35	2328	98.0
2599.6	0.999	.38	1772	66.7
3028.7	1.001	.36	2444	96.9
3256.2	1.002	.35	2413	97.7
3632.7	1.003	.34	2306	97.5
3968.7	1.003	.34	2317	98.0
4289.8	1.004	.34	2277	97.7
4716.8	1.004	.31	2100	97.6
5068.4	1.004	.30	1948	97.6
5597.3	1.004	.26	1758	98.0
5930.2	1.004	.23	1602	97.7
6294.8	1.004	.21	1449	97.7
6634.9	1.000	.21	449	97.7

Table 5.2-2 XTGBWR Calculated K_{eff} and Average Voids for Dresden-3 Cycle 6

Cycle Exposure MWD/MTU	K_{eff}	Average Voids	Power MWt	10^6 Flow lb/hr
250.9	1.006	.35	2218	83.3
330.3	1.006	.34	2382	93.6
550.8	1.007	.33	2445	97.3
719.1	1.004	.36	2103	74.6
876.3	1.005	.35	2364	91.8
993.6	1.006	.35	2418	95.3
1432.5	1.005	.35	2409	97.0
1674.0	1.005	.34	2408	94.5
1882.5	1.003	.35	2471	95.3
2221.2	1.004	.34	2458	97.7
2480.8	1.003	.36	2491	97.9
2825.6	1.003	.35	2338	98.0
3177.6	1.002	.38	2292	85.3
3275.2	0.997	.42	1894	63.1
3335.9	1.004	.36	2423	95.5
3657.1	1.004	.34	2376	95.4
3843.5	1.004	.35	2412	98.1
4216.8	1.006	.35	2450	97.8
4583.7	1.006	.34	2304	94.0
4874.1	1.000	.38	1903	67.6
5080.9	1.002	.34	1892	75.4
5305.1	1.004	.31	1877	83.7
5600.0	1.004	.34	1744	65.5
5987.3	1.001	.32	1808	65.3
6222.1	1.004	.31	1706	71.4
6481.6	1.003	.30	1701	72.7
6732.8	1.004	.27	1717	84.0
6923.4	1.005	.25	1718	94.3
7142.8	1.002	.25	1718	94.3

Table 5.2-3 XTGBWR Calculated K_{eff} and Average Voids for Oyster Creek Cycle 7

Cycle Exposure MWD/MTU	K_{eff}	Average Voids	Power MWt	Flow 10^6 lb/hr
121.3	1.005	.34	1766	56.4
293.0	1.006	.35	1752	55.7
565.9	1.005	.35	1877	55.8
869.0	1.004	.36	1828	51.5
939.8	1.003	.36	1795	51.8
1232.8	1.002	.36	1817	51.8
1536.0	1.002	.33	1787	52.2
1889.6	1.001	.35	1878	54.9
2401.2	1.001	.35	1833	53.4
2233.2	1.003	.35	1883	58.3
2536.4	1.002	.36	1867	55.9
2890.0	1.005	.32	1856	59.9
3021.4	1.005	.32	1892	60.5
3304.3	1.004	.34	1893	57.2
3668.1	1.005	.36	1893	57.6
3961.2	1.006	.33	1890	60.8
4254.2	1.006	.33	1892	60.6
4628.1	1.005	.37	1820	53.5
4890.8	1.006	.35	1887	61.0
5103.0	1.007	.35	1817	59.5
5244.5	1.005	.36	1781	61.0
5668.9	1.004	.35	1667	61.0
5937.6	1.005	.34	1594	61.0
6224.7	1.005	.34	1481	61.0
6558.1	1.006	.29	1372	61.0
6861.3	1.006	.27	1281	61.0

Table 5.2-4 XTGBWR Calculated K_{eff} and Average Voids for Oyster Creek Cycle 8

Cycle Exposure MWD/MTU	K_{eff}	Average Voids	Power MWt	10^6 Flow lb/hr
262.7	1.001	.36	1926	60.2
495.1	0.999	.38	1929	57.9
747.8	0.999	.38	1917	58.7
1253.0	0.997	.37	1914	59.5
1525.9	0.997	.38	1918	57.6
1748.2	0.997	.37	1912	57.6
2051.3	0.996	.37	1912	60.0
2405.0	0.997	.36	1806	53.3
2728.4	0.999	.34	1883	58.9
3132.6	0.999	.36	1779	53.8
3304.3	0.999	.35	1914	58.4
3516.6	0.999	.35	1921	58.0
3799.5	1.000	.34	1906	59.7
4102.6	1.000	.35	1906	59.3
4345.2	1.002	.35	1810	56.5
4729.1	1.001	.36	1910	59.6
4870.6	1.001	.37	1906	59.0
5133.3	1.002	.37	1892	60.1
5355.7	1.002	.37	1867	60.0
5689.1	1.001	.39	1777	59.5
5860.9	1.001	.38	1724	59.8
6103.4	1.000	.37	1660	60.0

Table 5.2-5 XTGBWR Calculated K_{eff} and Average Voids for Quad Cities Cycle 1

Cycle Exposure MWD/MTU	K_{eff}	Power MWt
272.3	0.997	2184
712.1	1.003	2235
881.9	1.002	2240
1470.6	1.003	2197
2238.9	1.002	2450
3190.2	1.000	2413
3836.2	0.998	2197
4074.2	1.001	2320
4730.1	0.997	2377
5301.6	0.997	2337
6559.2	0.997	2225
6807.3	0.998	2210
7397.0	0.996	2267
7659.4	0.997	2187
7980.2	0.997	2203

Table 5.2-6 XTGBWR Calculated K_{eff} and Average Voids for Quad Cities Cycle 2

Cycle Exposure MWD/MTU	K_{eff}	Power MWt
245.8	0.997	2171
677.9	1.002	2156
1136.5	0.995	2096
1502.5	0.998	2411
1855.2	1.000	2500
2886.9	1.000	2463
3951.7	0.997	2474
4648.3	1.000	2153
5609.5	0.999	1829
5911.5	0.998	1713
6324.5	0.998	1547
6954.5	0.998	1487

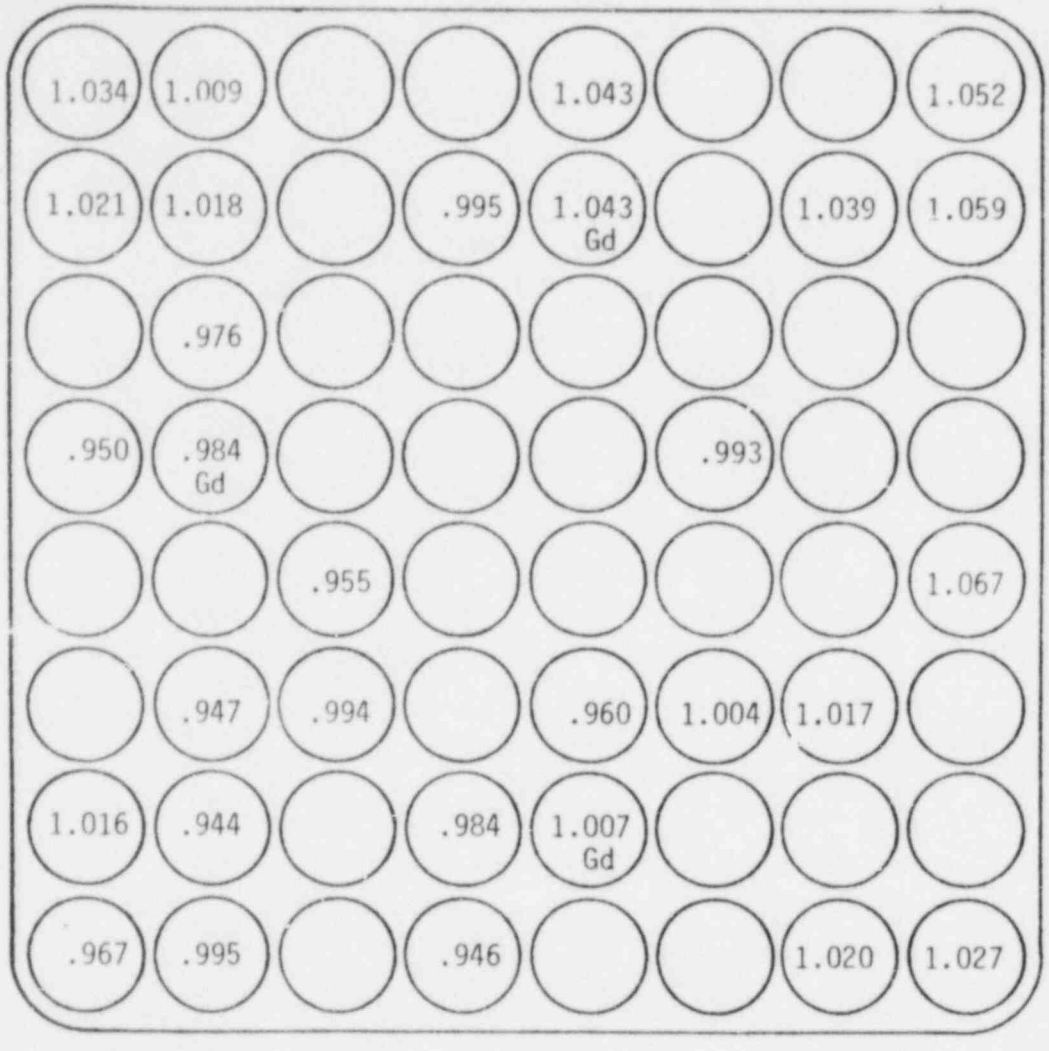

Calculation / Measured

OC Fuel Assembly - UD 3109

Distance Above Bottom of Fuel - 27.5 inches

Exposure - 4,500 MWD/MTU

Void Fraction - 0

Gamma Scan Data - La-140

Figure 5.1-1 Comparison of XFYRE Calculated/Gamma Scan Measured Local Power Distribution for ENC 8x8 Reload Fuel

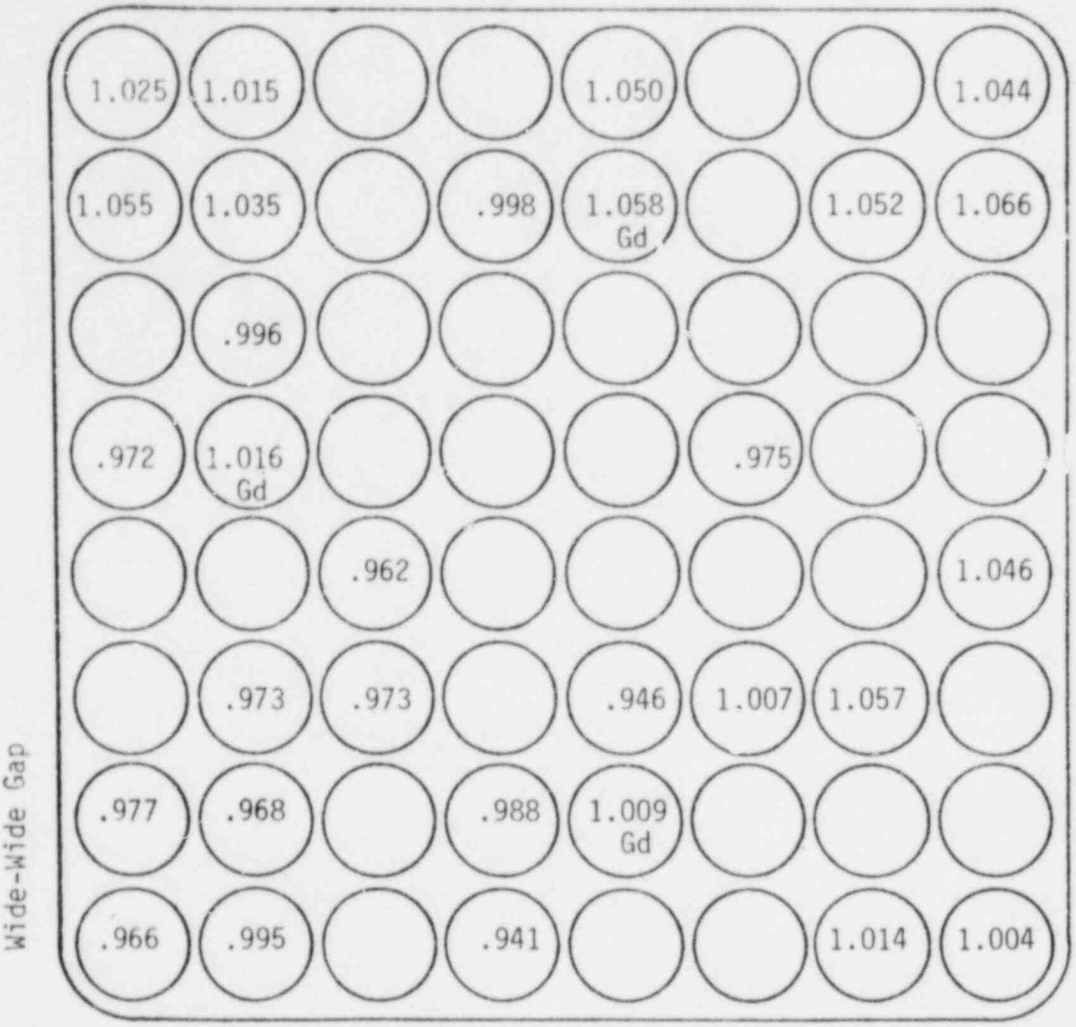

OC Fuel Assembly - UD 3109

Distance Above Bottom of Fuel - 47.0 inches

Exposure - 3,800 MWD/MTU

Void Fraction - 0.34

Gamma Scan Data - La-140

Calculation / Measured

Figure 5.1-2 Comparison of XFYRE Calculated/Gamma Scan Measured Local Power Distribution for ENC 8x8 Reload Fuel

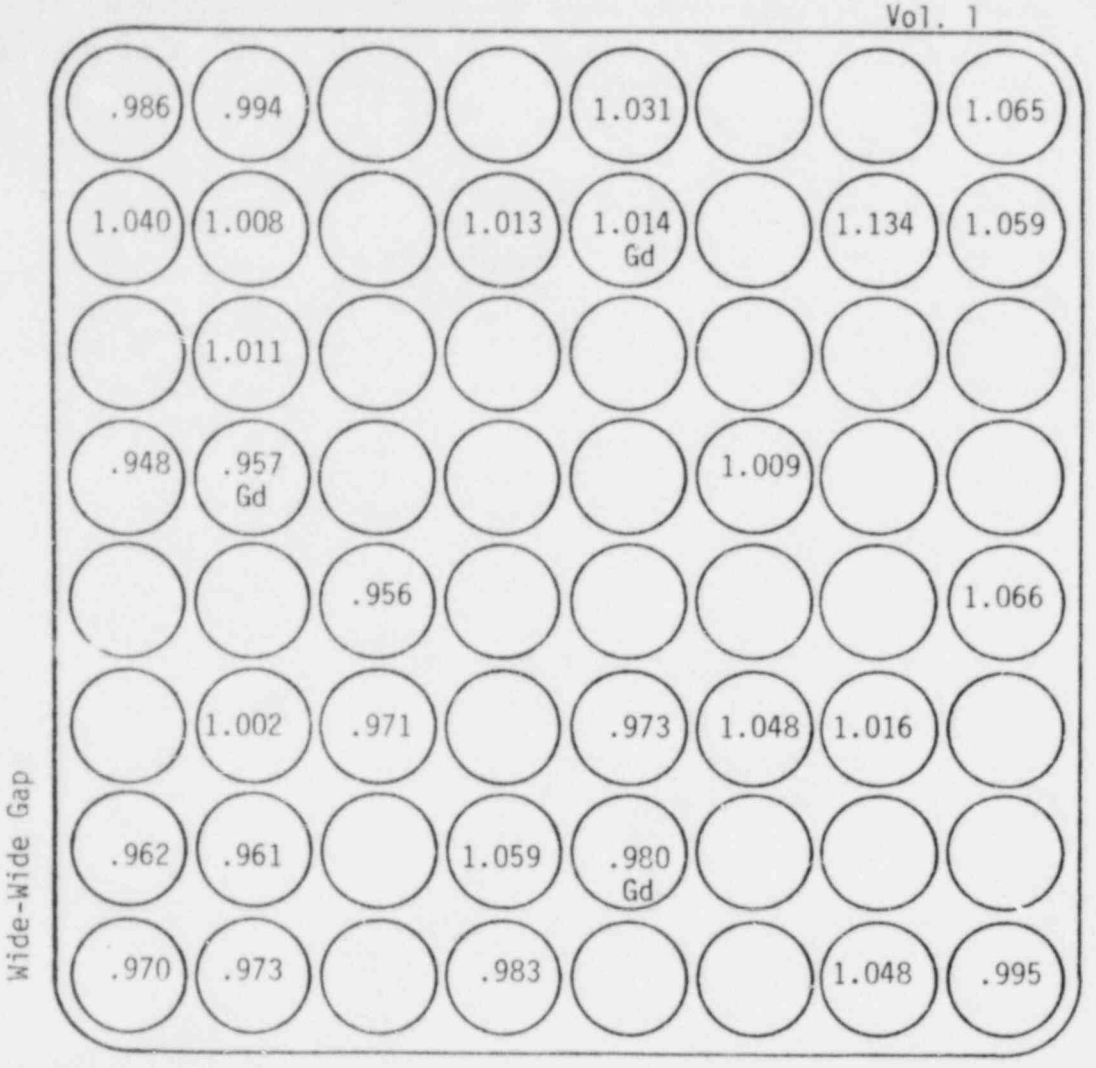

Calculation
Measured

OC Fuel Assembly - UD 3109

Distance Above Bottom of Fuel - 105.6 inches

Exposure - 3,400 MWD/MTU

Void Fraction - 0.65

Gamma Scan Data - La-140

Figure 5.1-3 Comparison of XFYRE Calculated/Gamma Scan Measured Local Power Distribution for ENC 8x8 Reload Fuel

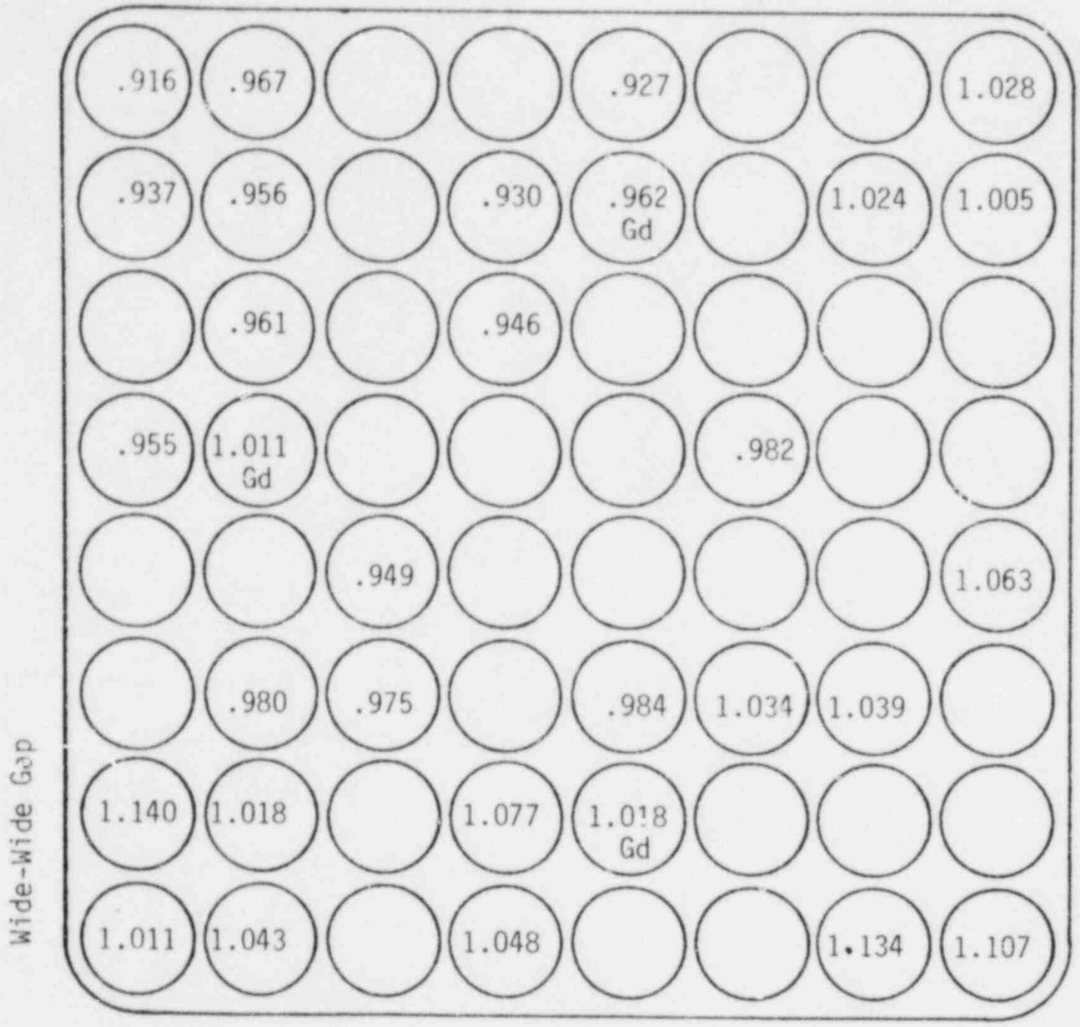

OC Fuel Assembly - UD 4070

Distance Above Bottom of Fuel - 47 inches

Exposure - 3,900 MWD/MTU

Void Fraction - 0.31

Gamma Scan Data - La-140

Calculation / Measured

Figure 5.1-4 Comparison of XFYRE Calculated/Gamma Scan Measured Local Power Distribution for ENC 8x8 Reload Fuel

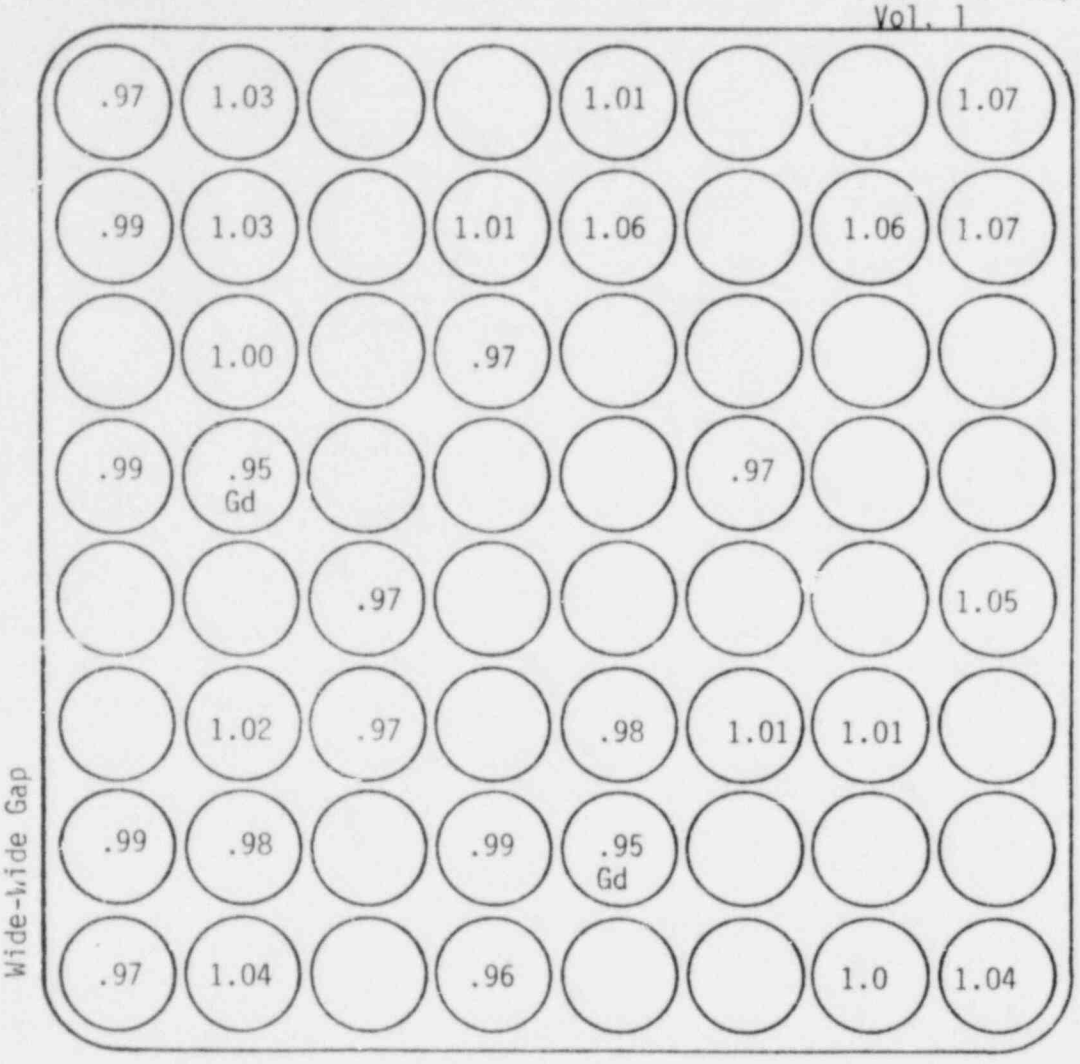

Calculation / Measured

OC Fuel Assembly - UD 4070

Distance Above Bottom of Fuel - 125 inches

Exposure - 3,100 MWD/MTU

Void Fraction - 0.66

Gamma Scan Data - La-140

Figure 5.1-5 Comparison of XFYRE Calculated/Gamma Scan Measured Local Power Distribution for ENC 8x8 Reload Fuel

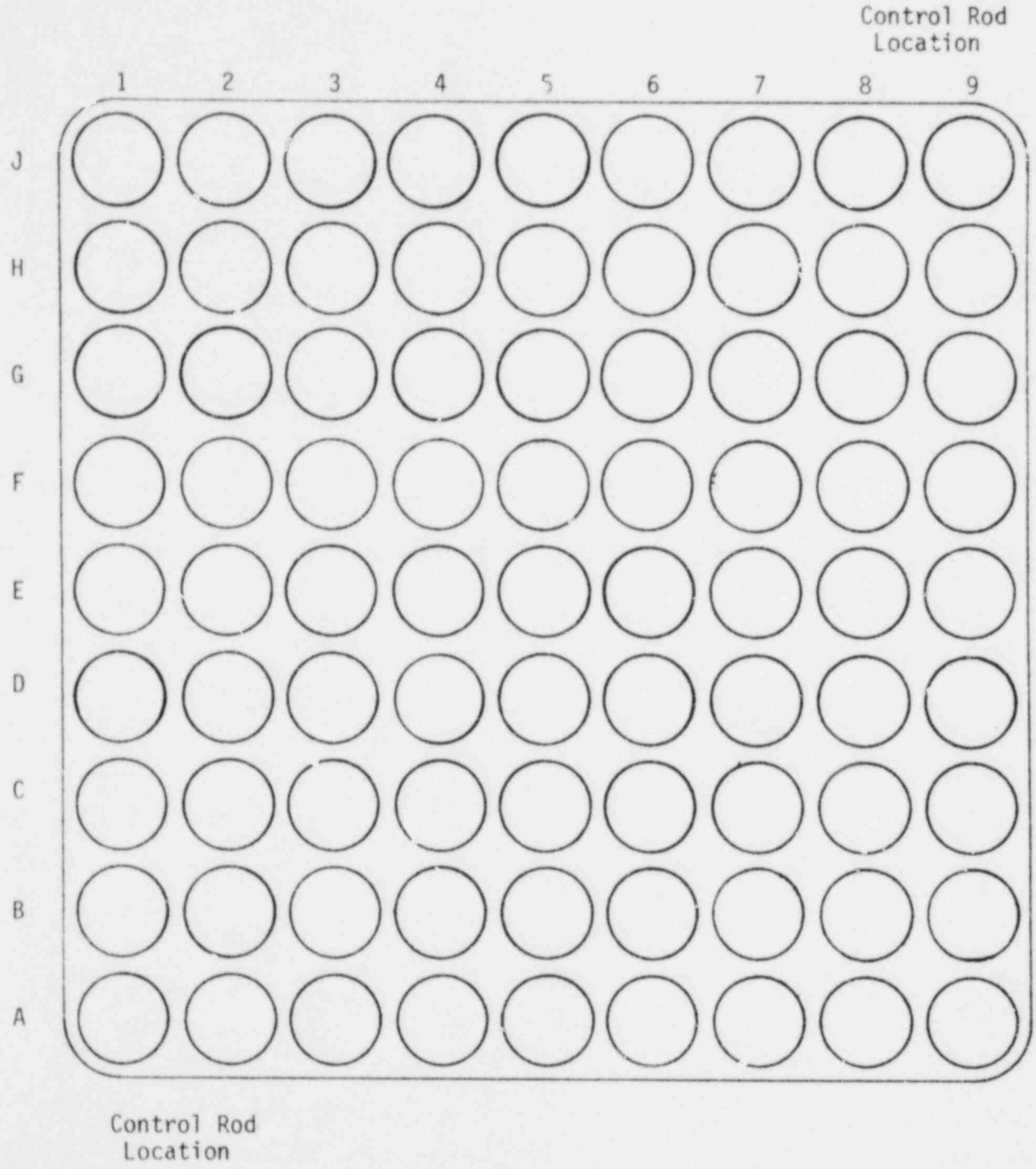

Figure 5.1-6 Fuel Rod Position Identification for Garigliano Isotopic Comparison

0.943 0.934 ±.010	1.077 1.072 ±.007	1.086 1.088 ±.009	1.035 1.060 ±.018	1.040 1.049 ±.016	1.101 1.104 ±.020	1.096 1.106 ±.030
1.168 1.146 ±.010	1.059 1.050 ±.013	0.936 0.947 ±.008	0.894 0.902 ±.011	0.900 0.911 ±.014	0.955 0.947 ±.018	
1.100 1.097 ±.011	0.991 1.010 ±.010	0.877 0.886 ±.011	0.840 0.841 ±.012	0.846 0.840 ±.013		
1.095 1.098 ±.010	0.984 0.970 ±.011	0.871 0.872 ±.009	0.833 0.849 ±.015			
1.152 1.167 ±.017	1.039 1.019 ±.014	0.914 0.883 ±.016				
0.924 0.919 ±.021	1.042 1.018 ±.020					
1.092 1.065 ±.018	XFYRE XMC ±1σ					

Figure 5.1-7 XFYRE/XMC (Monte Carlo) Calculated Local Power Distribution for Oyster Creek BWR Reload Fuel, 0% V - No Gadolinia - No Control

0.987 1.015 ±.009	1.109 1.129 ±.009	1.073 1.086 ±.012	0.975 0.969 ±.007	0.994 0.988 ±.013	1.079 1.058 ±.014	1.082 1.082 ±.017
1.229 1.255 ±.013	1.100 1.114 ±.011	0.905 0.884 ±.008	0.407* 0.380 ±.004	0.824 0.813 ±.011	0.922 0.898 ±.011	
1.167 1.188 ±.011	1.040 1.049 ±.008	0.872 0.873 ±.008	0.773 0.759 ±.006	0.775 0.755 ±.010		
1.173 1.173 ±.011	1.051 1.047 ±.009	0.899 0.898 ±.009	0.821 0.833 ±.011			
1.248 1.255 ±.011	1 128 1.117 ±.014	0.973 0.962 ±.014				
1.011 1.006 ±.011	1.143 1.139 ±.012					
1.193 1.216 ±.016	XFYRE XMC ±1σ					

* 1.0 w/o Gd_2O_3

Figure 5.1-8 XFYRE/XMC (Monte Carlo) Calculated Local Power Distribution for Oyster Creek BWR Reload Fuel 32% V - With Gadolinia - No Control

0.940 0.944 ±.013	1.074 1.076 ±.015	1.076 1.076 ±.015	1.016 0.994 ±.011	1.016 0.998 ±.012	1.075 1.083 ±.017	1.065 1.082 ±.018
1.170 1.182 ±.013	1.068 1.064 ±.010	0.935 0.912 ±.010	0.883 0.856 ±.011	0.885 0.848 ±.009	0.940 0.937 ±.016	
1.107 1.121 ±.013	1.002 1.007 ±.007	0.878 0.881 ±.005	0.829 0.840 ±.008	0.832 0.819 ±.012		
1.106 1.130 ±.011	1.001 1.001 ±.009	0.875 0.872 ±.008	0.827 0.825 ±.009			
1.169 1.203 ±.015	1.064 1.068 ±.012	0.928 0.940 ±.013				
0.943 0.942 ±.010	1.070 1.071 ±.012					
1.111 1.141 ±.019	XFYRE XMC ±1σ					

Figure 5.1-9 XFYRE/XMC (Monte Carlo) Calculated Local Power Distribution for Oyster Creek BWR Reload Fuel, 32% V - No Gadolinia - No Control

0.918 0.961 ±.009	1.176 1.188 ±.012	1.305 1.324 ±.012	1.328 1.341 ±.016	1.395 1.406 ±.013	1.518 1.527 ±.026	1.526 1.542 ±.028
0.948 0.966 ±.009	1.083 1.096 ±.011	1.093 1.079 ±.010	1.128 1.105 ±.009	1.193 1.181 ±.011	1.307 1.323 ±.015	
0.763 0.755 ±.009	0.929 0.944 ±.012	0.968 0.981 ±.011	1.015 1.001 ±.014	1.082 1.089 ±.016		
0.680 0.672 ±.009	0.843 0.843 ±.013	0.892 0.883 ±.013	0.944 0.928 ±.012			
0.645 0.620 ±.009	0.796 0.778 ±.008	0.840 0.846 ±.012				
0.465 0.435 ±.006	0.676 0.653 ±.014					
0.467 0.446 ±.011	XFYRE XMC ±1σ					

Figure 5.1-10 XFYRE/XMC (Monte Carlo) Calculated Local Power Distribution for Oyster Creek BWR Reload Fuel, 32% V - No Gadolinia - Controlled

0.917 0.968 ±.009	1.060 1.095 ±.012	1.062 1.070 ±.012	0.996 0.989 ±.009	0.989 0.984 ±.012	1.038 1.040 ±.009	1.013 1.035 ±.016
1.155 1.201 ±.012	1.077 1.083 ±.010	0.944 0.920 ±.013	0.884 0.848 ±.010	0.878 0.840 ±.011	0.925 0.908 ±.012	
1.102 1.138 ±.011	1.023 0.999 ±.008	0.894 0.853 ±.008	0.837 0.793 ±.008	0.832 0.791 ±.013		
1.109 1.119 ±.012	1.028 1.000 ±.009	0.899 0.863 ±.009	0.841 0.816 ±.009			
1.175 1.222 ±.009	1.097 1.101 ±.011	0.961 0.950 ±.012				
0.949 0.974 ±.010	1.097 1.116 ±.016					
1.102 1.184 ±.014	XFYRE XMC ±1σ					

Figure 5.1-11 XFYRE/XMC (Monte Carlo) Calculated Local Power Distribution for Oyster Creek BWR Reload Fuel, 64% V - No Gadolinia - No Control

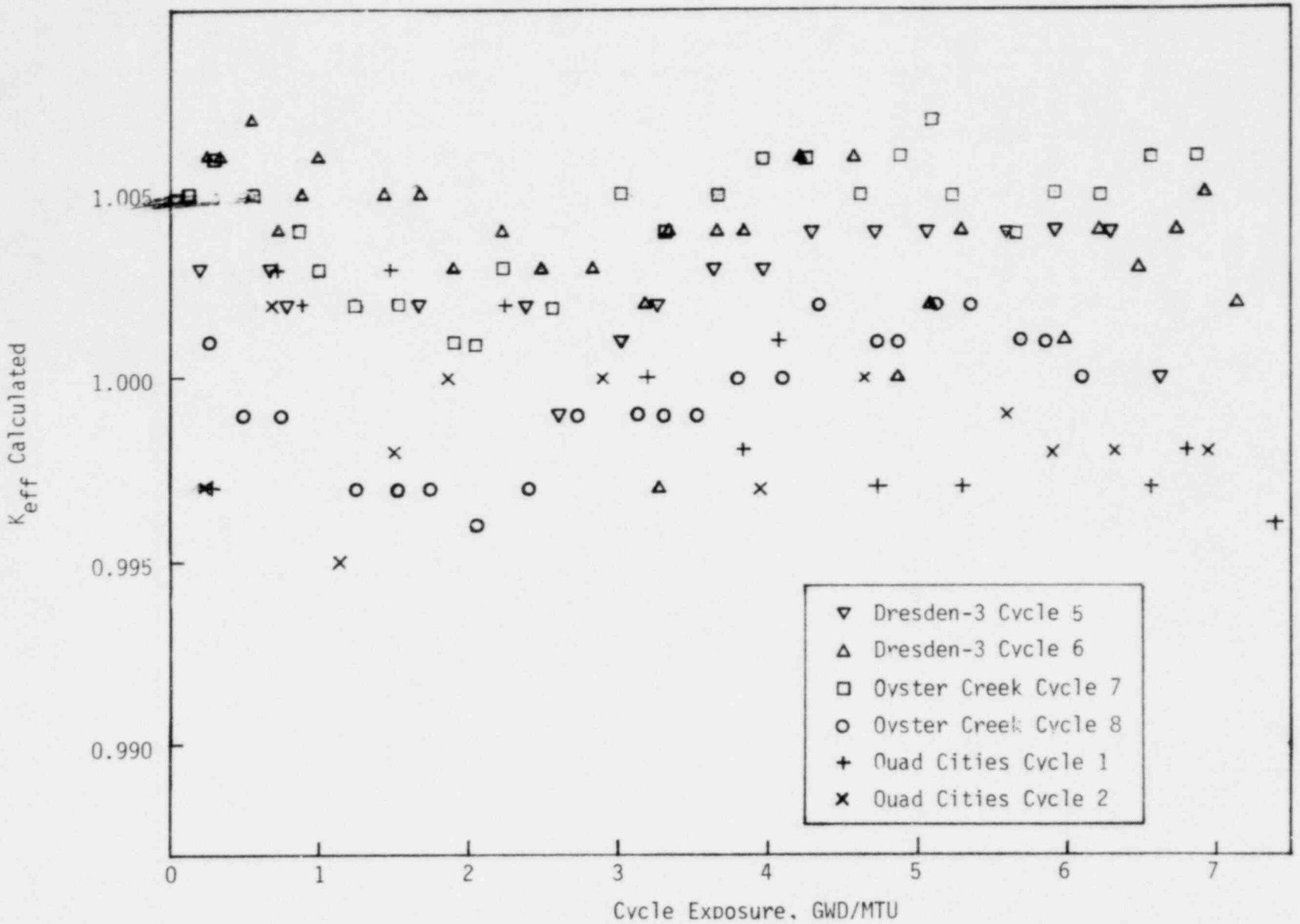

Figure 5.2-1 Calculated K_{eff} as a Function of Cycle Exposure

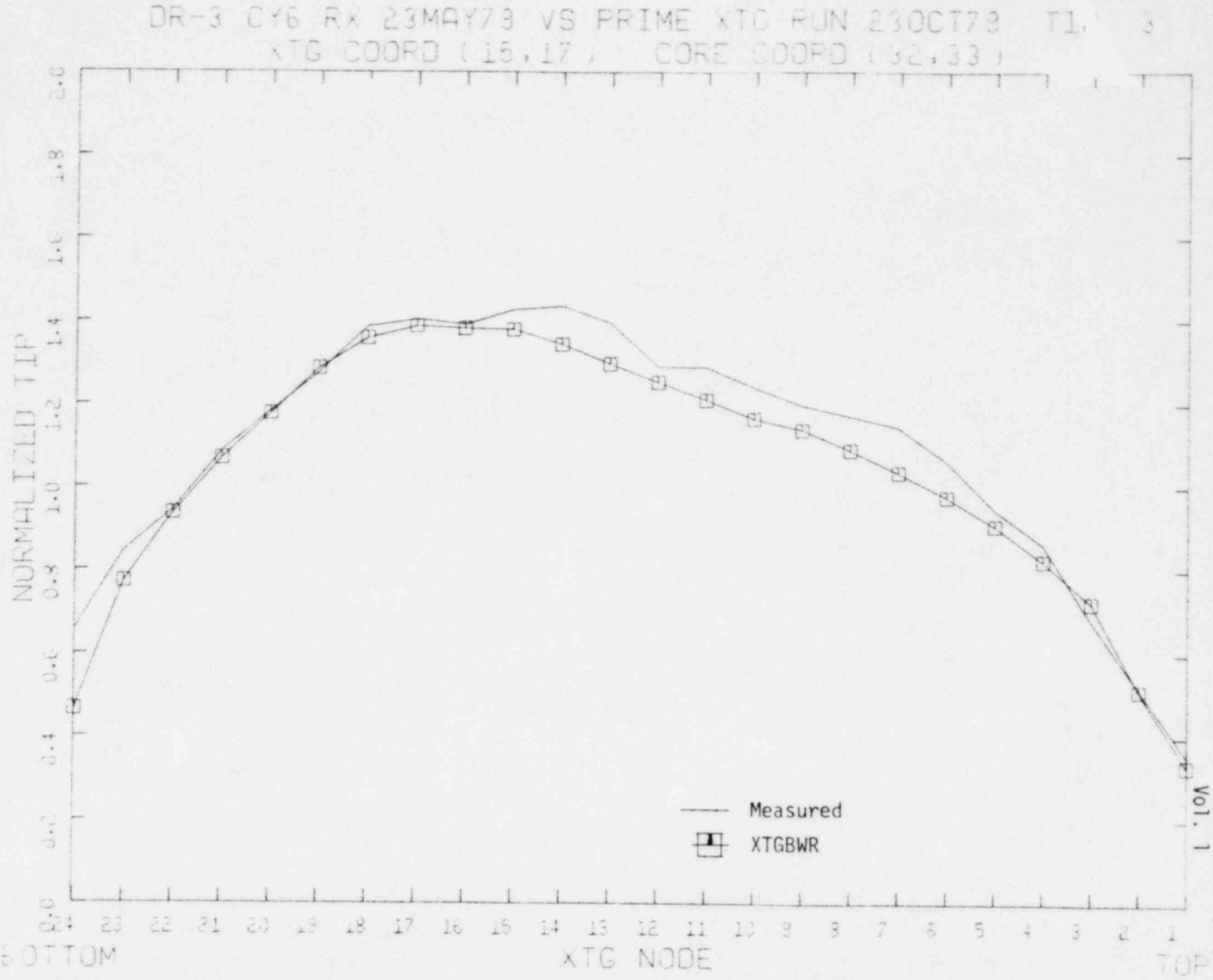

Figure 5.2-2 Dresden-3 Measured and XTGBWR Calculated TIP Comparison

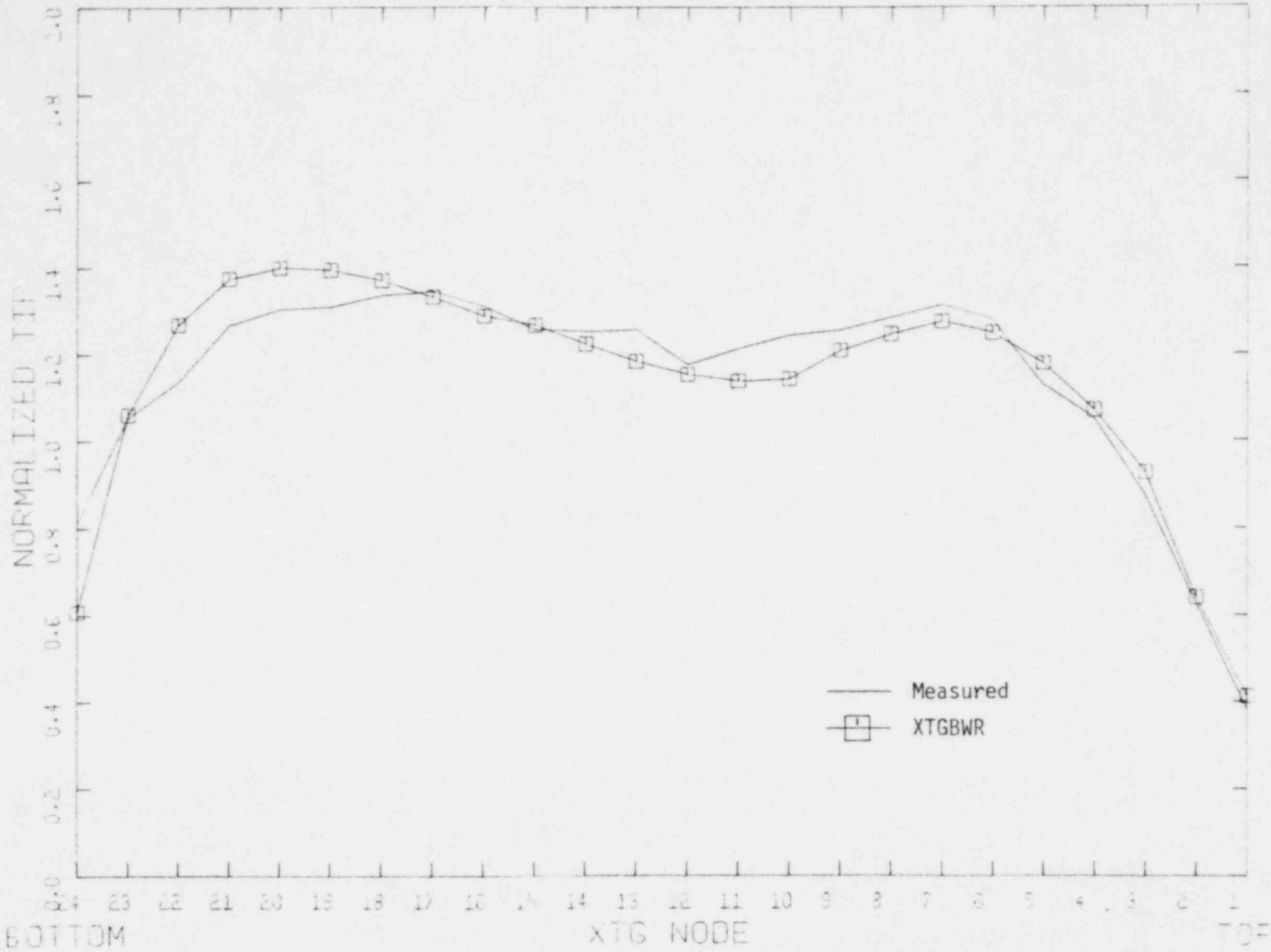

Figure 5.2-3 Dresden-3 Measured and XTGBWR Calculated TIP Comparison

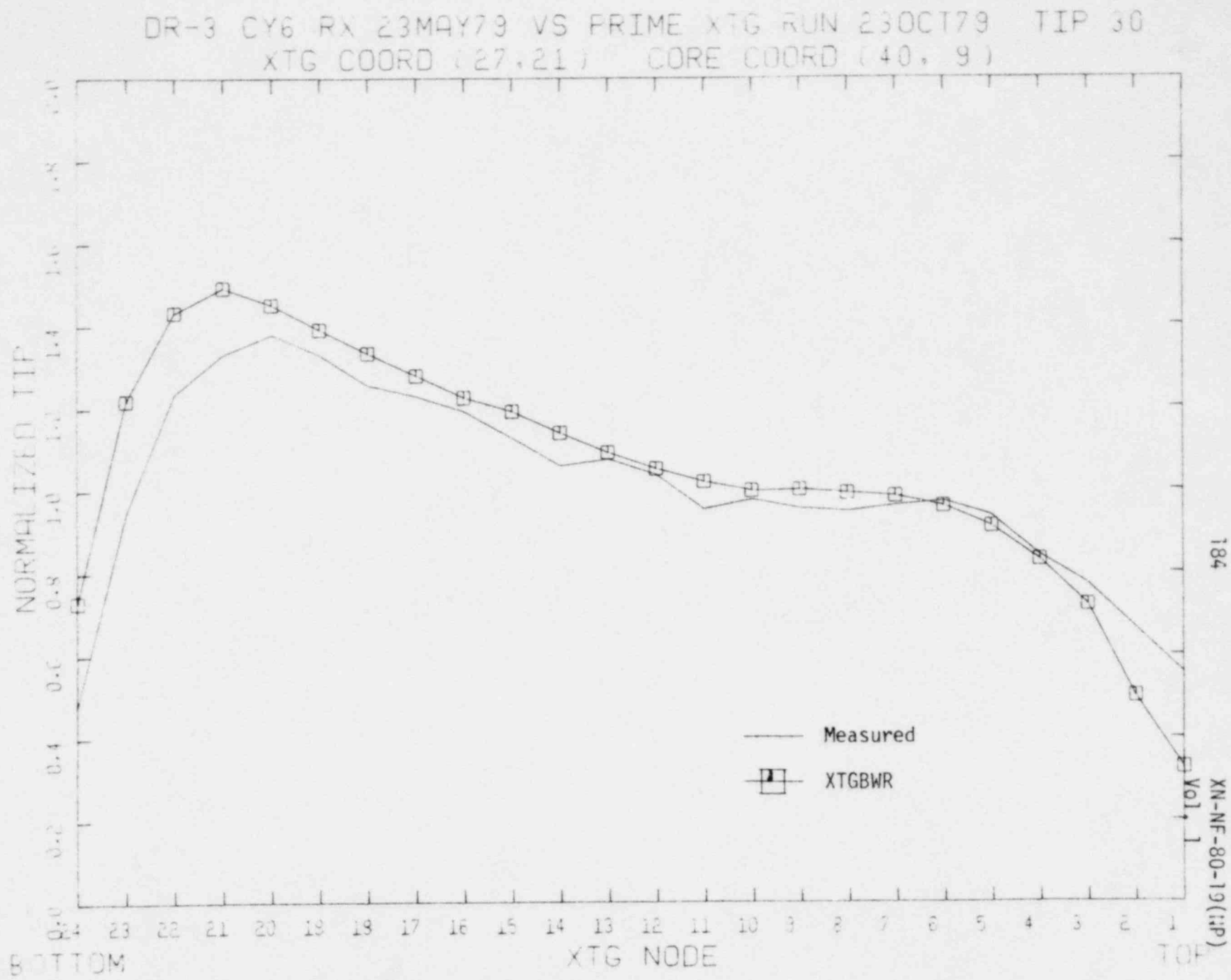

Figure 5.2-4 Dresden-3 Measured and XTGBWR Calculated TIP Comparison

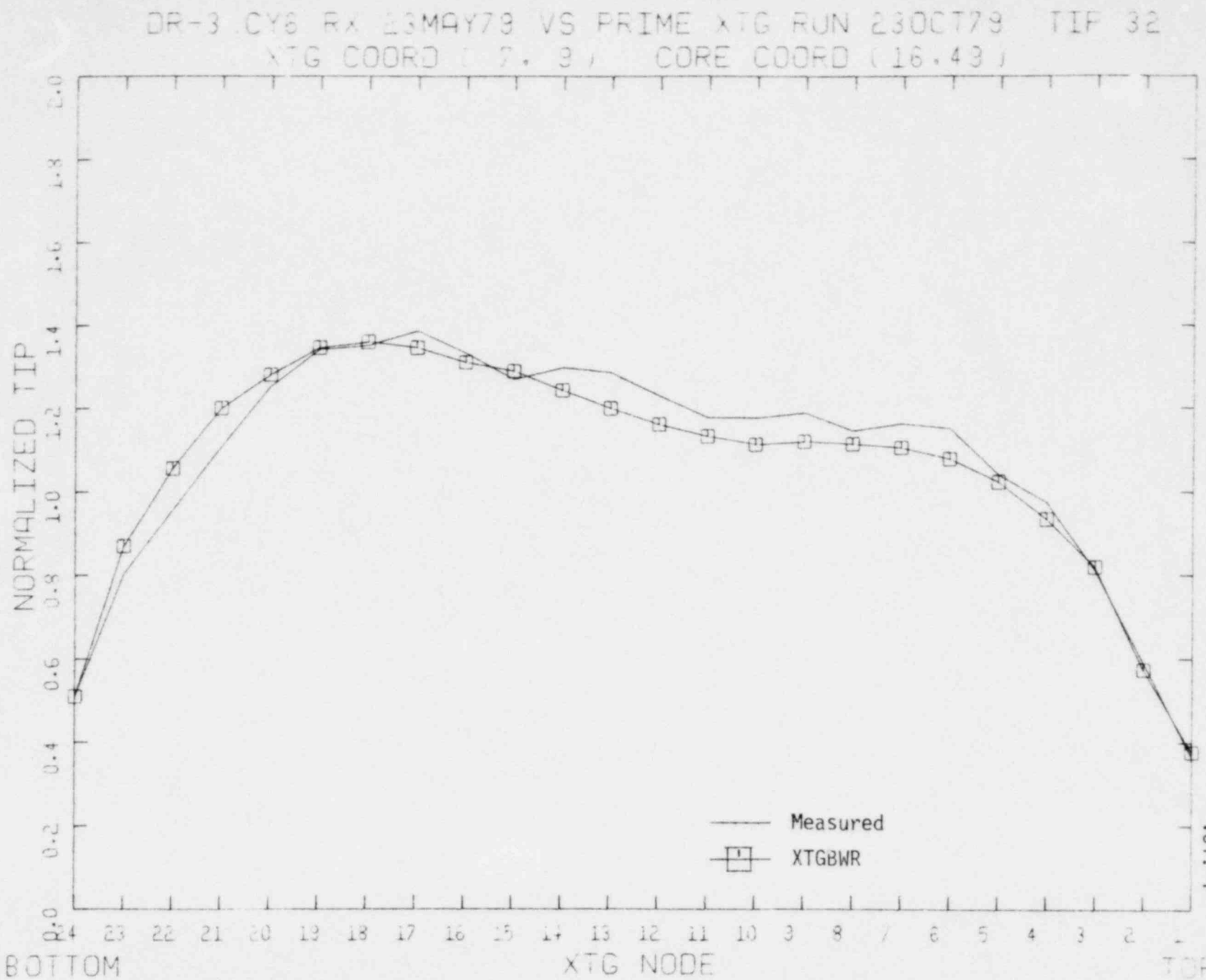

Figure 5.2-5 Dresden-3 Measured and XTGBWR Calculated TIP Comparison

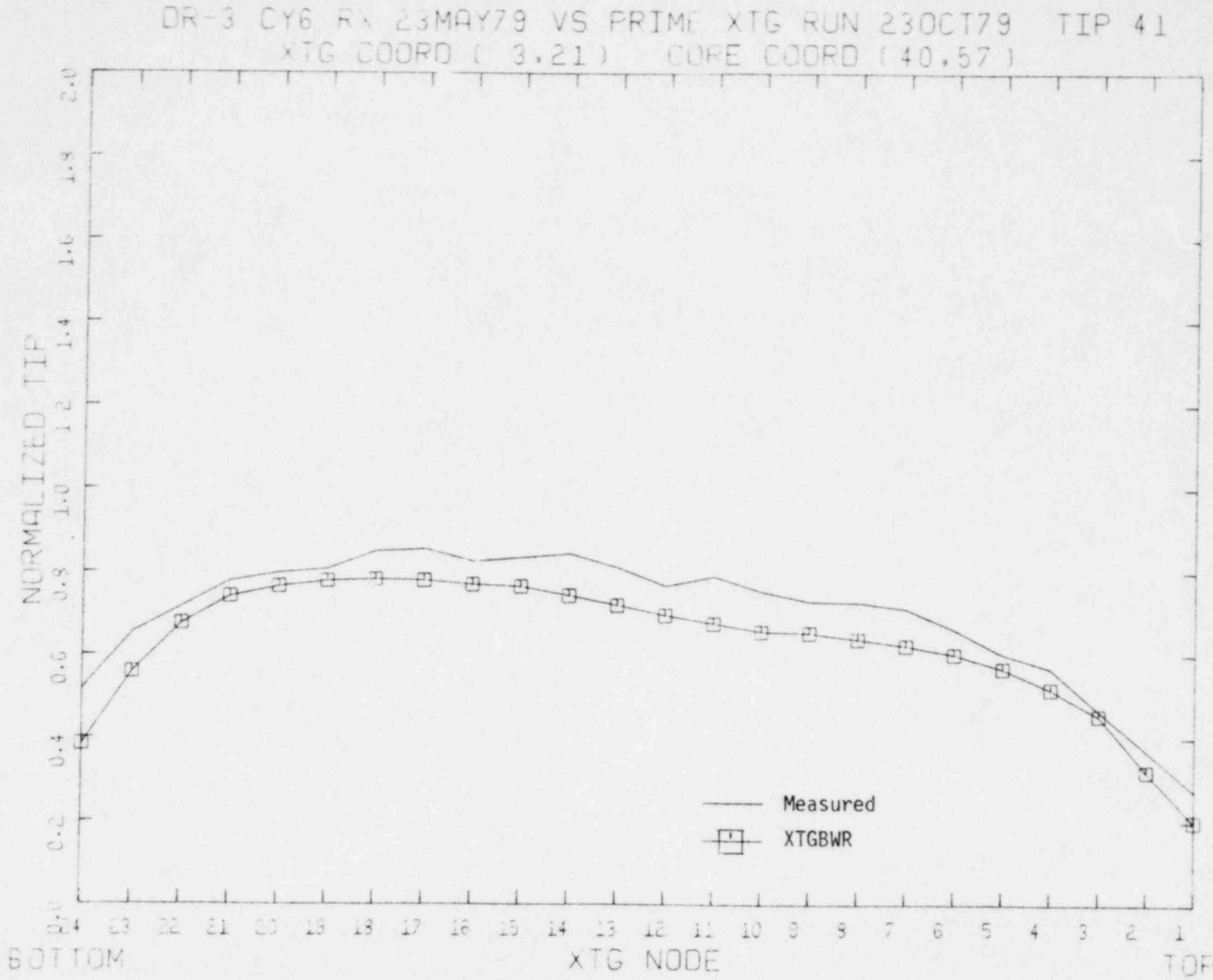

Figure 5.2-6 Dresden-3 Measured and XTGBWR Calculated TIP Comparison

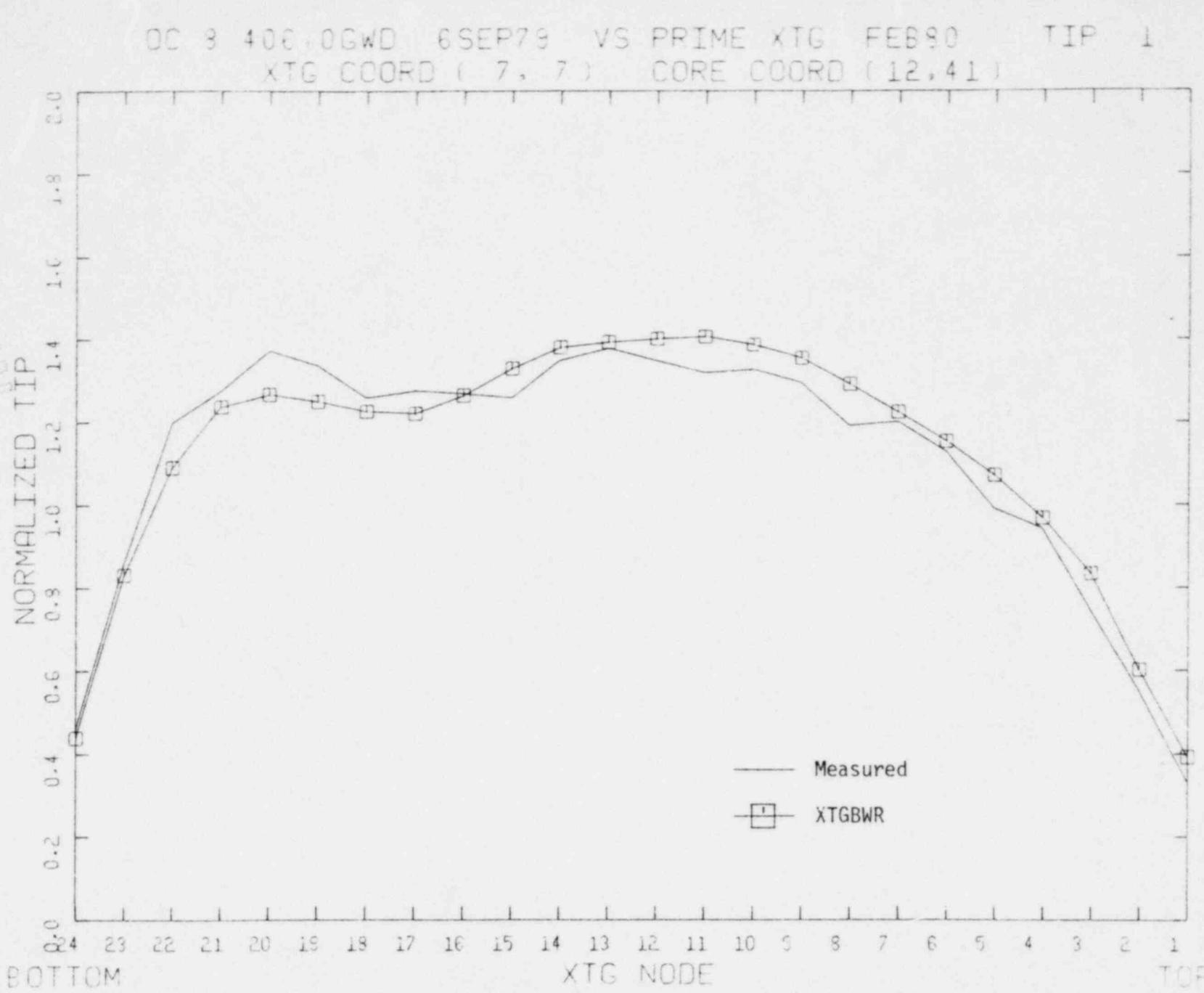

Figure 5.2-7 Oyster Creek Measured and Calculated TIP Comparison

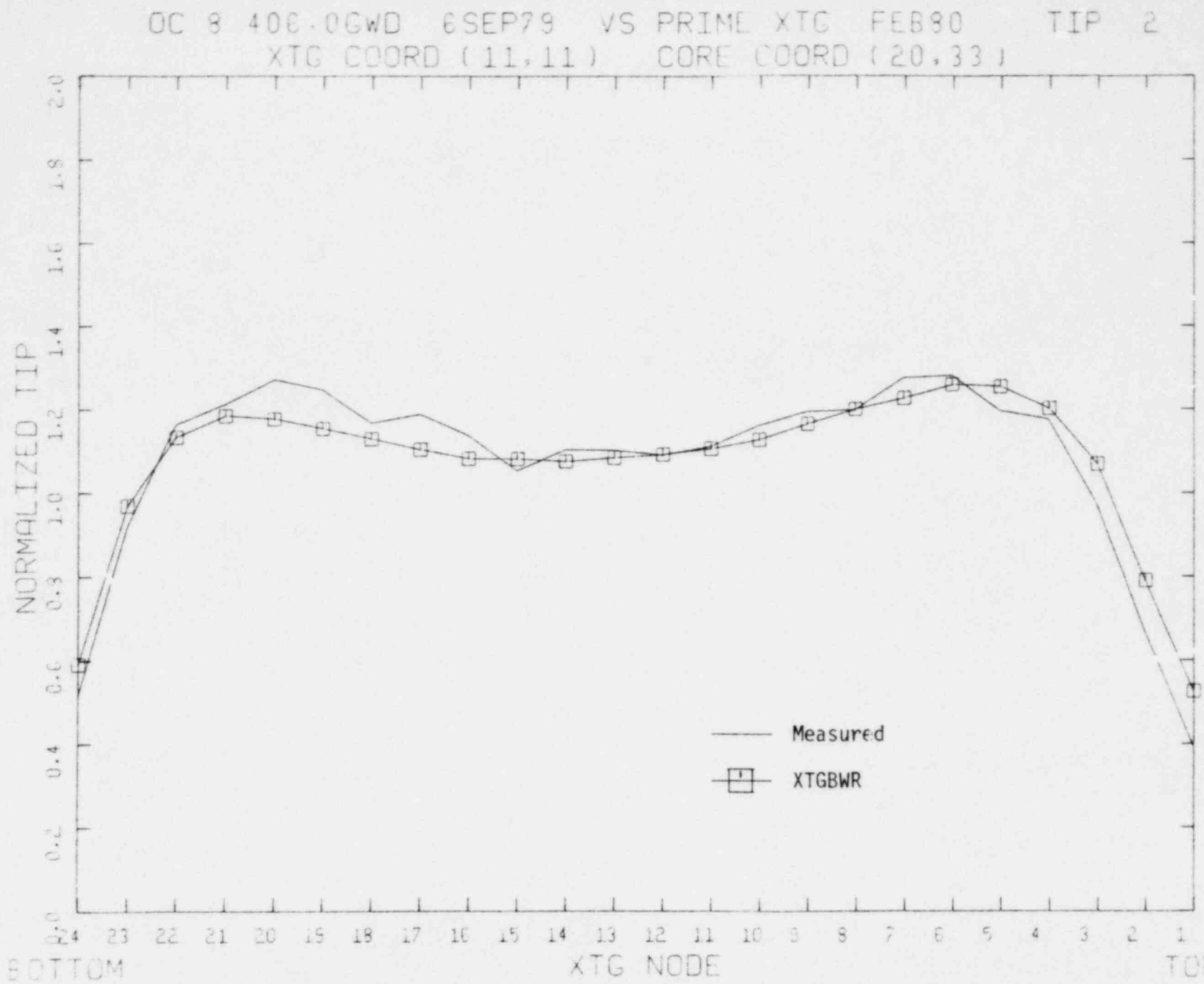

Figure 5.2-8 Oyster Creek Measured and Calculated TIP Comparison

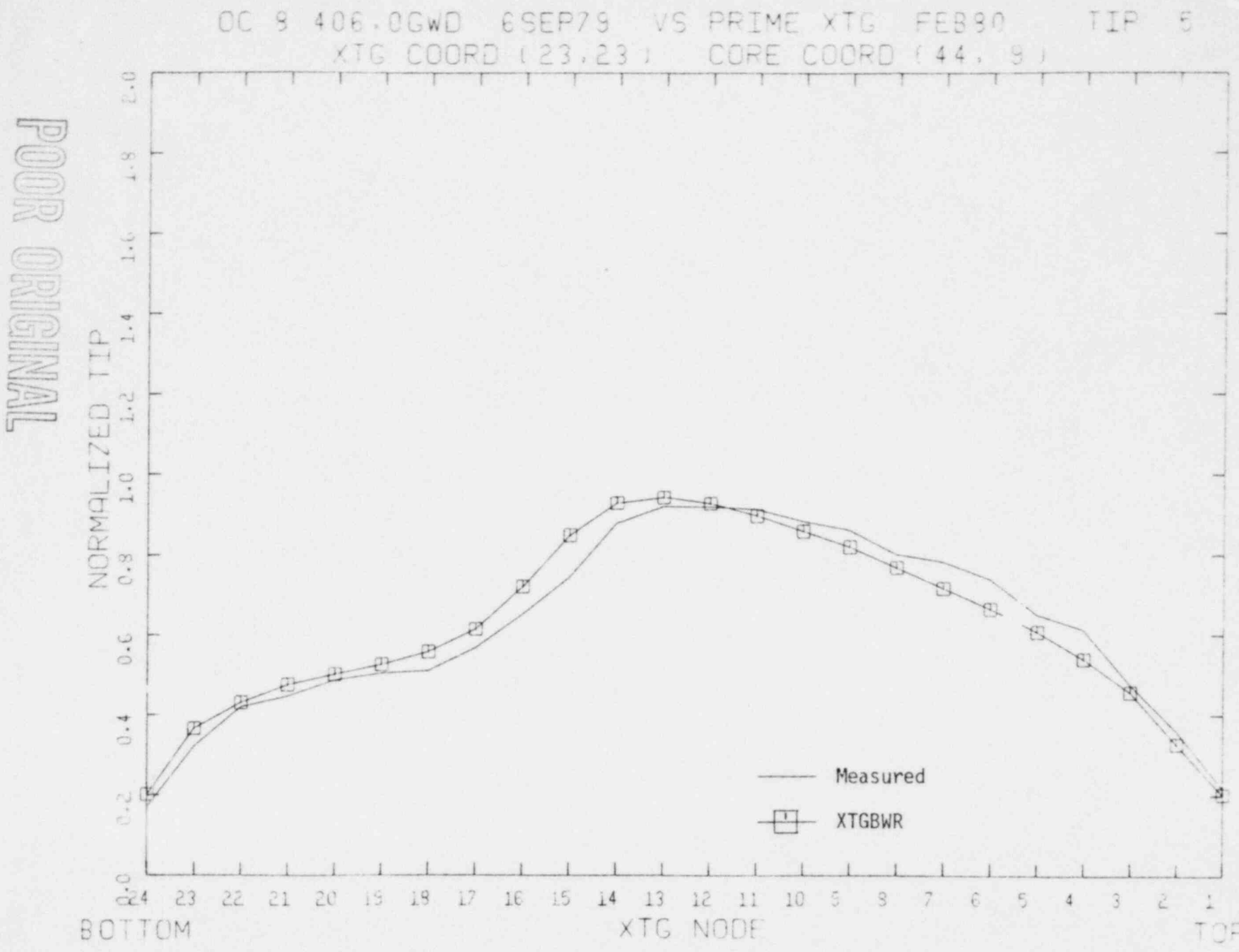

Figure 5.2-9 Oyster Creek Measured and Calculated TIP Comparison

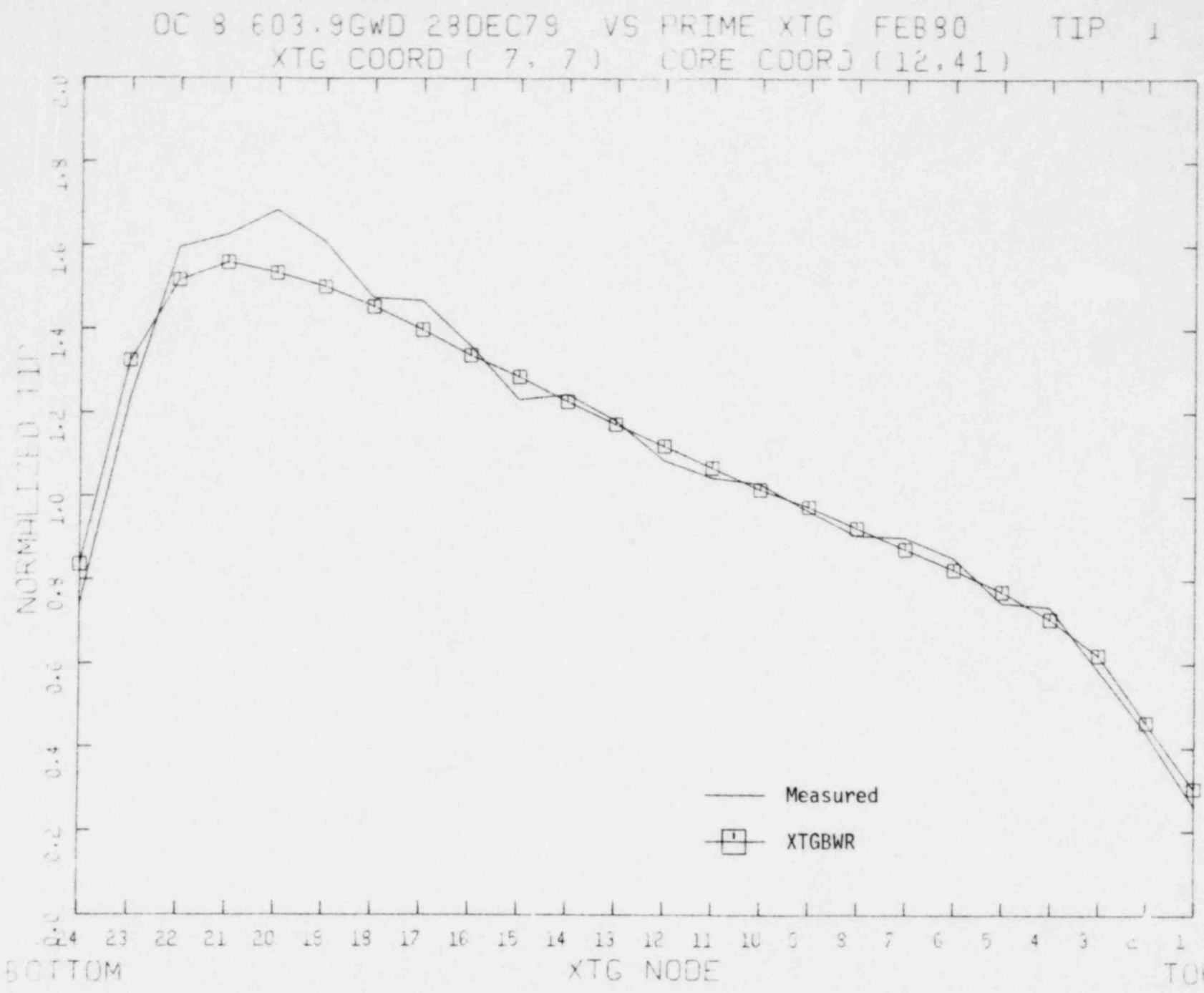

Figure 5.2-10 Oyster Creek Measured and Calculated TIP Comparison

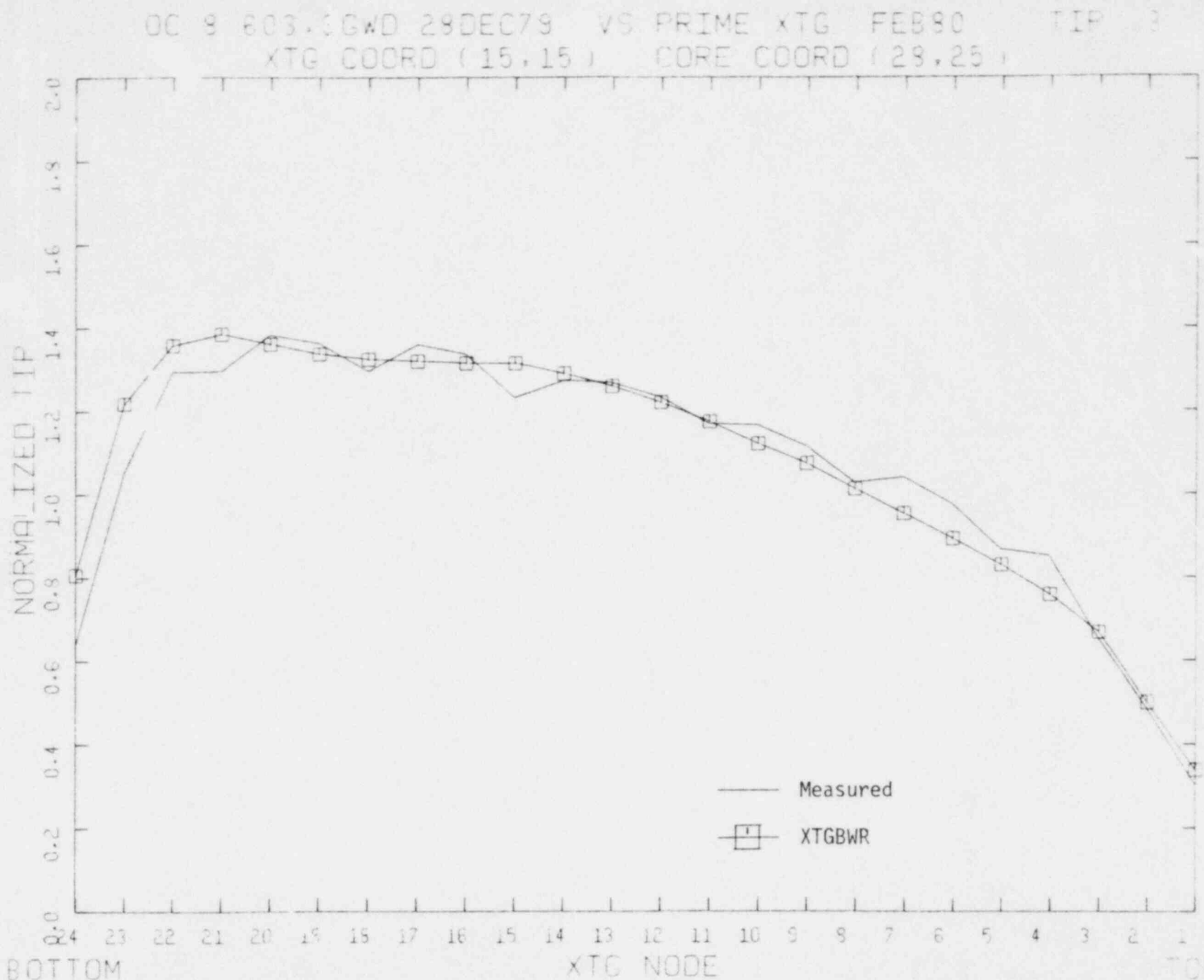

Figure 5.2-11 Oyster Creek Measured and Calculated TIP Comparison

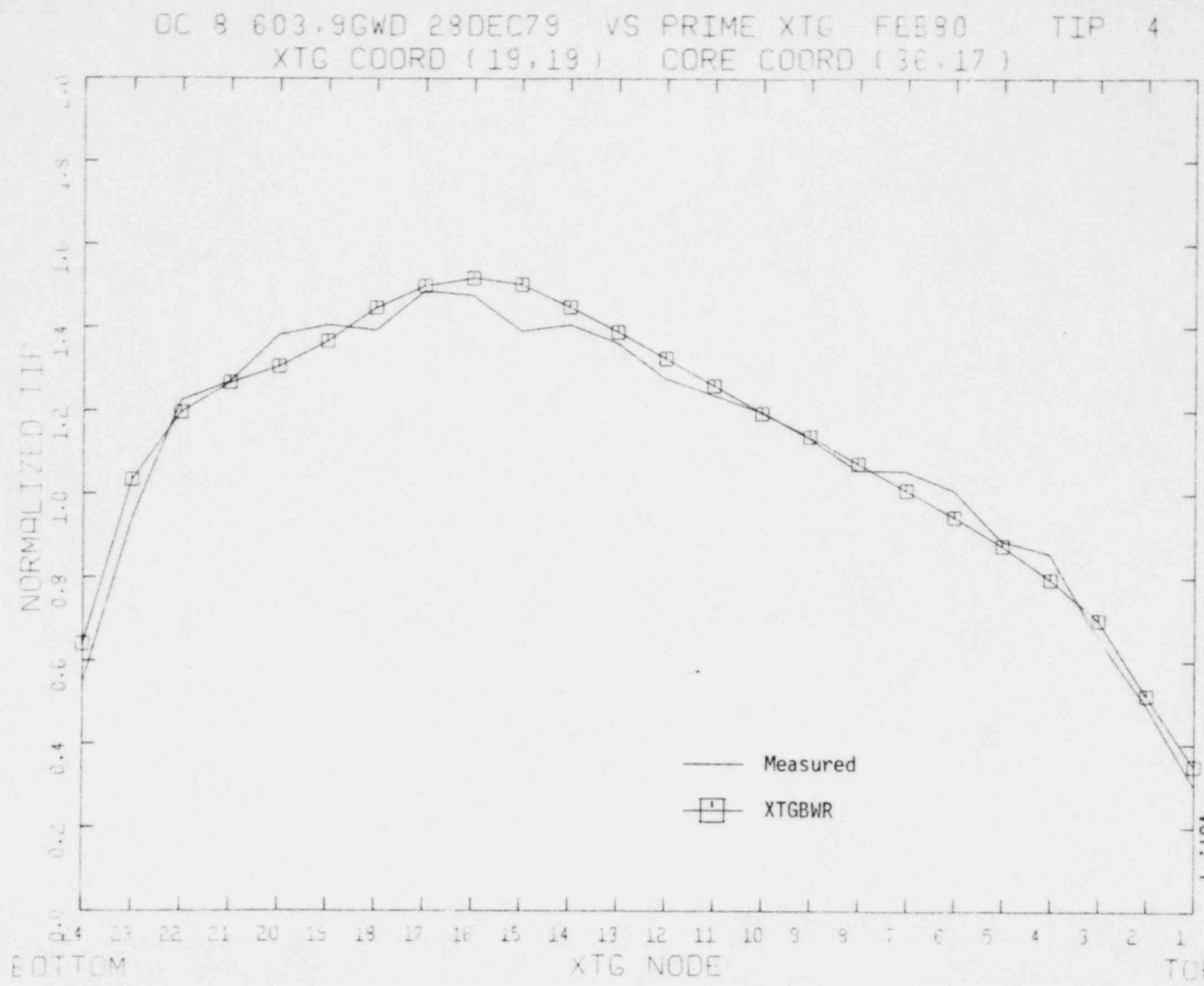

Figure 5.2-12 Oyster Creek Measured and Calculated TIP Comparison

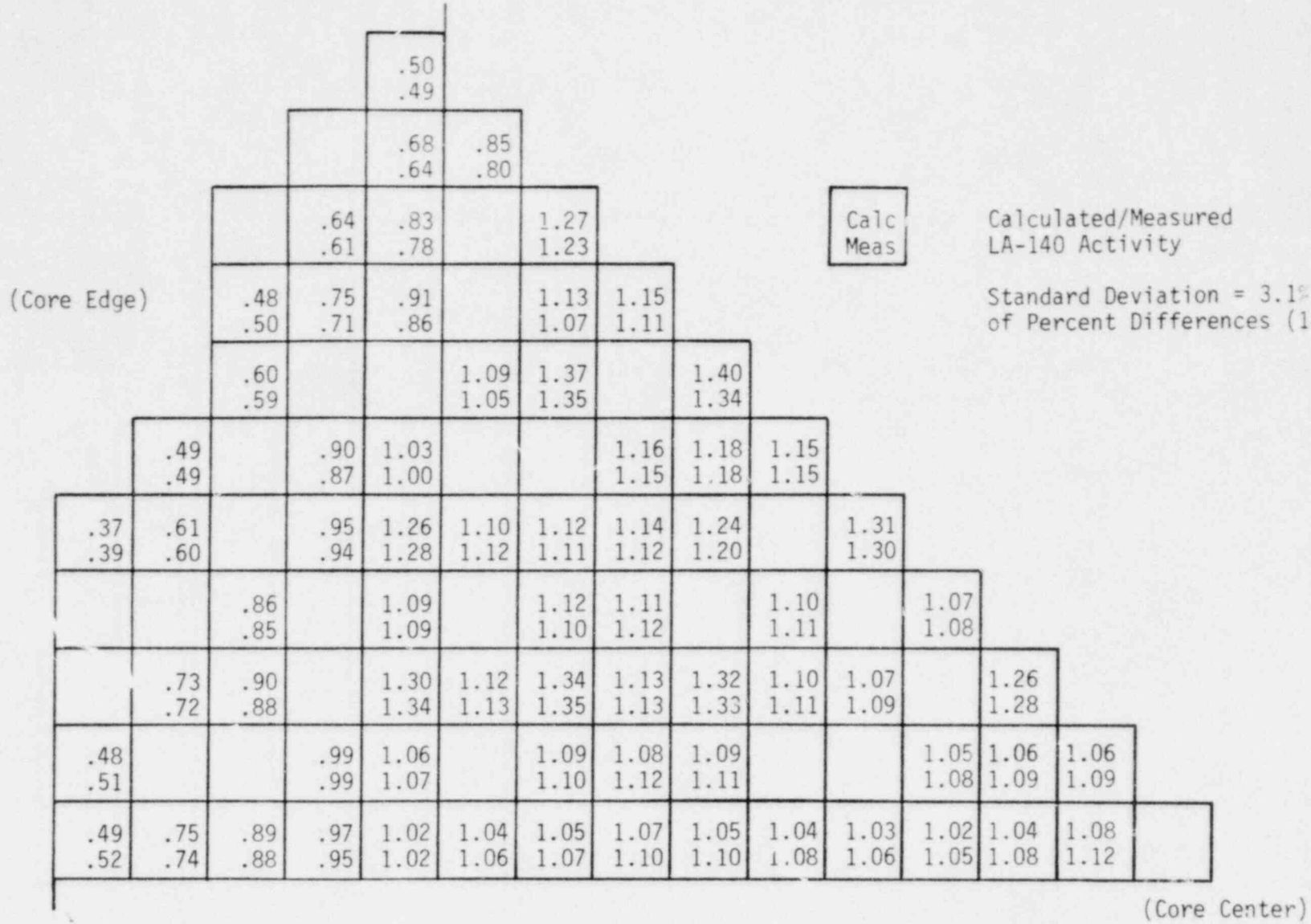

Figure 5.2-13 Quad Cities 1 EOC2 Fuel Assembly Gamma Scan Comparison, XTGBWR Calculated/Measured La-140

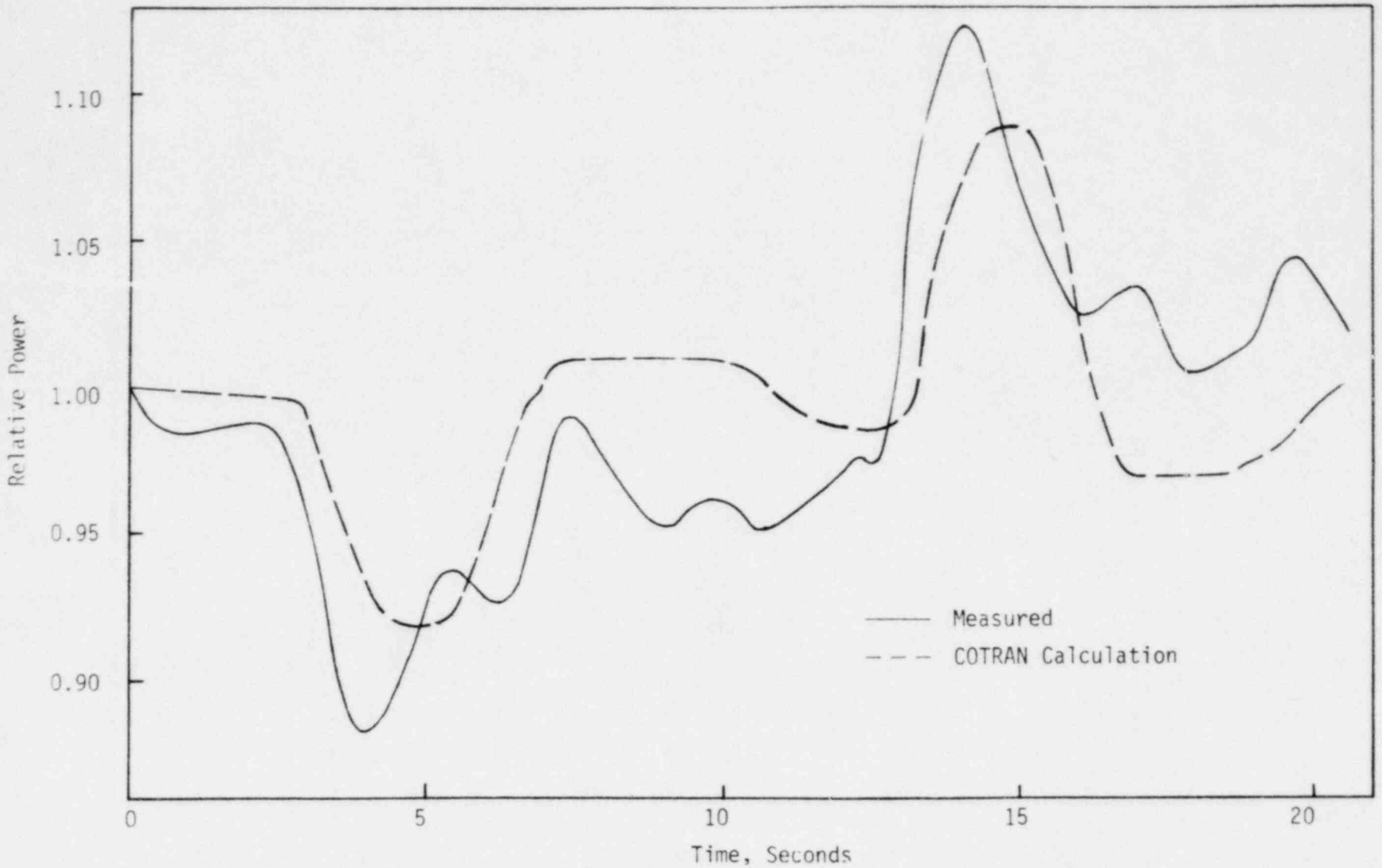

Figure 5.3-1 COTRAN - Peach Bottom-2 Low Flow Stability Test Comparison
Periodic Pressure Regulator Setpoint Step Changes

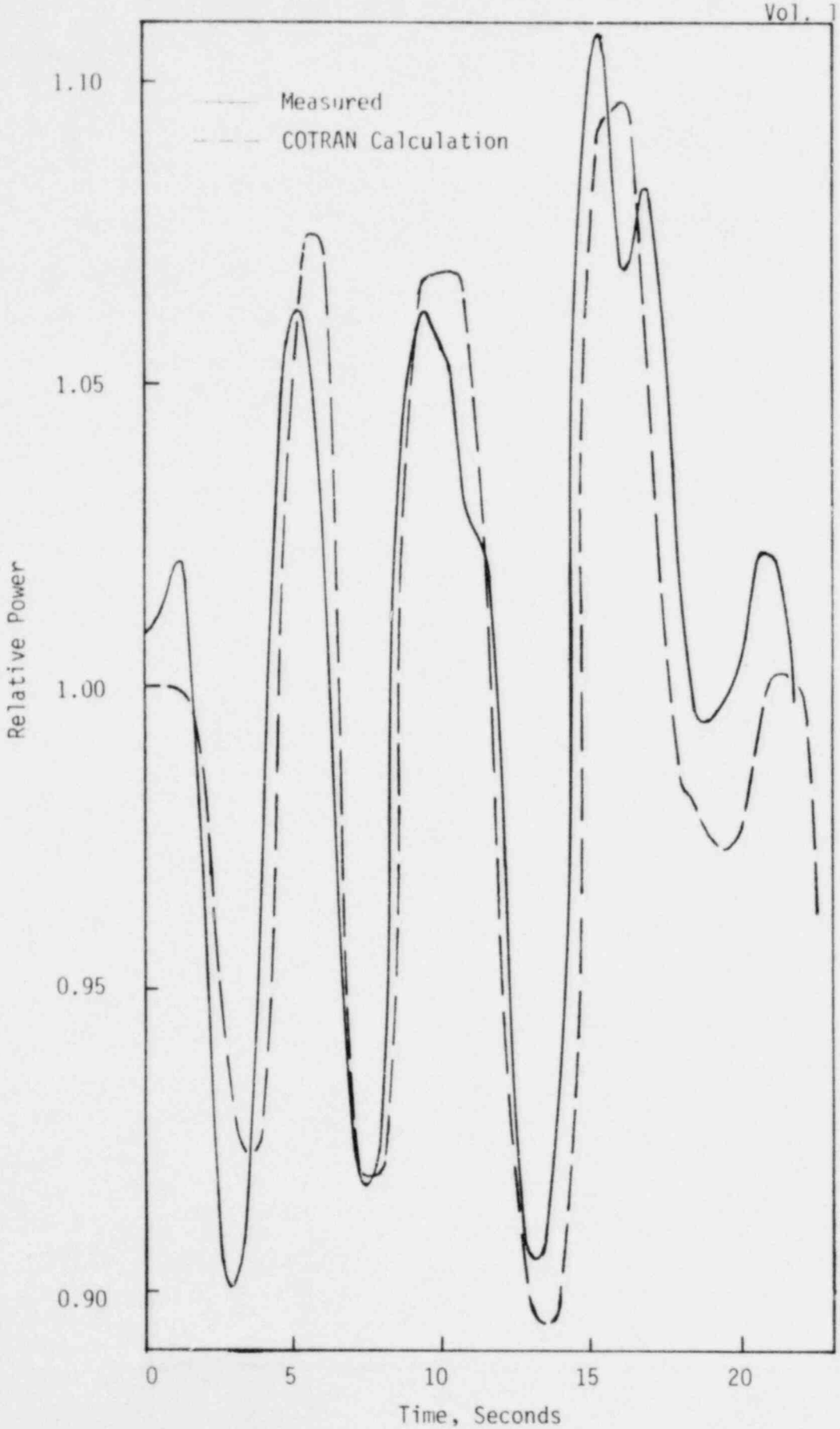

Figure 5.3-2 COTRAN - Peach Bottom-2 Low Flow Stability Test Comparison Random Pressure Regulator Setpoint Changes

5.4 REFERENCES

5-1 A. Ariemma, et., al., "Experimental and Theoretical Determination of Burnup and Heavy Isotope Content in a Fuel Assembly Irradiated in the Garigliano Boiling Water Reactor", EUR 4638, 1971.

5-2 M. B. Gutrone and G. F. Valby, "Gamma Scan Measurements at Quad Cities Nuclear Power Station Unit 1 Following Cycle 2", EPRI NP-214, July 1976.

5-3 L. A. Carmichael and R. O. Niemi, "Transient and Stability Tests at Peach Bottom Atomic Power Station Unit 2 at End of Cycle 2", EPRI NP-564, June 1978.

6.0 MEASURED POWER DISTRIBUTION UNCERTAINTY

The determination of the uncertainty associated with a measured power distribution is necessary to insure safe reactor operation. The safety analyses are performed to assure safe reactor operation with a certain quantified degree of confidence; thus, the uncertainty associated with the measured reactor power distribution must be quantified. The uncertainty analysis presented in this section begins with a concise mathematical expression of the method for determining the measured power distribution. The uncertainty is then defined in terms of the relative standard deviations of the independent variables involved in the measured power distribution determination. Methods to estimate the relative standard deviations of the independent variables from measured data are described. Using the relative standard deviation estimates in conjunction with the equation for the measured power distribution uncertainty, results in an estimate of the measured power distribution uncertainty expressed as a relative standard deviation.

6.1 MEASURED POWER DISTRIBUTION DETERMINATION

Reactor measured power distributions are combinations of measured reactor data and computer calculated data. The measured reactor power distribution data include the fixed local power range monitor (LPRM) in-core detector data and the traveling in-core probe (TIP) detector data.

The LPRM data are electric current readings proportional to the neutron flux level at four axial elevations in a number of radial locations. The radial locations are distributed in a uniform lattice throughout the

core. The LPRM detectors are fission chambers using U-235 as the fissionable isotope. The LPRM detectors are intercalibrated utilizing the TIP data. The TIP system consists of a number of movable fission chamber detectors (about 1" long) which can each enter a number of the radial locations at which the fixed LPRM detectors are located. The movable TIP detectors are all capable of entering one of the radial positions to allow intercalibration of the TIP system. Figure 6.1 is a drawing of an in-core instrument tube which contains both the four LPRM detectors and the TIP tube. Figure 6.2 depicts typical radial locations for both fixed and movable in-core detectors in a BWR core. Each radial location contains the equipment shown in Figure 6.1.

The computer calculated data include the relative core nodal power distribution, the in-core detector response distribution, and the local peaking factors for the fuel rods. The predicted relative nodal power and detector response distributions are calculated with the XTGBWR reactor simulator code described in Section 3.2. The XTGBWR code is a three dimensional modified two group diffusion theory reactor simulator program. The code uses large mesh sizes to perform full core nodal power calculations with time dependent xenon and samarium.

The local peaking factors are calculated by the XFYRE and XDT codes described in Sections 3.1 and 3.4. The XFYRE code is a single bundle depletion model that performs a microscopic depletion of each fuel rod in the fuel assembly. The XDT code is a diffusion theory program used to perform multibundle power distribution calculations.

The synthesis of the measured power distribution can be viewed to occur in two phases. Phase I consists of the fixed LPRM in-core detector calibration. Phase II consists of combining the individual fixed LPRM in-core detector distribution measurements with XTGBWR calculated data to produce the measured power distribution. An outline of the procedure is presented here.

[ ]

6.2 UNCERTAINTY DERIVATION

The uncertainty in the power distribution, P_{ijk}, can be derived based upon the measurement procedure formulation as expressed. The notation is simplified by rewriting for a single node ijk. In the following development, the index i will denote each fixed LPRM in-core detector used to determine P_{ijk} with ND denoting the number of detectors used.

[ ]

6.3 ESTIMATION OF UNCERTAINTY

The uncertainties, in terms of relative standard deviations, [ ] are determined by comparison to measured data. The measured data consist of distributions of TIP and fixed in-core detector responses plus gamma scans of bundles and pins. The majority of the data consists of TIP and fixed in-core detector distributions. This is due both to the limited amount of gamma scan data available, and to the limited core conditions represented by gamma scans.

6.3.1 Detector Measurement: δ_F

[ ] utilizes measured data which consist of a relative distribution of fixed in-core detector responses, F_i. The fixed detectors are located at four axial elevations in each of a number of radial locations, [ ]. The fixed detector responses are calibrated to TIP system measurements at regular intervals and are adjusted for the reduction in sensitivity to the neutron flux as a function of burnup between calibrations to the TIP system.

The uncertainty of the fixed in-core detector data [ ] is comprised of two sources. First, the uncertainty due to the TIP system which is acquired through the calibration process. Second, the uncertainty associated with the fixed in-core detector response itself.

The uncertainty in the TIP system measurements can be derived from symmetric TIP data. A core which is loaded 1/8 core symmetric and is operating with an 1/8 core symmetric rod pattern will have a number of pairs of instrumented radial locations which will have the same neutron flux distribution. Differences between the TIP responses in these positions can be used to define the TIP system measurement uncertainty.

The uncertainty in the TIP system measurements will be divided into two sources. First, the radial effects due principally to the random offset of the TIP from the center of the water region between channels,

[ ] is defined. Second, a term, [ ] is defined to represent all other sources of uncertainty. Define d_{ij} as the relative difference between symmetric TIP pair i at axial elevation j. The two sources of uncertainty can then be estimated as: [

]

The uncertainty in the fixed in-core detector response itself can be estimated from repeated measurements of the fixed detector response during a period of time when the power distribution is stable. The uncertainty associated with the fixed in-core detector lies in its ability to reproduce the response to which it was calibrated. The adjustment of the detector response due to a reduction in sensitivity through depletion of the U-235 introduces additional uncertainty, but this effect is negligible relative to that due to detector reproducibility and calibration to the TIP system. The uncertainty due to the fixed in-core detector reproducibility, [ ] is determined as follows.

Let [ ] represent the relative differences between two measurements j and k at position i.

[ ]

The uncertainty in the calibration, [ ] of a fixed in-core detector is the sum of the uncertainty in the TIP system measurement to which the fixed in-core detector is normalized and the uncertainty of the detector response being normalized.

[ ]

The uncertainty of the fixed in-core detector distribution [ ] is the uncertainty associated with the calibration plus the uncertainty of the fixed in-core detector reproducibility.

[ ]

6.3.2 Calculated Detector Response Distribution: δ_T

The uncertainty in the calculated detector response distribution can be determined by comparison to measured detector distributions, either from the TIP system or from the fixed in-core detectors. The relative standard deviation in the calculated detector response distribution can be determined as follows:

[ ]

To define the relative standard deviation in [ ] the calculated detector distribution, the uncertainty in [ ] must be removed from [ ] Equation 6.25 below represents the uncertainty in T if the TIP system measurements were used and Equation 6.26 represents the uncertainty if fixed in-core detector measurements are used [ ].

6.3.3 Calculated Nodal Power Distribution: δ_B

There are two sources of measured data which can be used in determining the uncertainty in the calculated nodal power distribution, [ ] The relative standard deviation [ ] can be derived from the calculated detector distribution uncertainty or it can be derived by comparing to gamma scan measurements of bundle power distributions. Both methods will be utilized.

The derivation of [ ] the relative standard deviation [ ] from the uncertainty in [ ] will be described first. The detector response distribution in XTGBWR is determined from the nodal power distribution using detector response-to-power factors. [

]. The equation from which T is determined can be written as follows, ignoring the normalization term.

[ ]

Following the approach described in Section 6.2, the relative variance [ ] can be written [ ] as in Equation 6.27. The random variables are treated as being independent. Covariance terms may need to be defined altering the equations, if analysis of the data indicates dependency among the random variables.

[ ]

6.3.4 Local Pin Distribution: δ_L

The pin power distribution is determined by multiplying the nodal power, [ ] by a local power distribution factor, [ ]. Local factors for each fuel type are calculated by the XFYRE and XDT codes and input to the XTGBWR code as a function of exposure, void, and control state (controlled or uncontrolled). XTGBWR interpolates among the input data to determine a value for the particular exposure, void and control state at node ijk.

The uncertainty in local peaking factors are determined by comparing the calculated pin powers to the pin by pin gamma scans of bundles which have been irradiated in a reactor. To perform the comparisons, the pin by pin power distributions from XFYRE/XDT must be converted to La-140 distributions, since the gamma scans measure La-140 distributions rather than power distributions.

[ ]

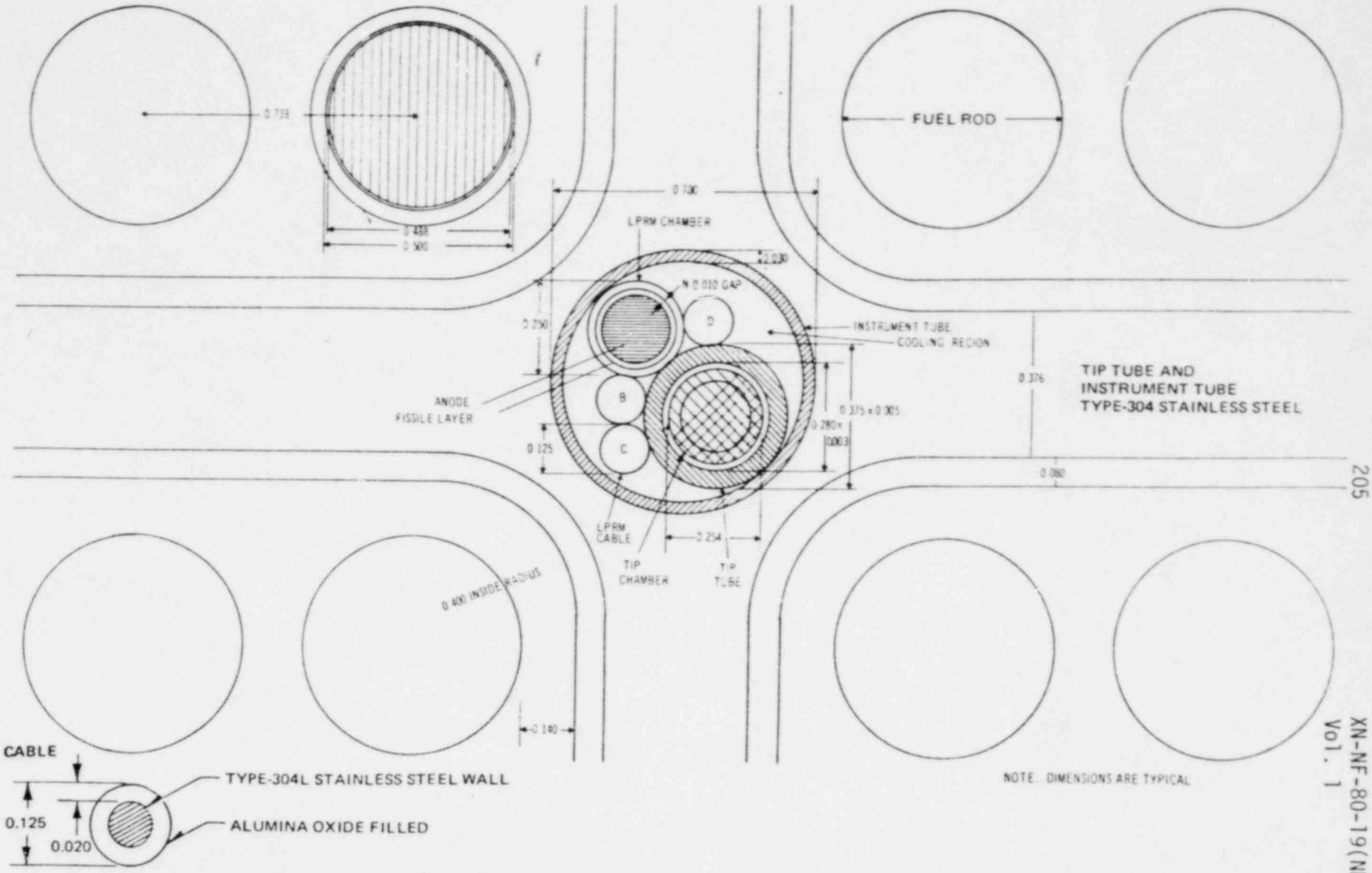

Figure 6.1 LPRM In-Core Assembly Cross Section

XN-NF-80-19(NP)
Vol. 1
08/07/80

DISTRIBUTION

T. L. KRYSINSKI
G. F. OWSLEY

NRC/G. F OWSLEY (20)
DOCUMENT CONTROL (5)